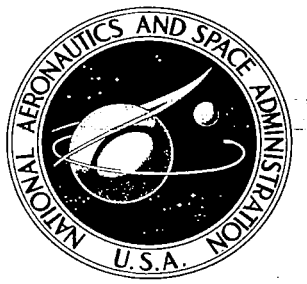

NASA CONTRACTOR REPORT

NASA CR-1715

STUDY AND DEVELOPMENT OF TURBOFAN NACELLE MODIFICATIONS TO MINIMIZE FAN-COMPRESSOR NOISE RADIATION

Volume V – Sonic Inlet Development

Prepared by
THE BOEING COMPANY
Seattle, Wash. 98124
for Langley Research Center

NATIONAL AERONAUTICS AND SPACE ADMINISTRATION • WASHINGTON, D. C. • JANUARY 1971

1. Report No. NASA CR-1715	2. Government Accession No.	3. Recipient's Catalog No.
4. Title and Subtitle STUDY AND DEVELOPMENT OF TURBOFAN NACELLE MODIFICATIONS TO MINIMIZE FAN-COMPRESSOR NOISE RADIATION. VOLUME V - SONIC INLET DEVELOPMENT		5. Report Date January 1971 6. Performing Organization Code
7. Author(s)		8. Performing Organization Report No. 10. Work Unit No.
9. Performing Organization Name and Address The Boeing Company Seattle, Wash. 98124		11. Contract or Grant No. NAS 1-7129 13. Type of Report and Period Covered Contractor Report May 1, 1967 to November 1, 1969
12. Sponsoring Agency Name and Address National Aeronautics and Space Administration Washington, D.C. 20546		14. Sponsoring Agency Code
15. Supplementary Notes		

16. Abstract Several sonic throat inlet concepts were investigated as a means of reducing the forward-radiated fan noise of turbofan JT3D-powered 707-320B/C airplanes. The acoustic, internal aerodynamic, and operational characteristics of a selected contracting cowl inlet were evaluated in model and full-scale ground rig tests. Static and in-flight inlet operation was simulated for both the noise-suppressed and unsuppressed modes of operation. Tests were conducted for a range of engine speeds, inlet Mach numbers, throat areas, and boundary-layer control configurations with both fixed and variable geometry inlets. Results are presented for fan noise attenuation, Mach number distributions, total and static pressure recovery, and effects on engine operation. Results are shown also for the dynamic response characteristics of the inlet and engine while operating with the inlet under automatic control. At simulated landing approach conditions, the results indicate that a 14- to 16-PNdB reduction of fan noise from the inlet was achieved with inlet center line Mach numbers of 0.7 to 0.8. Principal airplane performance penalties appear to be associated with the increased weight and drag of the acoustic nacelles.

17. Key Words (Suggested by Author(s))	18. Distribution Statement
707 airplane Sonic inlet Static tests Noise, aircraft	Unclassified - Unlimited

19. Security Classif. (of this report)	20. Security Classif. (of this page)	21. No. of Pages	22. Price*
Unclassified	Unclassified	123	$3.00

*For sale by the National Technical Information Service, Springfield, Virginia 22151

STUDY AND DEVELOPMENT OF TURBOFAN NACELLE MODIFICATIONS TO MINIMIZE FAN-COMPRESSOR NOISE RADIATION

OVERALL REPORT ORGANIZATION

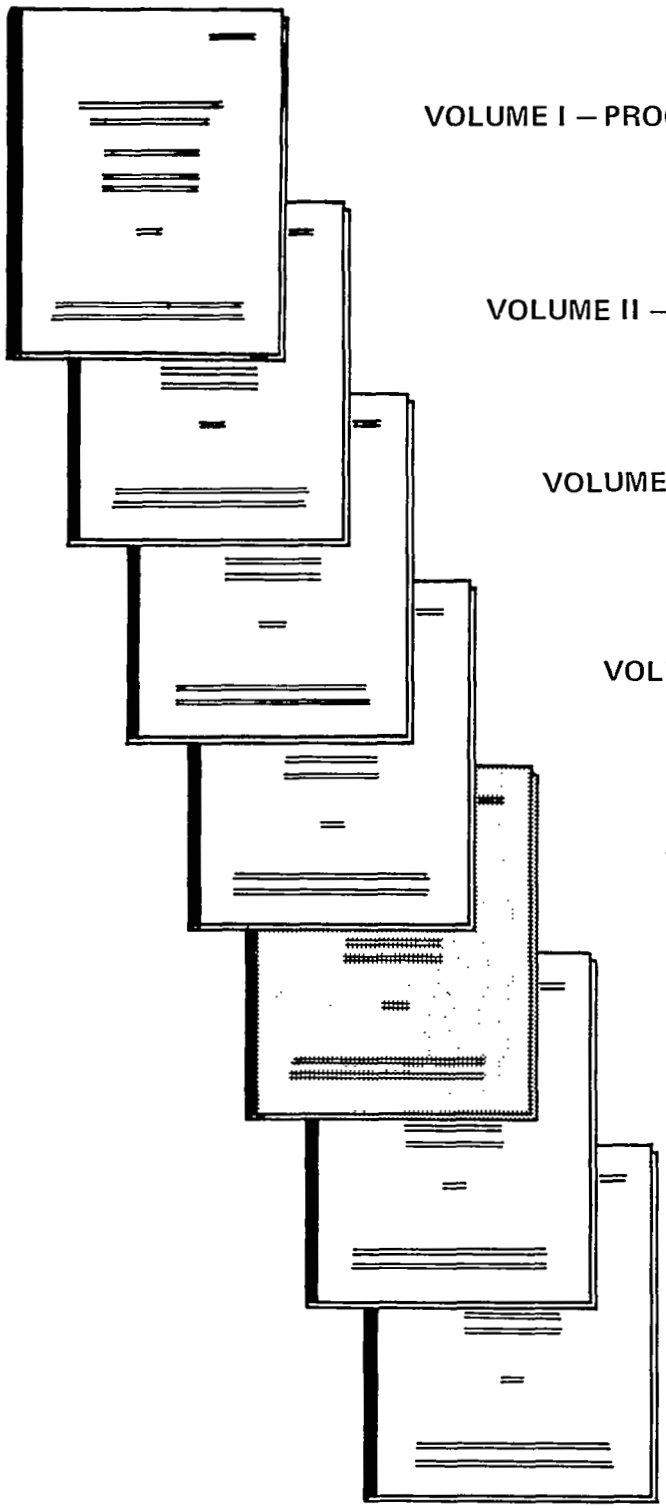

VOLUME I – PROGRAM SUMMARY

VOLUME II – ACOUSTIC LINING DEVELOPMENT

VOLUME III – CONCEPT STUDIES AND GROUND TESTS

VOLUME IV – FLIGHTWORTHY NACELLE DEVELOPMENT

VOLUME V – SONIC INLET DEVELOPMENT

VOLUME VI – ECONOMIC STUDIES

VOLUME VII – SUBJECTIVE EVALUATION TESTS

CONTENTS

TABLES

FIGURES

FIGURES—Continued

FIGURES—Continued

FIGURES—Continued

FIGURES—Concluded

STUDY AND DEVELOPMENT OF TURBOFAN NACELLE MODIFICATIONS TO MINIMIZE FAN-COMPRESSOR NOISE RADIATION

VOLUME V

SONIC INLET DEVELOPMENT

The Boeing Company
Seattle, Washington

SUMMARY

An investigation of turbofan engine noise suppression attainable as a result of sonic or near-sonic flow velocities through the engine inlet throat has been conducted. The investigation included conceptual studies and model tests followed by tests of full-scale boilerplate/prototype inlets. The inlet configuration selected for full-scale testing incorporated a variable cowl wall with automatic control for operation in the noise-suppressed mode. This configuration was evaluated in conjunction with acoustically treated fan ducts (described in vol. III) in static ground rig tests that simulated landing approach, takeoff, and cruise flight conditions for a 707-320B/C airplane equipped with JT3D engines.

Results show that the fan-generated discrete tones radiated forward through the inlet were virtually eliminated with inlet throat Mach numbers of 0.70 or greater at the inlet centerline. A reduction of 20 to 25 dB in sound pressure level (SPL) was measured in the 1/3-octave band containing the fan fundamental. However, definition of the magnitude of the fan tones propagating from the inlet during the noise-suppressed mode was limited by the masking effect from broadband noise components not associated with the fan-generated discrete tones. Therefore, reductions greater than 25 dB are estimated. Fan discharge noise appeared to be unaffected by suppression of the inlet noise.

Inlet perceived noise level reductions of 14 to 16 PNdB were obtained for conditions simulating landing approach. During simulation of cutback climb following takeoff, approximately 10-PNdB reduction of inlet noise was obtained. A reduction of inlet noise was also measured at maximum thrust conditions with the inlet in the unsuppressed mode; this reduction is attributed to the increased Mach number in the inlet as a result of the variable cowl wall configuration. This reduction in inlet noise will not materially affect the maximum noise levels since at maximum thrust these levels are established by the jet exhaust and fan discharge noise. To make most effective use of the sonic throat inlet, substantial reduction of other noise sources (fan discharge ducts, turbine, jet exhaust) is required for both landing approach and takeoff conditions.

When compared with a baseline (existing) inlet, it is estimated that takeoff thrust at 100 kn will be reduced by approximately 2 percent and cruise specific fuel consumption will be increased by 1 percent for the sonic throat inlet operating in the unsuppressed noise mode. For complete nacelles, which include both the sonic throat inlet and acoustically treated long fan ducts, principal airplane performance penalties appear to be associated with the increased weight and drag of the acoustic nacelle.

INTRODUCTION

Nacelle modifications that make use of acoustical linings in the inlet and fan discharge ducts to reduce the landing approach noise of turbofan JT3D-powered 707-320B/C aircraft have been described in volumes III and IV of this report. In this volume, another concept for the reduction of forward-radiated fan noise is presented in which high velocities within the inlet are utilized to aerodynamically oppose the propagation of fan-generated noise through the inlet. Because the concept becomes most effective when the velocity of the air within the inlet is sonic or near-sonic, an inlet of this type is often described as a sonic throat or "choked" inlet.

Achievement of the sonic or near-sonic inlet velocities requires that the flow area be reduced at some point within the inlet. Variable geometry is thus a feature of this type of inlet, with the area reduction provided whenever noise suppression is desired. During normal takeoff and cruise operation, when noise suppression is not required, it is planned that the inlet would return to a configuration similar to that of a conventional flight inlet.

The investigation of sonic throat inlets described in this report included conceptual studies, small-scale model tests, and full-scale boilerplate inlet tests. The conceptual studies were supported by both model and full-scale inlet tests, and these studies culminated in the selection of a contracting cowl wall inlet concept for full-scale evaluation with both fixed and variable geometry inlets. Of the latter, one inlet was manually adjustable, while a second inlet was fully mechanized and controlled. A nacelle installation that combined the mechanized inlet and acoustically treated boilerplate long fan ducts was evaluated with the inlet operating in both the suppressed and unsuppressed noise modes of operation. Evaluation of the selected inlet concept was supplemented by tests with 1/9-scale models.

SYMBOLS

A	area, inches^2
dB	decibel
E'	electrical voltage input, volts
E	electrical voltage output, volts
EGT	exhaust gas temperature, °R or °F
e	control reference voltage, volts
F_g	gross thrust, pounds
F_n	net thrust, pounds
g	*gravitational constant*
Hz	hertz (cycles/second)
L	length, inches
M	Mach number
m	momentum, foot pounds/second
N_1	low-pressure compressor rotor speed, rpm
N_{1-1}	basic control system input signal, low-pressure compressor rotor speed, rpm
N_{1-2}	model control system input signal, low-pressure compressor rotor speed, rpm
N_2	high-pressure compressor rotor speed, rpm
OASPL	overall sound pressure level, dB re 2 x 10^{-4} μbar
P	pressure, pounds/inch^2
PNdB	unit of PNL
PNL	perceived noise level, PNdB

SPL	sound pressure level, dB re 2×10^{-4} μbar
s	transfer function
T	temperature, ^{o}R or ^{o}F
W_A	inlet or engine airflow, pounds/second
W_f	fuel flow, pounds/hour
X	distance downstream of reference point, inches
δ	pressure ratio, P/P_o
Φ	vane sweep angle, degrees
θ	temperature ratio, T/T_o
μbar	microbar
Ω	angular displacement of rotating total pressure rake, degrees

Subscripts:

amb	ambient
BLC	boundary layer control
ch_1	forward BLC plenum chamber
ch_2	aft BLC plenum chamber
cw	cowl wall
R	total pressure with ram
S	static
T	total
th	throat
1	inlet entrance station
2	engine entrance station

2.45	fan discharge station
2.5	fan duct entrance station
7	turbine discharge station
∞	freestream

CONCEPTUAL STUDIES

During initial program investigations, a number of sonic throat inlet concepts were evaluated in terms of acoustic attenuation potential, aerodynamic and mechanical feasibility, and suitability for further development as a flightworthy inlet configuration. Specific design requirements were developed, and preliminary designs were analyzed for compatibility with these design requirements. Computer programs were used to predict the potential-flow and boundary layer growth characteristics of various inlet configurations, and two-dimensional water table studies were conducted to further evaluate boundary layer control (BLC) requirements. Insofar as practicable, results available from tests of both small- and full-scale inlets were used to assist in the evaluations.

Design Requirements

Design requirements established initially in the program included a 15-PNdB reduction in perceived noise level (PNL) during airplane landing approach, no compromise in flight safety, and no increase in crew workload. In addition, it was desired to maintain an economically viable airplane. The 707-320B airplane equipped with JT3D turbofan engines was selected for the installation studies. The sonic inlet was developed with these design requirements in mind.

Acoustic measurements on the JT3D engine established that the goal of 15-PNdB reduction in total noise during landing approach could be achieved with a 10- to 12-PNdB (or more) reduction of the noise radiated forward through the inlet, together with a 15-PNdB reduction of the noise radiated through the fan discharge duct. Studies also revealed that the 707-320B could not incorporate an inlet longer than 50 in. without major structural changes to the engine and airframe. Accordingly, inlet length was restricted to a maximum of 50 in. The constraint on inlet length was accompanied by a requirement to provide noise suppression at a minimum approach thrust of approximately 3000 lb per engine. At this thrust setting, the engine airflow, $W_A\sqrt{\theta}/\delta$, is approximately 250 lb/sec; consequently, the inlet throat area for sonic or near-sonic velocities was established at approximately 750 in^2 compared with a nominal throat area of 1570 in^2 required for cruise operation. Thus the inlet design problem became basically that of providing an inlet 50 in. long in which the throat area could be varied from 750 to 1570 in^2 while providing flow of the quality demanded by the engine for satisfactory operation.

To obtain satisfactory engine operation, total pressure recovery at the engine face must be sufficiently high and uniform to avoid both surge and excessive fan blade stresses. Also,

for those inlet concepts requiring engine bleed air for BLC, the quantity withdrawn from the engine must not result in excessive temperatures in the combustor, turbine, or exhaust ducts.

Proposed Concepts

A number of design concepts were proposed for test and evaluation. For discussion herein, these configurations have been categorized into three types:

- Variable cowl
- Variable centerbody
- Retractable vanes, struts, etc.

Two variable cowl concepts are illustrated in figures 1a and 1b. An eight-segment inlet concept, similar to that shown in figure 1a, appeared to be particularly promising during the conceptual studies. In the eight-segment design, the interior surfaces of the inlet were divided into eight circumferential segments separated by a similar number of fixed, triangular dividers; see figure 2. Each segment was further divided into three movable, overlapping panels that provided an essentially continuous flow surface axially through the inlet.

The eight-segment inlet concept evolved from an early variable cowl inlet designated as a "five-door" inlet. The "doors" of the five-door inlet were movable elements somewhat analogous to the segments of the eight-segment inlet except both inner and outer cowl surfaces moved as a unit. The refinement and evolution process began when the design constraints associated with the JT3D-powered 707 airplanes became more clearly defined. Compared to the five-door inlet, the eight-segment inlet was substantially shorter in length (50 versus 69 in.) and has a smaller inlet throat area in the minimum approach power configuration (750 versus 900 in^2). The number of fixed dividers (and segments) was increased to eight to minimize fan blade stresses when operating in the unsuppressed mode.

Variable centerbody inlet concepts are illustrated in figures 1c and 1d; variation of the throat area may be obtained by changes in the centerbody diameter or by axial translation of a centerbody within a suitably contoured outer cowl. A number of aerodynamic and mechanical problems became evident in evaluating this concept, particularly as a result of the limitations on inlet length inherent with the 707 series airplanes. Because of rapid diffusion associated with flow over the centerbody, model tests indicated that BLC would be required on both the centerbody and the interior surface of the cowl to prevent separation of the flow from these surfaces. Mechanical design problems also appeared to be formidable with the variable centerbody inlet, due in part to the wide range of area variation required for application to the 707 airplane.

Another sonic inlet concept is illustrated in figures 1e and 1f. In this concept, vanes, struts, or other elements that reduce the flow area through the inlet are inserted into the stream when noise suppression is desired. During normal operation (when noise suppression is not

required), it is anticipated that the vanes, struts, or other elements will be retracted and stowed within the cowl or centerbody, thereby minimizing performance losses during normal operation. This concept appears advantageous during takeoff and cruise operation; however, it is apparent that the aerodynamic and mechanical design problems must be considered carefully to achieve a satisfactory inlet.

Each of the various concepts appeared to offer certain advantages and disadvantages when compared on the basis of performance, weight, cost, controllability, safety, reliability, and maintainability. Performance estimates were based on analytical and experimental data obtained in potential-flow and boundary layer studies, water table tests, model tests, and tests of the full-scale, five-door inlet. Elements related to weight, cost, reliability, and maintainability were assessed for each configuration on the basis of preliminary design studies and layouts. The various concepts were also rated with respect to safety, feasibility, and suitability for flight applications. With sufficient development, it was believed that each of the three inlet concepts (i.e., variable cowl, variable centerbody, and element inserts) could provide the desired noise attenuation and aerodynamic performance. However, the variable cowl inlet appeared to offer the most advantages with respect to the aerodynamic and mechanical design of a sonic throat inlet, and it was selected for full-scale development. Models of the selected concept are shown in figure 2.

Advantages found for the variable cowl inlet include an internal flow distribution with high velocities near the cowl wall, least disturbance of the core flow entering the gas generator portion of the engine, adaptability to BLC, and a geometric arrangement favorable for the mechanical actuation and sealing of the variable geometry components. Experience gained in model and full-scale inlet tests of the variable cowl inlet was also favorable.

APPARATUS AND PROCEDURE FOR FULL-SCALE INLET TESTS

Test Installation

All full-scale tests were conducted at static conditions with the inlets installed on JT3D turbofan engines. Typical inlet and fan duct installations are shown in figures 3 through 5. For those tests in which the acoustic characteristics of the inlets were evaluated, the contribution of the fan discharge noise to the levels in the forward quadrant was minimized by acoustically treating the fan discharge ducts, thus suppressing the fan noise. The engine was suspended with its centerline at a height of 67 in. above a concrete pad approximately 30 ft wide and 50 ft long. A circular clearing with a radius greater than 300 ft provided an unobstructed area with low background noise levels.

Although details varied somewhat between tests, a typical system for supplying boundary layer control air to the inlet is shown in figure 6. Modulating valves provided control of the

flow from four high-pressure bleed ports on the engine to the inlet; flow rates were measured by calibrated flow tubes. During some of the early tests, BLC air was also supplied to the inlets from an external laboratory air supply.

A wind machine, which consisted of a large four-bladed propeller driven by a 2750-hp reciprocating engine and enclosed within a cylindrical shroud, was used to simulate landing approach conditions at wind speeds up to 100 mph and inflow angles up to 90° as measured with respect to the inlet centerline.

When operating at static and simulated approach flight conditions, an auxiliary 2.5-in.-radius lip was used to improve the flow entering the inlet. A large bellmouth lip shown in figure 7 was used to further reduce entrance losses when cruise operation was simulated.

Inlet Configurations

Four contracting cowl sonic throat inlets were evaluated in full-scale tests on a JT3D engine:

- Mechanized and controllable
- Adjustable
- Nonadjustable
- Five-door

A cross-section sketch of each inlet is shown in figure 8. A baseline inlet (used on 707-300B/C airplanes) was also tested. Although each sonic throat inlet was similar in general configuration, significant differences existed in the design details, as described below.

Mechanized and controllable inlet.—This inlet, shown in figure 8a, incorporated an actuation and control system that permitted simulation of flight operation with varying inlet throat area. Minimum throat area was 764 in^2, and maximum throat area was 1650 in^2. At the minimum throat area, the maximum diffuser wall angle (measured with respect to inlet centerline) was 21°; the equivalent conical diffuser half-angle was approximately 17°. Two BLC blowing slots that approximated two-dimensional convergent nozzles were included in the design. The first BLC blowing slot was located approximately 2.5 in. downstream of the geometric throat of the inlet, and the slot height was approximately 0.19 in. The second BLC slot was located near the midpoint of the diffuser, and the slot height was 0.14 in.; however, all tests were conducted with the aft slot passive.

Each of the eight movable segments consisted of forward, mid, and aft panels that overlapped to provide a faired inner cowl wall surface. The forward panel was hinged to the inlet lip ring, whereas the aft panel was hinged at its aft end to adjacent fixed dividers. Both boundary

layer blowing plenums were integral to the aft panel. The mid panel was supported by hinges and cam linkages to provide the overlapping action between panels. Each segment was operated by a separate linear hydraulic actuator mounted on the inlet frame below the panel, as shown in figure 8a.

A simplified diagram of the functional elements of the inlet control and actuation system used to vary the inlet throat area is shown in figure 9a. The control function was performed by an analog computer, and actuation was accomplished by the servohydraulic system. Although an analog computer was used to provide flexibility in programming the various control functions, an operational control system may use fluidic, mechanical, or simplified electrical equivalents to provide similar control functions.

A block diagram of the electrically equivalent inlet control system is shown in figure 9b. The command signals for control of inlet throat area were varied as a predetermined function of $N_1/\sqrt{\theta_{amb}}$. Values of inlet throat area measured at the completion of the tests are shown in figure 10a. Schedules of BLC and surge bleed valve operation were also preprogrammed. The BLC valve schedule is shown in figure 10b. The schedule for operation of the surge bleed valve is shown in figure 10c. Continuous modulation of surge bleed valve position was desired but was not worked into the design for this program because of time limitations.

The basic control system was designed with a capability to maintain inlet throat area at the values associated with an average Mach number of 0.85. The control system was designed also to maintain the selected Mach number to ±0.05, including variations due to subsystem transients. To meet the transient requirements, it was necessary to design for a servosystem response bandwidth of 200 rad/sec (corresponding to a time lag of approximately 0.005 sec).

A detailed functional diagram of the inlet control system is shown in figure 11a. The control system included duplicate functions, and comparator circuits were used to open the inlet in the event of a discrepancy between the two signals. A photograph of the control system and associated electronic equipment is shown in figure 11b.

Adjustable inlet.—This inlet, shown in figure 8b, was similar in design to the mechanized inlet, except for manual adjustment of inlet throat area. Only throat areas of 750, 900, and 1570 in^2 were evaluated. Forward and aft BLC slot heights were approximately 0.17 and 0.15 in., respectively. Both slots were designed as two-dimensional convergent nozzles. Tests were conducted with only the forward BLC slot active, as well as with both slots active. An auxiliary cowl inlet lip of 2.5-in. radius was used for ali of the tests. An instrumentation ring 6 in. long also was installed between the inlet and engine.

Nonadjustable inlet.—The nonadjustable inlet, shown in figure 8c, was designed as a simplified, fixed-geometry replica of the eight-segment inlet. To minimize fabrication time, the inlet was designed with straight-line elements (which gives the inlet its octagonal shape) rather than curved elements for each of the eight segments.

The inlet had a throat area of 750 in^2, and the diffuser walls formed an angle of 21° with respect to the inlet centerline. Two circumferential BLC blowing slots were incorporated in the diffuser at distances of 2.75 and 14.75 in. aft of the inlet throat. A cruise-type lip (i.e., small lip radius and contraction ratio) was used with this configuration.

The inlet was constructed as a multilayer laminate of resin-impregnated fiberglass, with metal fittings used for the BLC slots and manifolds. The BLC slots were designed as convergent nozzles in which the heights of the nozzles (slots) were varied by changing contoured steel plates; see figure 8c. The BLC slot heights evaluated were as follows:

Slot heights, in.	
Forward	Aft
0.114	0.090
0.171	0.136
0.250	2.200

Two different inlet centerbodies, designated as the 10-in. hemispherical and the 31-in. elliptical, were used. A 3.5° "droop" was also provided at the engine face for the inlet and centerbodies, consistent with the baseline inlet configuration.

Five-door inlet.—A cross-section sketch of the five-door inlet is shown in figure 8d. In minimum throat area position, the inlet had a geometric throat area of 928 in^2, a diffuser length of 57.5 in., a centerbody length of 31 in., a maximum diffuser wall angle of 11°, and an equivalent conical diffuser half-angle of 7°. The lip had a rounded leading edge, and BLC air was supplied through a row of discontinuous circumferential slots 0.25 in. wide, located 7.9 in. downstream of the geometric throat.

Instrumentation

The instrumentation used to measure the noise levels, inlet performance, and engine operation varied somewhat between tests of various configurations; however, principal results were obtained with the instrumentation described below.

Acoustic data recording.—Acoustic measurements were obtained using 24 microphones, as shown in figure 12. Output signals from the microphones were recorded on magnetic tape for subsequent analysis. An on-line analysis system was also used to continuously monitor the output signals. Sound pressure levels are presented with reference to a pressure of 0.0002 microbar (μbar).

Inlet instrumentation.—Principal inlet measurements consisted of total and static pressures at the engine face, static pressure distributions along the inner surfaces of the inlet, static pressures along the inlet centerline, and pressures, temperatures, and mass flow rates in the BLC system. Total temperatures were also measured at the engine face. Inlet instrumentation typical of that used during the tests is shown in figure 13. Pressure measurements were normally obtained with one or more pressure-scanning devices, each capable of scanning 48 pressures. Each pressure-scanning device contained a single transducer. Close-coupled rapid response transducers were used for some of the tests, particularly with the mechanized inlet, to record selected transient pressures up to at least 100 Hz.

Fourteen to 18 static pressures were sensed at approximately 1-in. intervals in the throat region of the inlet with the axial probe shown in figure 4a. Two of the static pressures were recorded directly with rapid response transducers during tests of the mechanized and controllable inlet. For some tests, the probe was traversed vertically from the inlet centerline to the upper divider. Mach numbers were based on the isentropic relationship for static to total pressure, with total pressure equal to ambient values. The maximum value of inlet centerline Mach number (minimum static pressure) was used to designate inlet operating conditions.

All steady-state inlet pressure and temperature data were digitized and recorded on magnetic tape for subsequent processing by a digital computer. Transient inlet data were recorded on 10- and 36-channel oscillographs; selected parameters were also displayed on X-Y plotters.

Engine operating instrumentation.—Axial thrust forces applied by the engine were sensed by a calibrated strain-gage-type load cell. Pressure and temperature instruments downstream of the fan are shown in figure 13. Standard pressure and temperature instrumentation provided by the engine manufacturer was used to measure gas generator (i.e., primary) exhaust conditions; see figure 13b. Rotational speeds of both the low- and high-pressure compressors were measured with tachometers. An additional tachometer was installed on the low-pressure compressor to provide an auxiliary input signal to the inlet control system. All steady-state engine operating data were digitized and recorded on magnetic tape for subsequent processing by a digital computer. Transient engine operating data were recorded on 10- and 36-channel oscillographs.

Test Procedures

Although test procedures were varied as necessary to accomplish specific test objectives, two general procedures were followed:

- Operation with fixed inlet throat area for varying engine rotor speeds (typical of tests with the five-door, nonadjustable, and adjustable inlets)

- Operation with varying inlet throat area and engine rotor speed (typical of tests with the mechanized inlet)

For tests with fixed inlet throat areas, acoustic and performance measurements were obtained at successively greater engine rotor speeds and inlet centerline Mach numbers. Maximum rotor speeds were usually limited by engine surge, excessive fan temperature differentials, or excessive turbine temperatures. If surge was encountered, engine rotor speeds were reduced sufficiently to obtain stable engine operation; data were then recorded. Data were recorded following a 3- to 5-min engine stabilization period at each test condition.

Acoustic data were recorded in two segments, each of 1-min duration. Engine performance and atmospheric data were recorded concurrently with the acoustic data. Each test was performed three times, and the acoustic data were averaged to minimize ground and meteorological effects. Acoustic data analyses were conducted in a manner similar to that described in volume III.

For tests with varying inlet throat areas and engine rotor speeds, both steady-state and transient (acceleration/deceleration) data were obtained. The steady-state data were recorded in the manner described above for fixed inlet throat areas; however, inlet throat area, BLC blowing rates, and surge bleed valve position were automatically controlled to preprogrammed values. Transient data were recorded for progressively faster power lever movements from idle to takeoff power, followed by a similar return to idle. Data were recorded continuously on both oscillographs and X-Y plotters during the accelerations and decelerations. Approximately 20 to 60 sec were required for each transient recording, depending on the rate of power lever movement used. The acceleration and deceleration tests were satisfactorily completed when surge-free operation was obtained for 1-sec power lever movements.

When landing approach conditions were simulated with the wind machine, corrections were made for the increased total pressure attributable to the axial velocity components.

RESULTS

The results obtained in this investigation are presented in figures 14 through 48, and in figures A-7 through A-20. Table I groups the data for the full-scale inlets according to type of data and inlet configuration for which the data were obtained. Results are shown first for the mechanized and controllable inlet because this inlet most closely represents the acoustic and performance characteristics of an inlet suitable for flight application. Results are also shown for the adjustable, nonadjustable, and five-door inlets. Results obtained with the nonadjustable inlet are summarized in table II. Results from the small-scale model tests are identified according to type in table III, and the data are presented in the appendix.

DISCUSSION

Mechanized and Controllable Inlet

The acoustic, control, and performance characteristics of this inlet are presented in figures 14 through 28.

Acoustic evaluation.—Acoustic data were recorded during steady-state and dynamic operation of the engine with the inlet at full area (unsuppressed mode) and with the inlet area under automatic control (noise suppression mode). However, the change of discrete blade passage frequency during rapid accelerations and decelerations made reliable determination of 1/3-octave band noise levels difficult. Thus, acoustic results are shown only for steady-state operation.

The maximum levels of the inlet radiated noise, as measured in the 1/3-octave band containing the fan blade passage fundamental frequency components, are shown in figure 14. At an inlet centerline Mach number of 0.70, the attenuation of fan-generated noise was 17 dB or greater. As shown by the acoustic spectra in figure 15, the fan-generated discrete tones were virtually eliminated in the inlet quadrant, but measurement of the absolute attenuation was limited by broadband noise levels of approximately 75 to 80 dB.

The relationship between inlet centerline Mach number and peak levels of inlet radiated noise is shown in figure 16 for various engine rotor speeds. These data indicate that a noise "floor" (which varied with engine rotor speed) effectively limited the attenuation at inlet centerline Mach numbers greater than 0.7.

For the inlet, the reduction in perceived noise level was 14 to 16 PNdB in the forward quadrant for conditions simulating an approach flyover at 400-ft altitude with a four-engine airplane, as shown in figure 17. Highest perceived noise levels during a flyover at approach power are associated with the fan discharge noise in the aft quadrant, both for the baseline and boilerplate nacelles. To fully use the mechanized inlet attenuation, fan discharge noise from the boilerplate nacelle must be reduced by an additional 4 PNdB during landing approach.

About 10-dB reduction in noise levels in the forward quadrant was also evident at maximum power with the inlet at full area, as shown in figure 14. This reduction in noise is attributed to the higher inlet centerline Mach number (0.58) with the mechanized inlet, compared to Mach 0.45 with the baseline blow-in door inlet.

Control operation.—The inlet centerline Mach number during steady-state operation in the approach power range varied from 0.60 to 0.83, as shown in figure 18a. Although inlet centerline Mach numbers were low at the lower speeds, higher Mach numbers could be provided by further reduction of inlet throat area. For these tests, minimum inlet throat area was 764 in^2.

As shown in figure 18b, thrust in the suppressed mode with automatic control was reduced in the approach power range, but the thrust losses were minimal at the higher power conditions. The variations in thrust and inlet Mach number at speeds of 5800 to 6200 low-pressure compressor rpm ($N_1/\sqrt{\theta}_{amb}$) were associated with closure of the BLC valve and the surge bleed valve (SBV). The surge bleed valve, because of the on-off action of its actuating system, made steady-state operation difficult in the range of 6000 to 6200 rpm ($N_1/\sqrt{\theta}_{amb}$). It was not considered feasible for this test program to further modify the actuation system of the SBV supplied by the engine manufacturer.

A series of accelerations and decelerations was completed with increasingly more rapid power lever (throttle) movements. Results obtained with power lever movements (idle to maximum power and vice versa) of 20 and 1 sec are shown in figure 19. These tests were completed without engine surge.

Largest variations from steady-state values of inlet centerline Mach number occurred during decelerations. Analysis of these results indicates that the BLC system was lagging in effectiveness during the transition from the unsuppressed to the suppressed mode of operation. Although BLC valve opening operation followed the programmed schedule satisfactorily, it appears that increased lead time was needed to fill the BLC manifold and distribution system.

A gain (amplification factor) of 200 in the servo loop was compatible with operation of the inlet and engine. The average time lag of the servoactuator system for the eight panels (without aerodynamic loads) was 0.009 sec in the extend direction (opening inlet) and 0.012 sec in the retract direction (closing inlet). The final overall inlet control system time lag was 0.015 and 0.018 sec in the extend and retract direction, respectively, without aerodynamic loads.

High actuator rates were required in the transition speed range between suppressed and unsuppressed modes of inlet operation. Operation in the constant throat Mach number range (i.e., suppressed mode) required a change in inlet throat area of approximately 25 in^2 per 100-rpm change in N_1. In the transition range (i.e., from unsuppressed to suppressed mode), a change of approximately 105 in^2 in throat area per 100-rpm change in N_1 was required.

Inlet and engine performance.—Principal factors influencing inlet and engine operation were boundary layer control blowing rates and inlet throat area.

Boundary layer control: The flow rates of bleed air used for inlet BLC in the noise-suppressed mode are shown as a function of engine rotor speed in figure 20a. It was necessary to reduce the BLC flow at engine rotor speeds greater than 5000 rpm ($N_1/\sqrt{\theta}_{amb}$) to remain within limits of exhaust gas temperature (EGT) established by the engine manufacturer.

Average values of EGT measured with and without BLC bleed are shown in figure 20b; the flow rates with BLC correspond to those shown in figure 20a. The 5-min operating temperature limit was not exceeded in these tests when using engine bleed air for BLC blowing.

Inlet centerline and cowl wall Mach numbers, with and without BLC, are shown in figure 20c. The results show that Mach numbers on both the cowl wall and inlet centerline were increased substantially when BLC was used; also, the Mach numbers on the cowl wall were significantly greater than those on the inlet centerline. Because the BLC valve is closed at approximately 5700 rpm, the Mach numbers measured at 5950 rpm or higher coincide for the two test runs with and without BLC.

Figure 20d shows the total pressure recoveries measured at the entrance to the fan, while figure 20e shows the total pressure recoveries measured at the entrance to the primary or gas generator section of the engine. Higher pressure recoveries at the fan entrance when using BLC resulted in higher fan exit pressures, as shown in figure 20f, and in lower fan exit temperature differentials, as shown in figure 20g. Without BLC, the fan exit temperature differentials were in excess of the engine manufacturer's recommended limits.

The results shown in figure 20g, together with results shown previously in figure 20b, clearly indicate the necessity for precise scheduling of the BLC valve position between 5600 and 6200 rpm ($N_1/\sqrt{\theta}_{amb}$) to remain within both fan exit temperature differential and EGT limits.

Use of high-pressure compressor bleed air for inlet BLC (while operating in the noise-suppressed mode) increased the thrust, as shown in figure 20h. The increased thrust is attributed to the improved fan performance shown previously in figure 20f.

Inlet throat area: Although inlet throat area was normally controlled as a function of engine rotor speed, selected tests were conducted in which inlet throat area was manually controlled as an independent variable. In each test, operation of the BLC and surge bleed valves remained under automatic control. Test results are summarized below for the three types of tests.

- Variable inlet throat area with constant approach rotor speed.—Mach numbers near the geometric throat of the inlet are shown in figure 21a. The engine rotor speed was maintained at approximately 5000 rpm ($N_1/\sqrt{\theta}_{amb}$) during these tests.

  Average total pressures measured at the entrance and exit of the fan are shown in figure 21b. As inlet throat area increased, the pressures increased rapidly, both at the entrance and exit of the fan. Thrust increased also, as shown in figure 21c.

- Variable inlet throat area with constant takeoff rotor speed.—Inlet Mach numbers attained during tests with reduced throat area at takeoff power are shown in figure 22a. As the throat area was decreased, the Mach number at the cowl wall increased to supersonic values, while the Mach number on the inlet centerline remained subsonic.

Pressure recoveries at the engine face and exhaust gas temperatures are shown in figures 22b and 22c. The thrust losses are shown in figure 22d. At a centerline Mach number of 0.79 the thrust loss was approximately 4.6 percent of that for the unsuppressed mode.

- Constant minimum inlet throat area with variable rotor speed.—To simulate a control failure in the noise-suppressed mode, the inlet was fixed at minimum throat area, and engine rotor speed was varied from approach to takeoff values. The results obtained at steady-state operating conditions are shown in figure 23.

  Surge was not encountered during any of the steady-state or moderate acceleration/deceleration tests. These results, considered with those of figures 23a and 23b, indicate that pressure recovery at the fan has little or no direct relationship to engine surge characteristics.

  Figure 23b shows that fan exit pressure decreases markedly with increasing engine speed. Fan exit temperature differential increased very rapidly over the speed range in which the BLC blowing was reduced, as shown in figure 23c, but no apparent difficulties were encountered when operating at the high fan temperature differentials. Fan blade stresses were not measured during these tests; additional tests to determine the blade stresses should be conducted prior to extended operation at these conditions.

  Turbine exit temperatures remained within acceptable limits, as shown in figure 23d.

  The thrust measured during operation with minimum inlet throat area is shown in figure 23e. Approximately 45 percent of engine thrust is available, at least on an emergency basis, with the inlet fixed in the minimum throat area position, as shown in figure 23f.

  A further indication of the operational capability of the engine with the inlet in the minimum area position is shown in figure 24. Both rapid accelerations and decelerations were accomplished, but surge was encountered on a very rapid deceleration.

  Other test results that show an operational capability with an inlet control or mechanical failure of one movable segment are presented in figure 25.

Simulated crosswinds: Crosswinds simulated by a wind machine (100 mph at 25° and 25 mph at 90°) had only a minor effect on inlet Mach numbers when operating in the noise-suppressed mode, as shown in figures 26a and 26b. Figures 26c and 26d show that inlet total pressure recovery was not greatly influenced by the simulated crosswinds, and surge was not encountered during either crosswind simulation. All tests were conducted at steady-state conditions with the 2.5-in.-radius takeoff lip installed.

As shown by figures 26e and 26f, the measured (or net) engine thrust was reduced by the ram effects produced when the wind machine was in the 25° location. With the wind machine in the 90° location, ram influence was negligible.

Takeoff performance, unsuppressed noise mode: Estimated takeoff thrust with the mechanized inlet is shown in figure 27a. The thrust loss, compared to specification thrust, was 2.5 percent at 0 kn and 2.2 percent at 100 kn. The inlet pressure recovery used for these estimates is shown in figure 27b. Measured inlet pressure recoveries (at static conditions) for a 2.5-in.-radius lip and a cruise simulation bellmouth lip are shown in figure 27c.

The radial distribution of inlet total pressure recovery, based on an average of six pressure rakes, is shown in figure 27d for several engine rotor speeds. These data indicate that the losses were confined to an area near the cowl wall. The total pressure recovery for the individual rakes is shown in figure 27e.

No engine surging occurred in the unsuppressed noise mode, even when crosswinds of 100 mph at 25° and 25 mph at 90° were simulated and snap accelerations and decelerations were executed. The time to accelerate from idle to takeoff power was similar to that obtained with the baseline inlet. Inlet total pressure recovery with crosswind was slightly lower than that measured at static conditions, as shown in figure 27f.

Cruise performance, unsuppressed noise mode: Inlet centerline Mach numbers for the takeoff and simulated cruise inlet configurations at various power settings are shown in figure 28a. It is believed that high velocities in the throat region are responsible for the reduction in noise shown previously at takeoff power in figure 14.

Radial total pressure distribution for the simulated cruise inlet configuration is shown for various engine rotor speeds in figure 28b. The total pressure distributions at various circumferential locations are shown in figure 28c.

Estimated thrust specific fuel consumption (TSFC) for the simulated cruise inlet configuration is shown in figure 28d. These results indicate an increase of 0.9 percent in TSFC for the mechanized inlet over that of a very low-loss reference bellmouth inlet.

When the inlet performance is combined with that of the boilerplate long ducts, propulsive performance of the resultant nacelle is estimated to be approximately 1.5 percent lower in thrust for takeoff and approximately 2.2 percent lower in TSFC at cruise, excluding external drag. When external nacelle and interference drag is included, the decrease in range is estimated to be 0.5 to 1.0 percent. An additional decrease in range is associated with the increased weight of the nacelles.

Adjustable Inlet

During the initial tests, it was established that use of the maximum allowable BLC blowing air produced the greatest reduction of fan noise and temperature differentials across the fan; consequently, nearly all tests were conducted with maximum allowable BLC blowing air.

Acoustic performance.—Results obtained from the acoustic measurements at inlet throat areas of 750 and 900 in^2 are summarized in figures 29 and 30. No acoustic data were obtained at the 1570-in^2 throat area. Noise measurements in the forward quadrant (0^o to 90^o) are believed to be indicative of inlet attenuation whereas measurements in the aft quadrant (90^o to 180^o) are primarily indicative of attenuation due to the acoustically lined 3/4-long fan discharge ducts and directionalizer. Combined effects due to attenuation of both the inlet and fan discharge noise would be anticipated at angles near 90^o.

As shown in figures 29a and 29b, fan-generated noise was reduced as inlet centerline Mach numbers increased from 0.5 to 0.8; only small additional reductions in noise level were observed at centerline Mach numbers greater than 0.8. At a Mach number of 0.8, the fan noise attenuation was greater than 23 dB (1/3-octave band analysis) for angles of 30^o to 50^o from the inlet centerline.

In the low thrust range, the fan noise attenuation was lower, as shown in figures 29c and 29d, because throat Mach numbers were limited to values less than 0.70 by the minimum attainable inlet flow area and engine airflow characteristics. These results indicate that a minimum throat area of somewhat less than 750 in^2 may be needed if uniform attenuation through the full thrust range is desired.

Acoustic spectra obtained with the eight-segment adjustable inlet, shown in figure 30a, indicate that broadband noise levels were significantly higher with the eight-segment inlet than with the five-door inlet. Acoustical absorbing materials were not used around the inlet and fan ducts in the tests of the adjustable inlet; hence, noise transmission through the inlet and duct structure may have contributed to the higher broadband noise levels.

The perceived noise levels as determined for the adjustable inlet are shown in figure 30b, corrected to a line parallel to, and 200 ft from, the axis of the engine. Figure 30c shows that a maximum PNL reduction of 16.5 to 17.5 PNdB is obtained with the adjustable inlet at an angle of 30^o to the inlet centerline.

Aerodynamic performance.—Maximum Mach numbers attained on the inlet centerline $M_{\mathbb{C}_L}$ increased with increasing engine rotor speed, as shown in figure 31a. Mach numbers on the cowl wall (M_{cw}) also increased with engine rotor speed. For inlet centerline Mach numbers up to 0.8, higher values of Mach numbers on the cowl wall were found with the 750-in^2 throat area than with the 900-in^2 throat area; see figure 31b. Sonic flow on the cowl wall occurs

when inlet centerline Mach numbers exceed 0.63 to 0.7. Mach number gradients across the inlet throat, shown in figures 31c and 31d, were also greater with the 750-in^2 throat area.

For a fixed inlet area, total pressure recovery decreased with increasing engine speed, as shown in figure 32a. The decrease in recovery was related to both an increasing inlet centerline Mach number and a decrease in available BLC airflow rate, as shown in figure 32b. For a given Mach number and recovery, lower BLC airflow rates were required when using only the forward BLC slot, as shown in figure 32c.

For a constant inlet centerline Mach number, reduction of the BLC airflow rate from the maximum allowable produced lower total pressure recovery, as shown in figure 33a. Blowing through both slots or through only the forward slot with the maximum allowable airflow rate produced similar recovery profiles; see figure 33b. Because the EGT limit restricted permissible BLC airflow rates, the pressure recovery (at an 0.8 inlet centerline Mach number) was lower at an inlet throat area of 900 in^2 than at 750 in^2, as shown in figure 33c.

Radial total pressure recovery profiles measured with the six individual rakes at the engine face are shown in figures 34a through 34e. Repetition of the test conditions of figure 34a gave the results shown in figure 34c. Although significant changes in circumferential distribution occurred, the average pressure recovery was nearly equal for the two tests. At lower BLC blowing rates, pressure recovery for the flow entering the fan section was reduced, as shown in figures 34a and 34d.

Wall static pressure profiles are shown in figures 35a and 35b. A shock pattern was indicated upstream and downstream of the forward slot, particularly with high-pressure blowing; see figure 35b. Reduction of BLC airflow rates from the maximum allowable resulted in lower static pressure recovery in the diffuser and a higher static pressure in the throat region, as shown in figures 35a and 35c. Wall static pressures measured with a 900-in^2 throat indicated less variation in the BLC slot region, as shown in figures 35d and 35b.

With the inlet throat area increased to the maximum value of 1570 in^2, similar values of total pressure recovery at the engine face were measured with the rotating rake and with six fixed total pressure rakes, as shown in figure 36a. Relative to the exposed dividers, similar total pressure recovery profiles were measured with the six fixed rakes and with the rotating rake, as shown in figures 36b and 36c. It is believed that a vortex action may be energizing the flow on either side of the dividers, as shown in figure 37.

Engine performance.—Engine parameters are shown in figure 38 for two inlet throat areas and two BLC blowing conditions. During these tests, the surge bleed valve was maintained in the open position. The maximum available BLC airflow rate was used up to an inlet throat Mach number of 0.7 for the 750-in^2 throat area and up to 0.6 for the 900-in^2

throat area. At higher throat Mach numbers, it was necessary to reduce the BLC airflow to maintain exhaust gas temperature within the limit, as shown in figures 38a and 38b.

When operating in the noise-suppressed mode, the fan nozzle pressure ratio was greatly reduced at the higher speeds (and throat Mach numbers), as shown in figure 38c. Exhaust pressure ratio (EPR) of the primary section of the engine was also reduced, as shown in figure 38d. With both fan and primary nozzle pressures lower, thrust was also reduced; see figure 38e. The thrust losses increased rapidly at the higher inlet centerline Mach numbers for both the 750- and 900-in^2 inlet throat areas, as shown in figure 38f. At the 0.8 centerline Mach number presently contemplated for inlet operation during approach, thrust losses of approximately 17 percent may be anticipated. However, sufficient thrust is available to prevent the airplane becoming thrust limited at any time during approach.

Maximum fan temperature differentials $\Delta T_{2.45}$ are shown in figure 38g, together with limits recommended by the engine manufacturer. The limit was not exceeded except at a condition where centerline Mach number = 0.9 when using both BLC slots.

Results of static ground tests of the sonic throat inlet with a throat area of 1570 in^2 are presented in figure 39. A comparison of the performance of the adjustable inlet to the reference bellmouth inlet indicates a thrust loss of 2.2 percent (at constant $N_2/\sqrt{\theta}_{amb}$) and a specific fuel consumption increase of 1.3 percent (at constant thrust).

Nonadjustable Inlet

The operation of the inlet and engine at high inlet centerline Mach numbers is summarized in table II; these results indicate that satisfactory operation was achieved up to Mach numbers of 0.84. Operation was demonstrated at higher Mach numbers, but fan temperature differentials exceeded recommended operating limits.

Inlet centerline Mach number.—Without BLC, the maximum Mach number attainable on the inlet centerline was limited to approximately 0.7 or less. With BLC blowing, the attainable Mach number was increased to 0.84 or greater, as shown by figures 40a and 40b. With BLC blowing through the forward slot only, the highest inlet centerline Mach number without engine surge was attained with the 0.250-in. slot height. By contrast, the combination of the 0.171-in. forward BLC slot and the 0.136-in. aft BLC slot provided the highest inlet centerline Mach number without surge when using both BLC slots.

Inlet centerline Mach numbers of approximately 1.0 were obtained with the wind machine operating to simulate a 100-mph approach flight condition, as shown in figure 40c. These results were obtained using only the 0.171-in. forward BLC slot (aft slot passive); in addition, the area of the surge bleed valve was increased. The effect of the wind machine was small, except at the higher engine speeds. A similar effect was found also in tests of the 0.171-in. forward and the 0.136-in. aft BLC slots, as illustrated in figure 40d.

Fan exit temperature differential.—The effect of increasing BLC slot height (and flow rate) upon $\Delta T_{2.45}$ is shown in figure 41a. At the largest BLC slot height tested, a facility limitation on the BLC rate resulted in a slight increase in $\Delta T_{2.45}$.

The minimum quantities of BLC blowing air necessary to operate within the recommended limit of $\Delta T_{2.45}$ are shown in figure 41b. Of the three forward BLC slot heights tested (aft slots passive), BLC air was a minimum with the 0.171-in. slot at a given centerline Mach number. For operation within $\Delta T_{2.45}$ limits at an inlet centerline Mach number of 0.8, BLC bleed air (from the engine) equal to 3.5, 2.5, and 4.8 percent of the mass flow entering the inlet throat would be required with the 0.114-, 0.171-, and 0.250-in. forward BLC slots, respectively. Greater quantities of BLC bleed air were required with two BLC blowing slots to attain similar centerline Mach numbers.

Engine surge characteristics.—As shown in figure 41a, surge was encountered during tests with both the 0.114- and 0.171-in. forward BLC slots (aft slots passive). By contrast, surge did not occur with the 0.250-in. slot. When both forward and aft BLC slots were used, higher plenum chamber pressures were required for the forward slot than the aft slot to avoid surge. Attempts to correlate surge with inlet pressure recovery or other inlet flow characteristics were not conclusive, although high values of inlet pressure recovery for the flow entering the primary section of the engine appeared to be necessary to avoid surge.

With the surge bleed valve closed, surge occurred at inlet centerline Mach numbers of approximately 0.5. Opening the SBV permitted operation at centerline Mach numbers of 0.9, but surge at lower Mach numbers was likely with nonoptimum BLC blowing slot pressures and geometries. A significant improvement in the engine surge characteristics was noted following removal of an annular restrictor in the SBV.

With the SBV restrictor removed, large variations of primary and fan total pressure recovery were measured prior to surge, as shown in figures 42a and 42b. Corresponding values of inlet centerline Mach number and fan temperature differential are shown in figures 42c and 42d. The low value of pressure recovery at the primary section appears to be the cause of surge at approximately 5200 rpm. High values of pressure recovery at the primary section were found when BLC was not used, but fan temperature differentials were excessive.

Inlet centerbody.—Increased sensitivity to surge was noted when a short (10 in.) hemispherical centerbody was replaced with a longer (31 in.) centerbody with an elliptical contour. Lower values of total pressure recovery were associated with the longer centerbody, as shown by figures 43a and 43b.

Diffuser static pressure recovery.—Highest static pressure recoveries were obtained when blowing at the maximum rate through the forward BLC slot (aft slot passive), as shown in figure 44. These data were obtained at approximately the same engine speed (4400 rpm) and with the same BLC slot height (0.171 in.) installed.

Five-Door Inlet

Inlet characteristics related to noise, thrust, BLC requirements, and internal aerodynamics are presented in figures 45 through 49.

Noise.—A progressive reduction of inlet radiated fan noise was measured as inlet centerline Mach numbers increased to 0.80, as shown in figure 45a. At Mach numbers greater than 0.80, the noise levels remained nearly constant, and it is concluded that a noise floor due to other sources was encountered at approximately 75 to 80 dB. Wrapping the fan ducts with acoustical materials lowered the noise floor by approximately 4 dB.

A maximum reduction of 32 dB in fan noise was obtained at an angle of 40° to the inlet centerline, as shown in figure 45b. The corresponding reduction of maximum perceived noise was 25 PNdB. As shown by the typical spectra in figure 46c, both the discrete tones and broadband noise above 500 Hz were significantly reduced.

Thrust.—Figure 47a shows that gross thrust losses of approximately 2 to 12 percent may be anticipated when operating the five-door inlet with BLC in the approach thrust range, with the higher losses associated with Mach numbers near 1.0.

BLC requirements.—BLC bleed rates of approximately 2.4 to 3.4 percent of the inlet throat airflow rates were used at inlet centerline Mach numbers of 0.6 and 1.0, respectively. At the latter condition, further reduction of the BLC flow rate resulted in engine surge.

The primary exhaust gas temperature was higher with the five-door inlet due to the use of high-pressure bleed air, as shown in figure 47b. The EGT temperature limit of 1310°R, established by the engine manufacturer for continuous operation with bleed, was not exceeded. The circumferential spread in EGT when using high-pressure bleed air did not exceed 101°F for any test condition.

Internal aerodynamics.—The maximum Mach number in the inlet throat region at various radial distances from centerline to cowl wall is shown in figure 48. Highest Mach numbers were found at the cowl wall, with the flow becoming sonic on the cowl wall when centerline Mach numbers exceeded 0.7. The distribution of Mach numbers axially through the throat region of the inlet is shown in figures 49a and 49b for nominal inlet centerline Mach numbers of 0.6 and 1.0, respectively. At the lower centerline Mach numbers, the rate of Mach number change with axial distance is gradual; however, at the higher centerline Mach numbers, there is a rapid decrease from supersonic to subsonic flow, particularly in the area adjacent to the cowl wall. It is believed that this rapid compression is the result of the flow passing through a series of oblique shocks. Mach numbers at the cowl wall (determined from static pressure measurements on the cowl wall for centerline Mach numbers of 0.6 and 1.0) are also shown in figures 49a and 49b. From these results it is apparent that the BLC blowing slot locally influences static pressure near the cowl wall. Wall static pressures also indicate that one or more shock systems may be present in the flow near the cowl wall.

One-Ninth-Scale Model Inlets

Results obtained with models representing each of the proposed inlet concepts (i.e., contracting cowl wall, expanding centerbody, and retractable vanes) are presented in Appendix A. For similar inlet configurations and operating conditions, the small- and full-scale inlet test results were found to be similar with respect to both acoustic and aerodynamic characteristics. However, interpretation of model test results related to full-scale engine operation (particularly surge) was difficult because of uncertainties associated with the effects of inlet losses and flow distortion on engine operation. Operation of the engine is also influenced by other factors, such as compressor bleed rates, interstage and interspool matching, and dynamic acceleration characteristics, which make full-scale tests necessary for a complete evaluation of inlet and engine operation. Yet model tests do provide a useful means for investigating inlet acoustic and aerodynamic characteristics, often at conditions which are difficult to achieve in full-scale tests. For maximum effectiveness, model tests should precede full-scale tests.

CONCLUDING REMARKS

Model and full-scale tests of the contracting cowl sonic throat inlet indicate the following.

- The sonic throat inlet is highly effective as a means of reducing forward-radiated fan noise. Reductions of 14 to 16 PNdB or more in inlet radiated noise are attainable during landing approach of a JT3D-powered 707-320B/C airplane. Other engine noise sources,such as fan noise radiated from the fan exhaust duct and jet noise, would have to be reduced significantly to take full advantage of the inlet noise reduction afforded by the sonic throat.

- Measurable attenuation was found at inlet centerline Mach numbers as low as 0.5, and substantial attenuation (greater than 20 dB in the peak 1/3-octave band) was obtained at inlet centerline Mach numbers of 0.7 to 0.8. At the latter conditions, the flow was supersonic near the cowl wall.

- Boundary layer control blowing (up to 4.5 percent of inlet mass flow rate) was necessary to achieve satisfactory inlet and engine operation with the eight-segment inlet.

- A thrust loss of approximately 2 percent is estimated at takeoff and an increase of 1 percent in cruise specific fuel consumption is estimated with the eight-segment inlet.

- For a complete acoustic nacelle on JT3D-powered 707-320B/C airplanes, principal airplane performance penalties appear to be associated with the increased weight and drag of the nacelle.

- Sonic throat inlet development must be closely integrated with the operating characteristics of the engine, and future development should be closely coordinated with the engine manufacturer.

- Application of the sonic throat inlet must be based on economic and/or environmental requirements that will justify the additional weight, complexity, and cost of the inlet and other nacelle treatment.

The Boeing Company
Commercial Airplane Group
Seattle, Washington, September 1969

APPENDIX A

MODEL TESTS

The internal performance and acoustic attenuation characteristics of contracting cowl wall, expanding centerbody, and stowable (radial) vane inlet concepts were evaluated in tests of 1/9-scale inlet models. The tests were conducted using a static ejector rig, a 5-in.-diameter powered model fan, and a low-speed wind tunnel (0 to 200 kn).

Description of Small-Scale Models

Eight-segment contracting cowl wall inlet.—Several configurations of the eight-segment inlet were evaluated with the models described below.

750-in^2 simulation inlet: The landing approach model that simulated the adjustable boilerplate inlet is shown in figure A-1. The takeoff lip modification is shown in figures A-1a and A-1b. The aft view of figure A-1b shows the BLC blowing slots. The height of each BLC slot was 0.01 in.

900-in^2 simulation inlet: The 900-in^2 boilerplate simulation model consisted of the same hardware as that used for the 750-in^2 simulation. The inlet segments were relocated to provide the larger throat area. Photographs of the 900-in^2 simulation appear in figure A-1c.

1370-in^2 simulation inlet: A front view of the 1370-in^2 boilerplate simulation model showing the takeoff lip modification and protruding dividers is presented in figure A-1d. The 0.01-in.-wide BLC blowing slots are shown in the rear view of figure A-1d.

Takeoff and cruise simulation model: The same basic inlet model was used for both takeoff and cruise performance evaluation with the only difference being in the lip employed. The takeoff lip modification was used for static evaluation of takeoff performance. Similarly, a large bellmouth inlet lip was used for static evaluation of cruise performance. Figure A-1e shows the cruise configuration with the bellmouth.

Eight-sided nonadjustable inlet: A sketch of the nonadjustable inlet model is shown in figure A-2. The height of each BLC blowing slot was 0.01 in.

Non-BLC inlet: A circular cross-section inlet model having the wall contour indicated in figure A-3 was fabricated as a reference non-BLC inlet configuration representative of that used in the noise-suppressed mode.

Five-door inlet.—Sketches of the models that simulated landing approach, takeoff, and cruise configurations of the five-door inlet are shown in figure A-4a. A photograph of the takeoff simulation models, with each of the lips tested, is shown in figure A-4b.

Five-door inlet, centerbody extended.—The same basic five-door inlet model in its approach configuration with the rounded leading-edge flap lip was tested with a 31-in. centerbody in several extended positions as indicated in figure A-4a. A view of the model with the centerbody forward, simulating an inlet with a 700-in^2 throat, is shown in figure A-4c.

Expandable centerbody inlet.—A cross section of the test model is shown in figure A-5. Cowl wall BLC consisted of two rows of holes to enable extraction to 1 percent of diffuser throat mass flow rate by suction. The centerbody was equipped for blowing BLC. However, suction BLC was also investigated by reversing the flow direction through the BLC slot.

Radial vane inlet.—A sketch of the radial vane inlet model is shown in figure A-6. Provisions were made to position the vanes at angles of 0°, 20°, and 30.8° (0° corresponds to minimum throat area) to simulate the throat area associated with three different power settings during approach flight conditions. An extended centerbody was tested with the 30.8° vane position. Additionally, two diffuser extensions (3.36 and 6.72 in. long) were fabricated. The 3.36-in.-long diffuser extension provided a diffuser-length to vane-chord relationship representative of that which would exist in a full-scale inlet.

Baseline inlet.—A scale model of the inlet used on many of the 707 airplanes appears in figure A-4b. This model was used for baseline comparisons with the eight-segment takeoff simulation model.

Model Test Facilities

The small-scale inlet models were evaluated by using one or more of the following Boeing facilities:

- Ejector rig
- Powered model fan
- Low-speed wind tunnels
- Water table

The ejector rig facility provided a means for inducing airflow through the static model and a means for measuring static pressure distributions along the cowl wall and inlet total pressure recoveries at the simulated engine face. A 32-probe rotating rake assembly was used to obtain detailed surveys at the simulated engine face. The powered model fan used a single-stage inducer section from a Boeing T-50 gas turbine engine to simulate turbofan operation behind a sonic throat inlet. The powered model fan and its air-driven turbine were enclosed

within an anechoic chamber, and measurements of the noise emanating from the inlet were made for a range of fan speeds and inlet throat velocities.

Other tests were conducted in low-speed (up to 200 kn) wind tunnels, with either 4- by 9-ft or 9- by 9-ft test sections. Internal performance of the inlets and effects of lip geometry on inlet operation during takeoff simulation were evaluated. Approach and takeoff operation was also simulated at inflow angles up to 25°. A large vacuum pump was used to induce the desired flow rate through the inlet, and pressures along the cowl wall and at the simulated engine face were measured in a manner very similar to that used for the ejector rig.

Tests of two-dimensional inlet models were conducted on a large water table. These tests permitted observation of the general flow characteristics of several inlet configurations. The water table tests were also used to supplement analytical studies of suction and blowing boundary layer control as applied to the inlet diffuser.

Description of Model Tests

Test conditions were established by progressive increases of mass flow rate through the inlet. Data were recorded at stabilized conditions for a wide range of mass flow rates and inlet throat Mach numbers. Pressures were measured with one or more pressure-scanning devices, each capable of scanning 48 pressures with one transducer. The data were digitized and recorded on punched cards or paper tape for subsequent processing on a large digital computer.

For the low-speed wind tunnel tests, tunnel speed was set and maintained prior to final inlet airflow adjustment. Cruise operation was simulated at static test conditions by the use of a large bellmouth lip that faired smoothly into the throat contour of the inlet.

Acoustic measurements were obtained only during tests with the powered model fan. Acoustic surveys were made using a boom-mounted microphone capable of traversing in an arc of 180° around the front of the inlet at a radius of approximately 40 in. Sound pressure levels were recorded as a function of microphone position. Suitable filters were used to provide 1000-Hz bandwidth SPL covering the blade passage frequency range. Most inlet acoustic data presented herein are based on the narrowband SPL obtained at the blade passage frequency ±500 Hz. Measured overall sound pressures levels included all frequencies between 50 and 50 000 Hz.

Results and Discussion

Eight-segment contracting cowl wall inlets.—Test results for the various eight-segment inlet models are presented in figures A-7 through A-12.

750-in^2 simulation inlet: Ejector rig tests were conducted with single- and double-slot BLC blowing over a wide range of inlet airflows and BLC supply pressures. Figure A-7a shows

a typical distribution of total pressures at the diffuser exit when using high BLC blowing pressures. The distribution of total pressure at the diffuser exit when BLC was not used is shown in figure A-7b; the preferential flow separation apparent in the figure appears to be characteristic of flow through rapidly diffusing passages without BLC. For specified BLC flow rates, highest values of inlet total pressure recovery were measured when using only the forward BLC slot, as compared to use of both BLC slots.

As shown in figure A-8a, highest Mach numbers and lowest sound pressure levels of the fan blade passage frequency were measured at the highest BLC blowing pressure. For this blowing condition (60 psia at the forward slot), the results show a maximum reduction of 24 dB from the non-BLC case. Fan exhaust noise was also reduced with BLC blowing. Measured inlet wall static pressure distributions are shown for a constant fan speed of approximately 31 000 rpm in figure A-8b.

900-in^2 simulation inlet: An abbreviated series of ejector rig tests with the simulated 900-in^2 inlet model was conducted without the benefit of BLC blowing. Figure A-9a shows that the same type of preferential flow separation and flow distortion was encountered with this simulation model without BLC as with the 750-in^2 simulation model and the eight-sided inlet model.

Tests using the powered model fan facility were terminated when blade fatigue failure of the fan occurred during the first test incorporating BLC following a non-BLC baseline run. Only the lowest (20 psia) forward BLC slot blowing pressure was used. Results obtained up to the time of fan failure are presented in figure A-9b.

1370-in^2 simulation inlet: During these tests, it was found that the aerodynamic throat of the inlet occurred between the two BLC slots. Performance gains were not apparent for either the forward blowing slot or blowing pressures in excess of 40 psia. BLC blowing through the aft slot with 2.2 percent of inlet throat airflow rate increased the inlet pressure recovery 3 percent and eliminated large regions of flow instability. When the losses associated with engine bleed (for BLC) are taken into account, a thrust loss of approximately 5 percent results.

Takeoff and cruise simulation model: Figure A-10a shows the effects of tunnel velocity and inflow angle on inlet total pressure recovery for takeoff airflow conditions; inlet throat area was maximum in these tests.

The total pressure distribution at the diffuser exit for a 0° inflow angle, 150-kn test condition is shown in Figure A-10b. The takeoff lip was installed throughout these tests.

Results of tunnel tests with the cruise lip (takeoff lip removed) indicate that the takeoff lip may be completely stowed at a flight speed of approximately 200 kn. Performance for this configuration is shown in figure A-11a.

Internal cruise performance was evaluated by simulating flow conditions statically with the aid of an elliptic bellmouth. Inlet total pressure recovery at the simulated cruise conditions

was 0.995, as indicated on the total pressure contour plot of figure A-11b. The effect of the dividers on inlet recovery was small.

Nonadjustable inlet: Test results without BLC are shown in figure A-12a. A preferential flow distortion pattern is evident for tests both with and without BLC, as shown in figures A-12a and A-12b. Internal aerodynamic performance of the inlet for various BLC blowing pressures is shown in figure A-12d. As shown by the slope of the curve in figure A-12e, the momentum introduced by BLC blowing was not fully used.

Use of BLC eliminated the flow separation at Mach numbers less than 0.52, but separation could not be completely eliminated at the higher Mach numbers with the BLC available in the model. The test results obtained with this inlet on the ejector rig indicated that an acoustic evaluation on the powered model fan was not warranted.

Non-BLC inlet: Test results obtained with the non-BLC inlet of circular cross section are presented in figures A-12c and A-12d. These results indicate that the flow through the inlet diffuser consisted of a high-velocity core surrounded by a low-velocity or fully separated flow region. As indicated by the results in figure A-12d, the total pressure recovery and distortion characteristics of the non-BLC inlet were similar to those of the nonadjustable inlet without BLC.

Five-door inlet.—Results obtained during tests on the powered model fan simulating landing approach are shown in figure A-13. These results indicate that inlet lip geometry may significantly influence the noise reduction attainable with sonic throat inlets.

Five-door inlet, centerbody extended.—Results obtained with various inlet throat areas are shown in figure A-14; for these tests, inlet throat area was varied by varying the length of the centerbody. These results indicate that a centerbody may significantly influence the total pressure recovery and diffuser flow separation characteristics of a sonic throat inlet.

Expandable centerbody inlet.—Results of tests of a model incorporating a large centerbody are shown in figure A-15. Maximum suction capability was insufficient to maintain attached flow. Blowing from the centerbody slot improved performance over that attainable with suction, but the flow would not remain attached to both the cowl wall and centerbody as sonic throat velocity was approached. Sufficient BLC to control flow along one wall produced turning of the main flow, thus inducing separation on the opposite wall.

Radial vane inlet.—Initial tests indicated that flow separation was occurring on the vanes. Following an investigation of several types of trip strips as a means of ensuring turbulent flow over the vanes, No. 80 mesh grit was applied to the vanes in the manner shown in figure A-16. Aerodynamic performance for each of the vane positions is shown in figure A-17a. For each vane angle tested, the lowest recovery was measured near the hub.

Results obtained with various centerbody positions are shown in figure A-17b. Small gains in recovery and distortion were apparent as the centerbody was moved aft.

Results with various vane angles and centerbody positions on noise and vibration levels of the powered model fan are shown in figure A-18.

Baseline inlet.—Tests representing severe inlet flow conditions were performed with the 1/9-scale model of the baseline inlet. Static performance of the baseline inlet model was slightly lower than that of the eight-segment inlet; however, the baseline inlet was much less sensitive to the effects of inflow angle.

Comparison of model and full-scale inlets.—A comparison of the acoustic attenuation characteristics of the model and full-scale eight-segment inlets is given in figure A-19. The aerodynamic flow characteristics of these inlets, as indicated by total pressure recovery and total pressure distortion at the exit of the diffuser, are compared in figures A-20a and A-20b.

Figure A-20c shows a comparison of static pressures on the internal surfaces of the inlets. Despite large differences in Reynolds numbers and blade passage frequencies between the model and full-scale inlets, close agreement was found with respect to both aerodynamic and acoustic characteristics. Full-scale tests are required, however, to evaluate operational characteristics such as surge and blade stresses.

TABLE I.—FULL-SCALE SONIC THROAT INLET TEST CONFIGURATIONS

Inlet configuration	Throat area, in^2	Flight condition simulated	Figure no. of sketch	Figure no. of photograph	Figure no. of data	Remarks
Mechanized and Controllable	764 to 1650	All	6a, 8a, 9, 11a	3, 6b, 7, 11b	14 to 28	Installation included boilerplate long ducts on JT3D-3B engine
Automatic control	764 to 1650	Suppressed landing approach	6a, 8a, 9, 11a	---	14 to 20, 26	2.5-in.-radius takeoff lip used
Manual control	1650	Unsuppressed static takeoff	8a, 11a	3 (shown without 2.5-in.-radius lip)	27	2.5-in.-radius takeoff lip used
Manual control	1650	Unsuppressed cruise	7, 8a, 11a	7	28	Cruise bellmouth lip used
Manual control	780 to 1050	Suppressed landing approach, constant rpm	6a, 8a, 11a	---	21	Variable $M_{\mathbb{C}}$ at 5000 $N_1A\sqrt{\theta}_{amb}$
Manual control	1330 to 1650	Suppressed static takeoff, constant rpm	6a, 8a, 11a	---	22	Variable $M_{\mathbb{C}}$ at 6700 $N_1/\sqrt{\theta}_{amb}$
Manual control	764	Suppressed landing approach with go-around	6a, 8a, 11a	---	23, 24	Failure simulation of all segments at minimum throat area
Automatic control	875 to 1650	Suppressed landing approach with go-around	6a, 8a, 9, 11a	---	25a	Failure simulation of one segment at maximum throat area position
Automatic control	764 to 1539	Suppressed landing approach with go-around	6a, 8a, 9, 11a	---	25b	Failure simulation of one segment at minimum throat area position
Adjustable	750, 900, 1570	Landing, takeoff	8b	4	29 to 39	Installation included 3/4-long fan ducts and directionalizer on JT3D-3B engine
	750	Suppressed landing approach	8b	4a	29 to 35, 38	2.5-in.-radius takeoff lip used
	900	Suppressed landing approach	8b	---	29 to 35, 38	2.5-in.-radius takeoff lip used
	1570	Unsuppressed static takeoff	8b	4b	36, 37, 39	2.5-in.-radius takeoff lip used
Nonadjustable	750	Suppressed landing approach	8c	5	40 to 44	BLC supply independent of engine; BLC slot configurations varied, JT3D-1 engine with production ducts
Five-Door	928, 986	Suppressed landing approach	8d	---	45 to 49	Installation included 3/4-long fan ducts and directionalizers on JT3D-1 and JT3D-3B engines
Blowing BLC	928	Suppressed landing approach	8d	---	45 to 49	Test terminated prematurely by BLC system failure and resultant inlet damage
Suction BLC	928	Suppressed landing approach	---	---	---	Limited suction capability; results were not conclusive
Initial (no BLC)	928	Suppressed landing approach	---	---	---	Various lip and vortex generator configurations evaluated; results indicated need for BLC

TABLE II–MAXIMUM INLET CENTERLINE MACH NUMBERS

Test configuration		Maximum Mach no. on centerline	Remarks
Without BLC	SBV closed	0.48	Near surge; fan temperature differential excessive
	SBV open	0.63	Near surge; fan temperature differential excessive
	SBV open; SBV area increased	0.72	Fan temperature differential excessive
Two-slot BLC; SBV[a] open	0.114-in. fwd slot 0.090-in. aft slot	0.89	Random surging
	0.171-in. fwd slot 0.136-in. aft slot	0.94	Fan temperature differential excessive
	0.250-in. fwd slot 0.200-in. aft slot	0.86	At fan temperature differential limit
Forward slot BLC (aft slot passive); SBV open	0.114-in. fwd slot 0.090-in. aft slot	0.84	Near surge; exceeds fan temperature differential limit
	0.171-in. fwd slot 0.136-in. aft slot	0.84	Near surge
	0.250-in. fwd slot 0.200-in. aft slot	0.90	Exceeds fan temperature differential limit
One- and two-slot BLC; SBV open; SBV area increased	0.171-in. fwd slot 0.136-in. aft slot	0.97	Fan temperature differential excessive
	0.171-in. fwd slot 0.136-in. aft slot passive	1.00	Near surge; fan temperature differential excessive

[a]Surge bleed valve

TABLE III.—1/9-SCALE MODEL INLET TEST CONFIGURATIONS

Inlet configuration	Equivalent full-scale throat area, in^2	Flight condition simulated	Test facility	Figure no. of sketch	Figure no. of photograph	Figure no. of data	Remarks
Eight-segment adjustable	750	Landing approach	Ejector and powered fan	A-1a	A-1b	A-7, A-8, A-19, A-20	Takeoff lip used; models evaluated with and without BLC; BLC slot width = 0.010 in.
	900	Landing approach	Ejector and powered fan	A-1a	A-1c	A-9	
	1370	Takeoff	Low-speed wind tunnel	A-1a	A-1d	---	
	1570	Takeoff	Low-speed wind tunnel	A-1a	---	A-10	Takeoff lip used; no BLC
	1570	Cruise	Low-speed wind tunnel	A-1a	A-1e	A-11	Cruise bellmouth lip used; no BLC; small-radius cruise lip also used
Eight-sided nonadjustable	750	Landing approach	Ejector	A-2	---	A-12	Takeoff lip used; model evaluated with and without BLC
Non-BLC (circular reference)	750	Landing approach	Ejector	A-3	---	A-12	Takeoff lip simulated; no BLC used
Five-door	925	Landing approach	Powered fan	A-4a	---	A-13, A-14	Rounded, slotted, and sharp edge lips evaluated; vortex generators on lips and in diffuser evaluated; all models non-BLC
	1570	Takeoff	Low-speed wind tunnel	A-4a	A-4b	---	
	1570	Cruise	Low-speed wind tunnel	A-4a	---	---	
Five-door with extended centerbody	630	Landing approach	Ejector	A-4a	---	A-14	All models with rounded lip; no BLC used
	700	Landing approach	Ejector	A-4a	A-4c	A-14	
	770	Landing approach	Ejector	A-4a	---	A-14	
	830	Landing approach	Ejector	A-4a	---	A-14	
Expandable centerbody	750	Landing approach	Ejector	A-5	---	A-15	Bellmouth lip used; suction BLC used on outer wall and blowing BLC used on centerbody
Radial vane $\Theta = 0°$	750	Landing approach	Ejector and powered fan	A-6	A-16 (vanes only)	A-17, A-18	Bellmouth lip used; no. 80 grit applied to forward 15 percent of chord of vanes; 24 vanes used; all models non-BLC; two diffuser extensions and various centerbody configurations also evaluated
$\Theta = 20.5°$	800	Landing approach	Ejector and powered fan	A-6	---	A-17, A-18	
$\Theta = 30.8°$	935	Landing approach	Ejector and powered fan	A-6	---	A-17, A-18	
Baseline (707)	1570	Takeoff	Low-speed wind tunnel	---	A-4b	---	Blow-in doors open; no BLC used

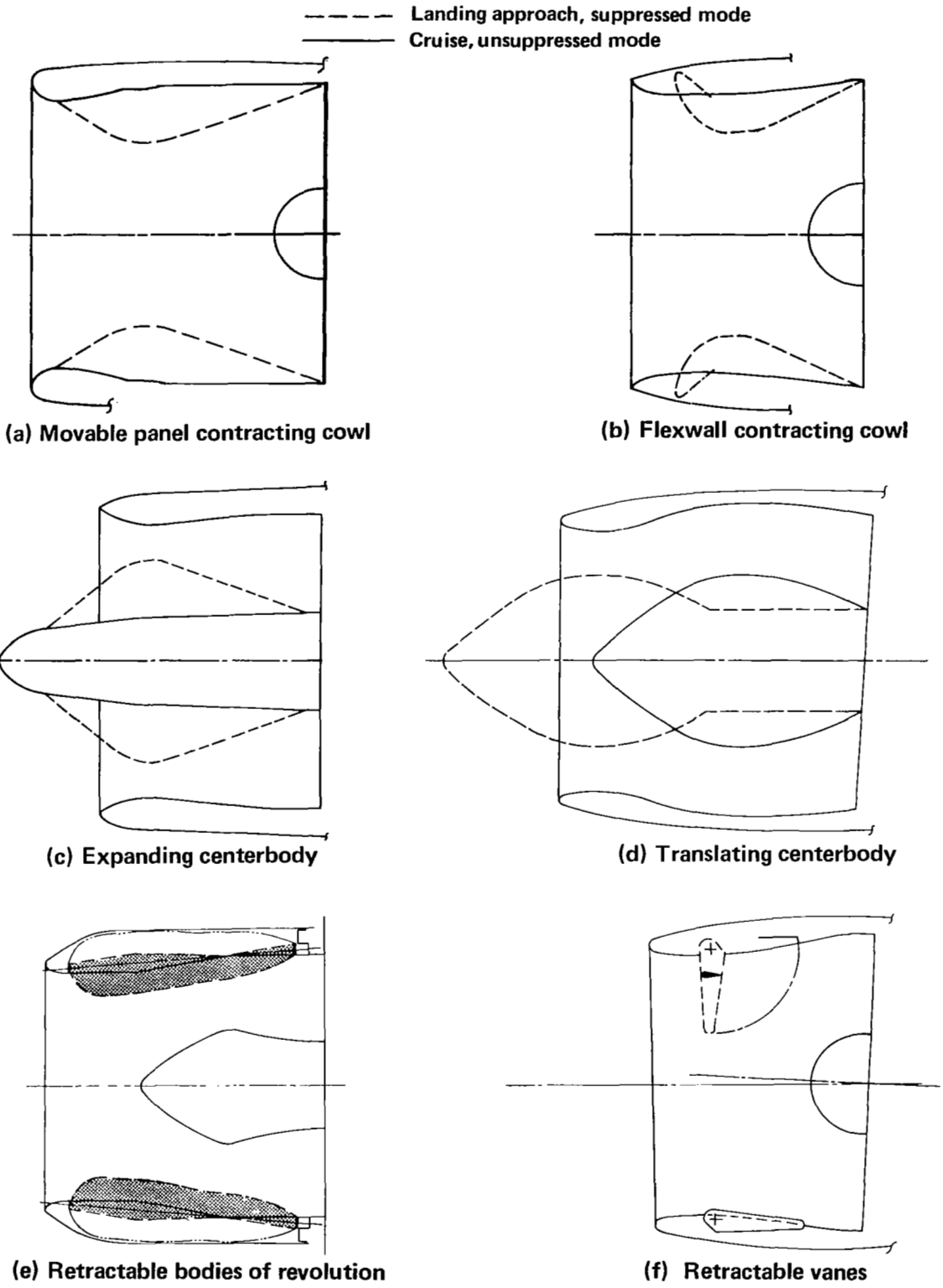

FIGURE 1.—SONIC THROAT INLET CONCEPTS

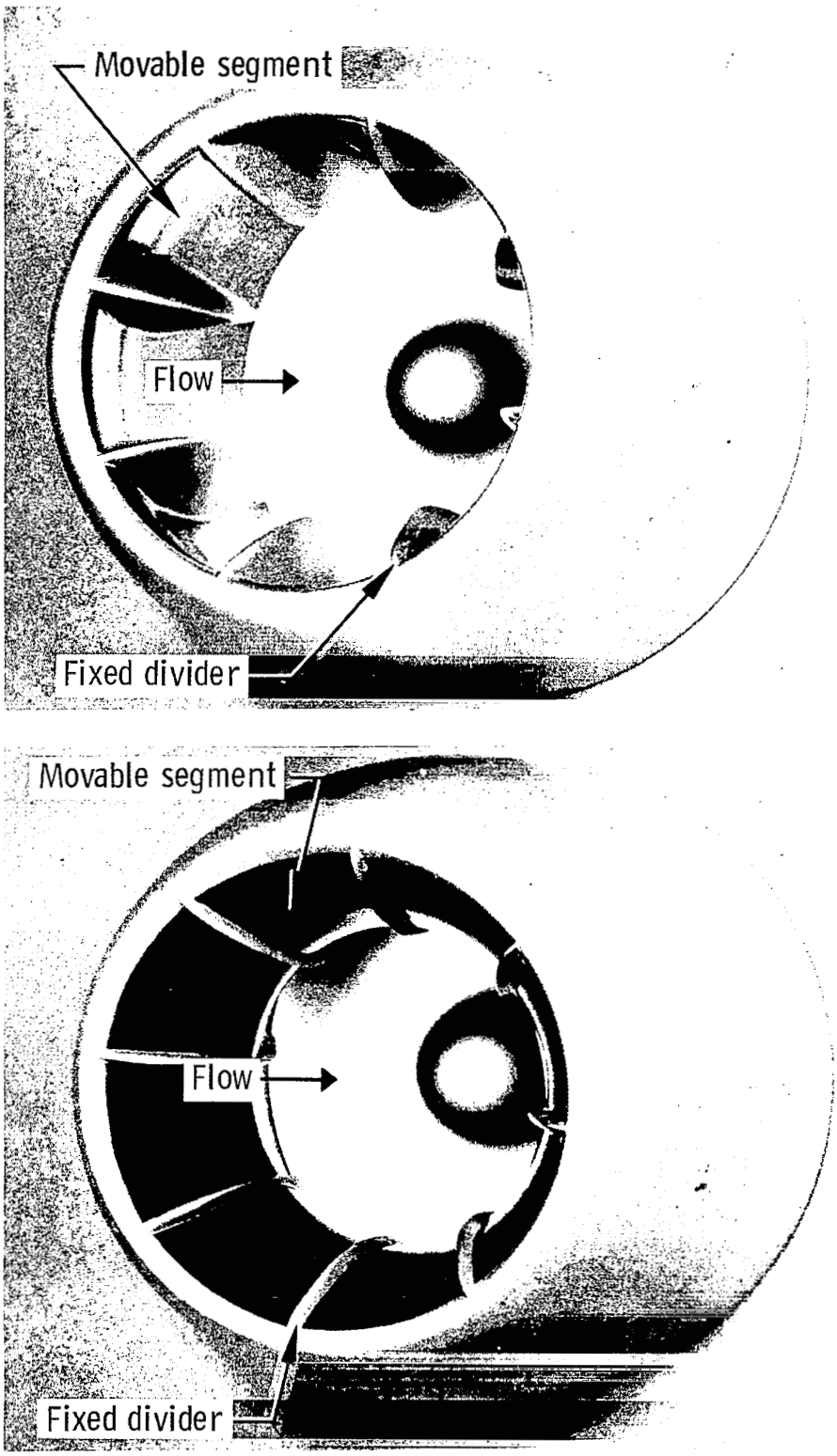

(a) Cruise

(b) Landing approach

FIGURE 2.—MODELS OF EIGHT-SEGMENT CONCEPT

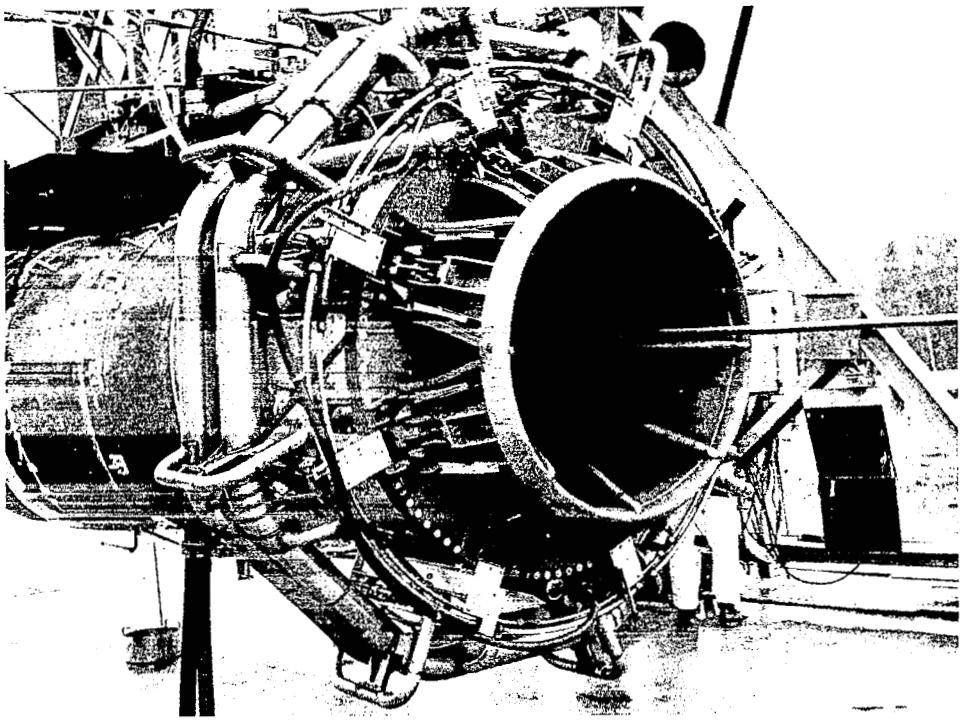

(a) Front view, unsuppressed mode

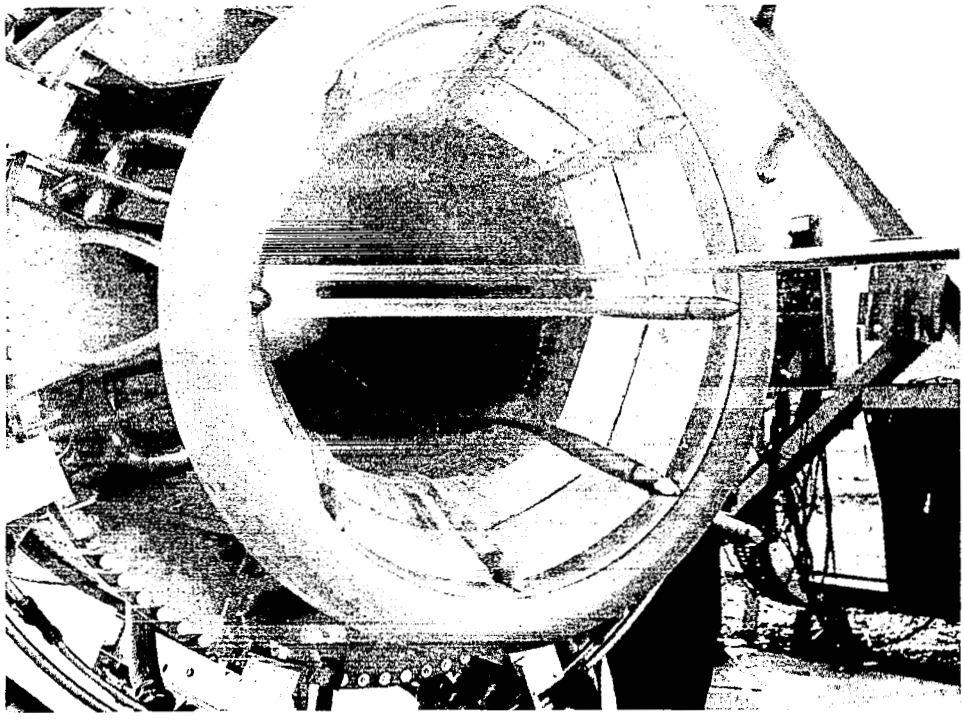

(b) Front view, suppressed mode

FIGURE 3.–MECHANIZED INLET INSTALLATION

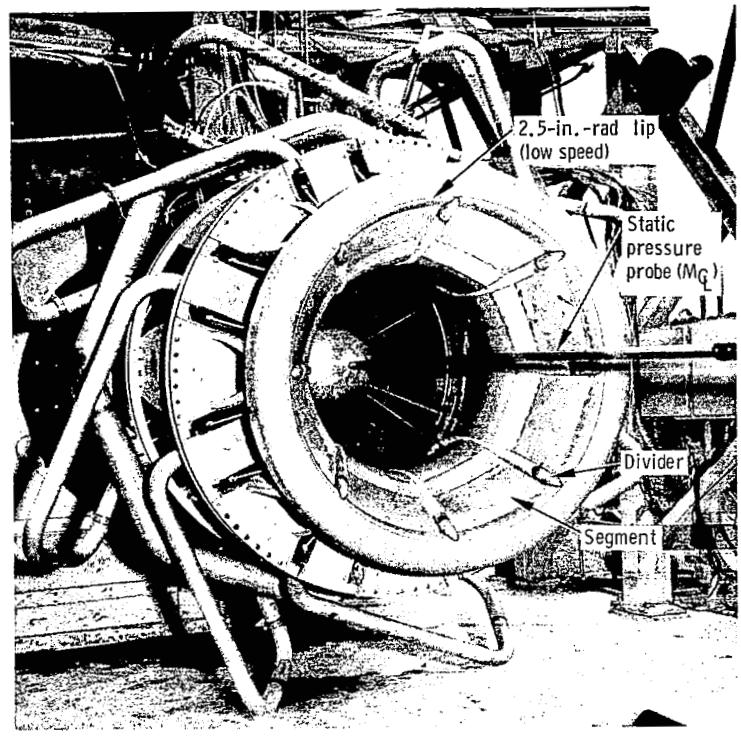

(a) Landing approach

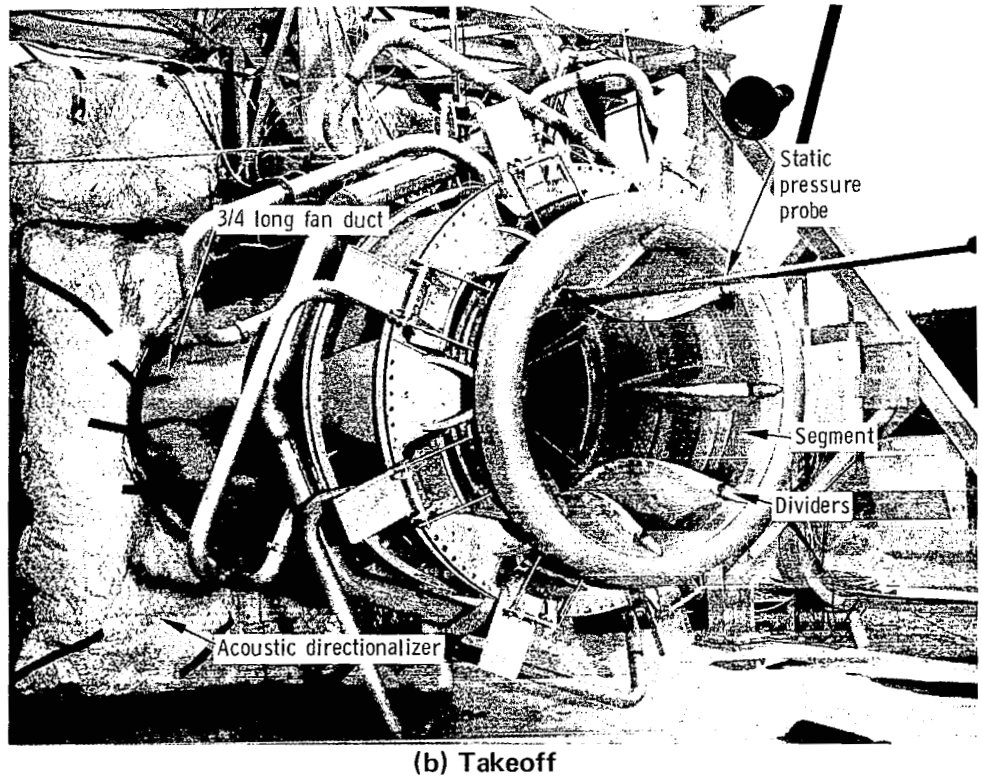

(b) Takeoff

FIGURE 4.—ADJUSTABLE INLET INSTALLATION

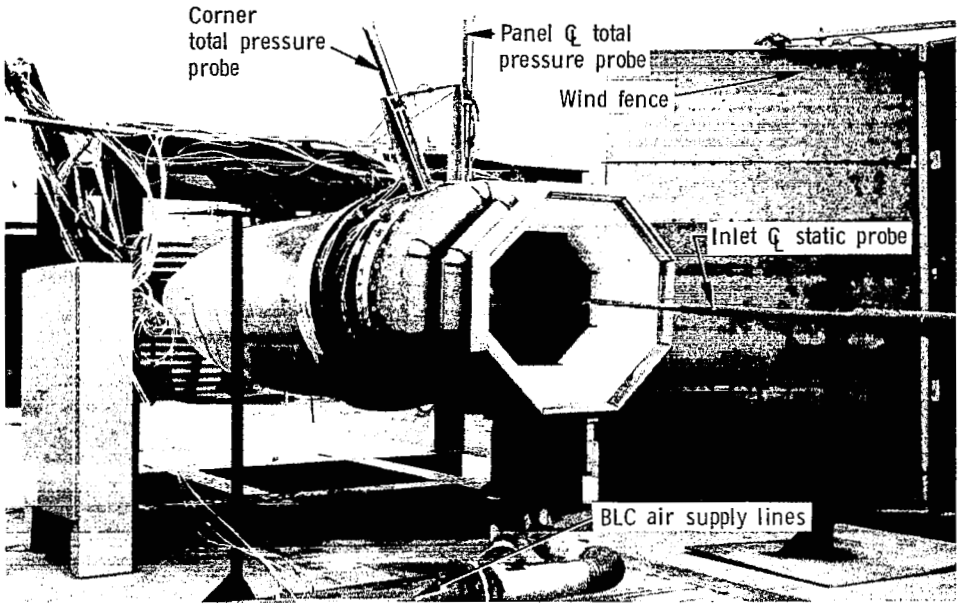

(a) Inlet installed on engine

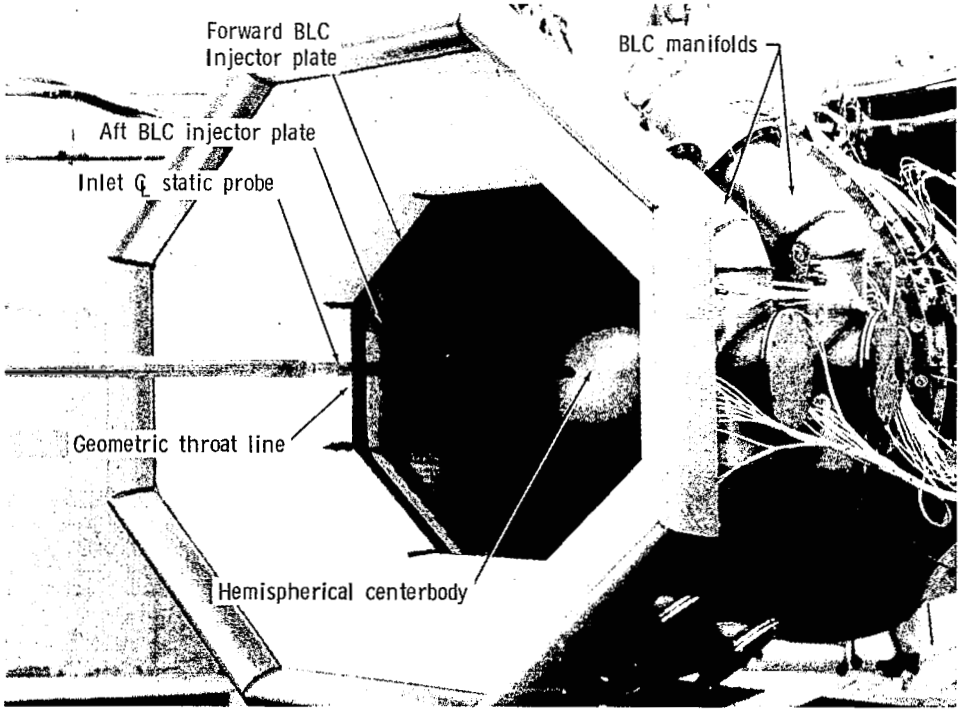

(b) Closeup view of inlet

FIGURE 5.—NONADJUSTABLE INLET INSTALLATION

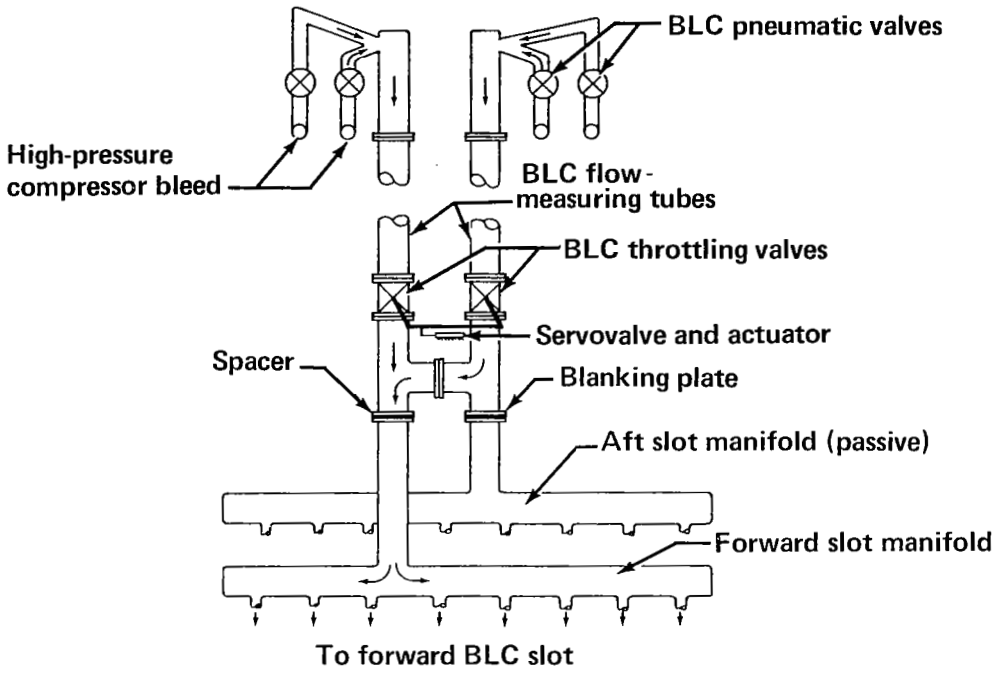

(a) BLC system schematic

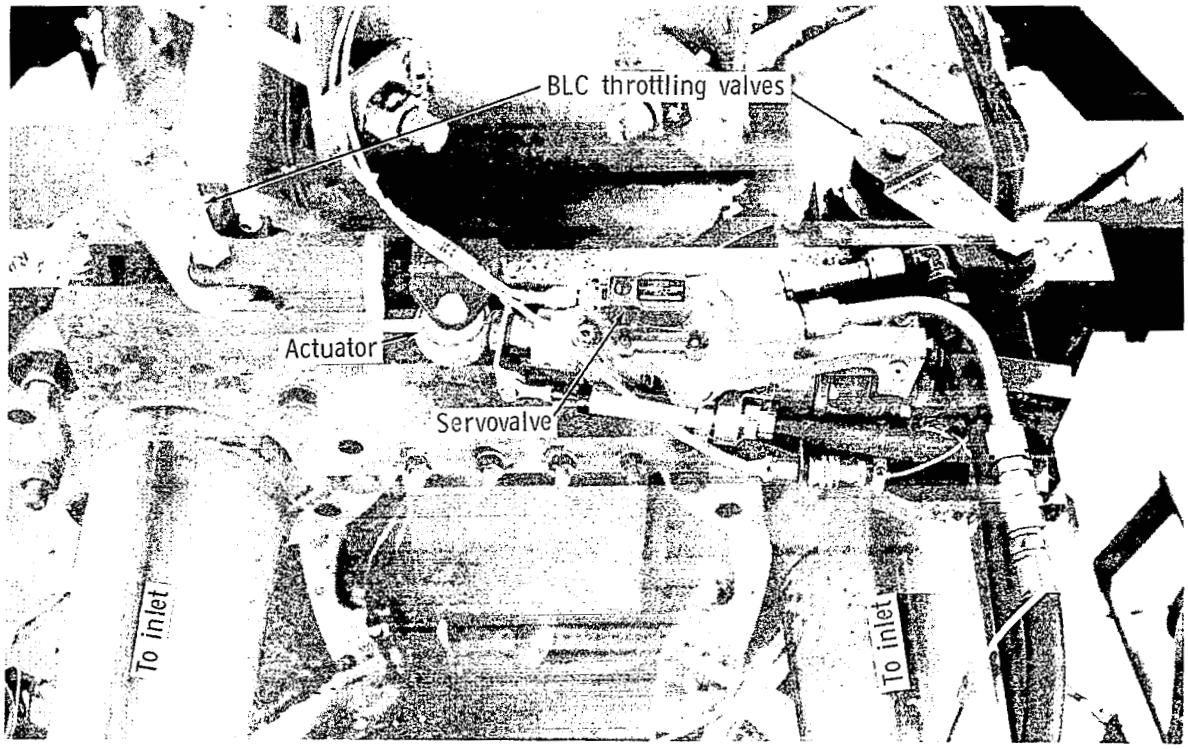

(b) BLC servovalves and control valves

FIGURE 6.—BLC SYSTEM FOR MECHANIZED INLET

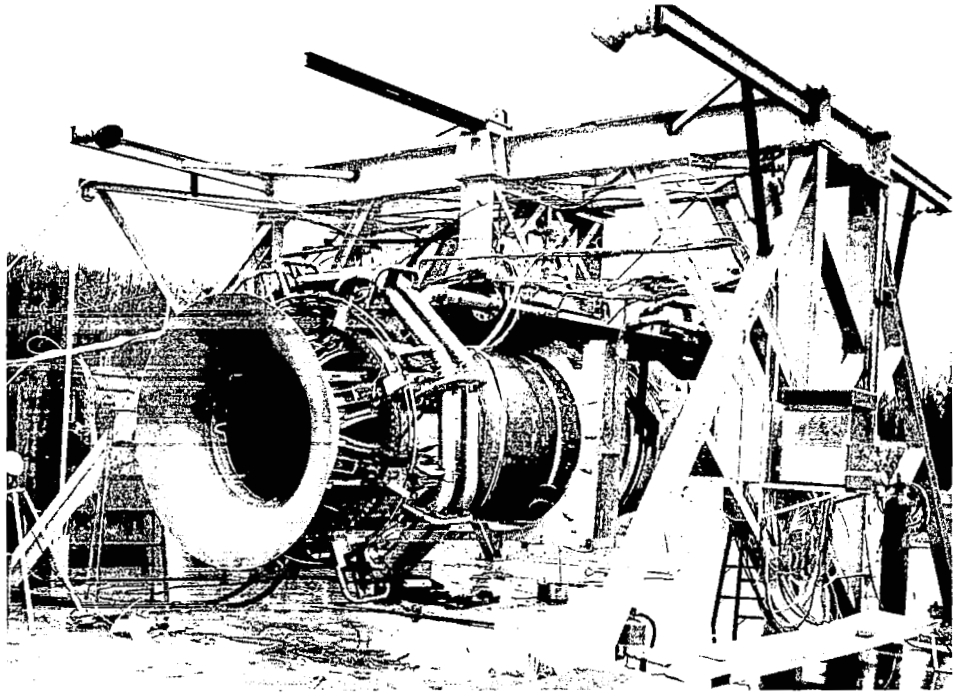

(a) Cruise simulation bellmouth lip

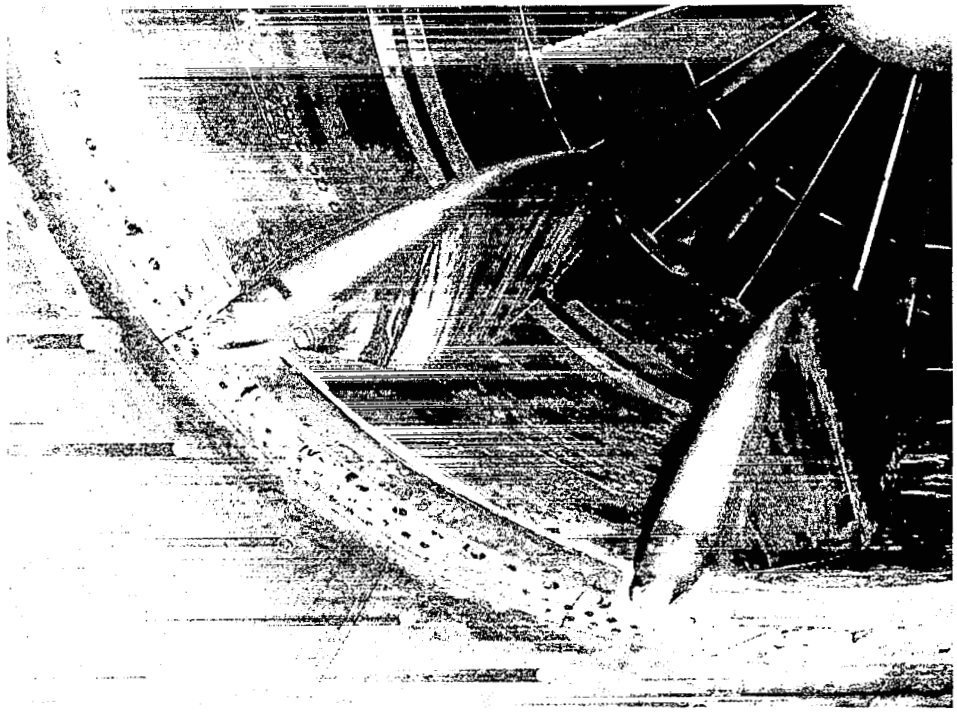

(b) Closeup view of cruise simulation bellmouth lip

FIGURE 7.–DETAILS OF CRUISE SIMULATION BELLMOUTH LIP INSTALLATION

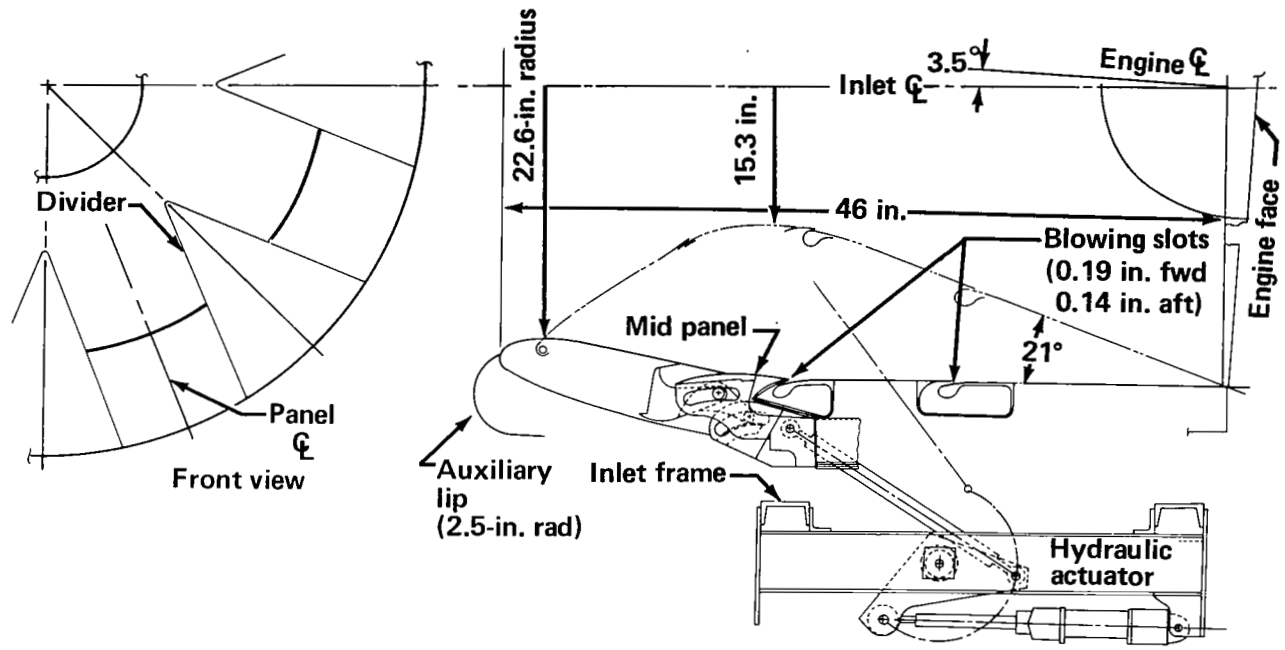

(a) Mechanized inlet

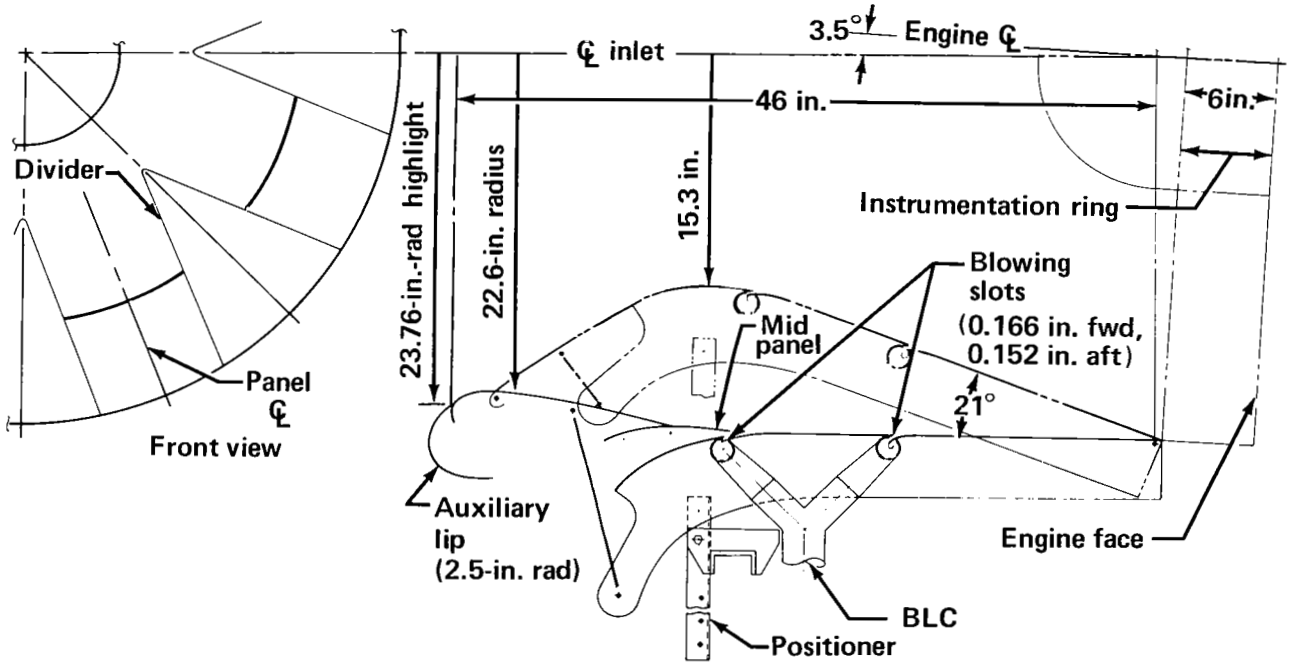

(b) Adjustable inlet

FIGURE 8.–CROSS-SECTION SKETCHES OF FULL-SCALE INLETS

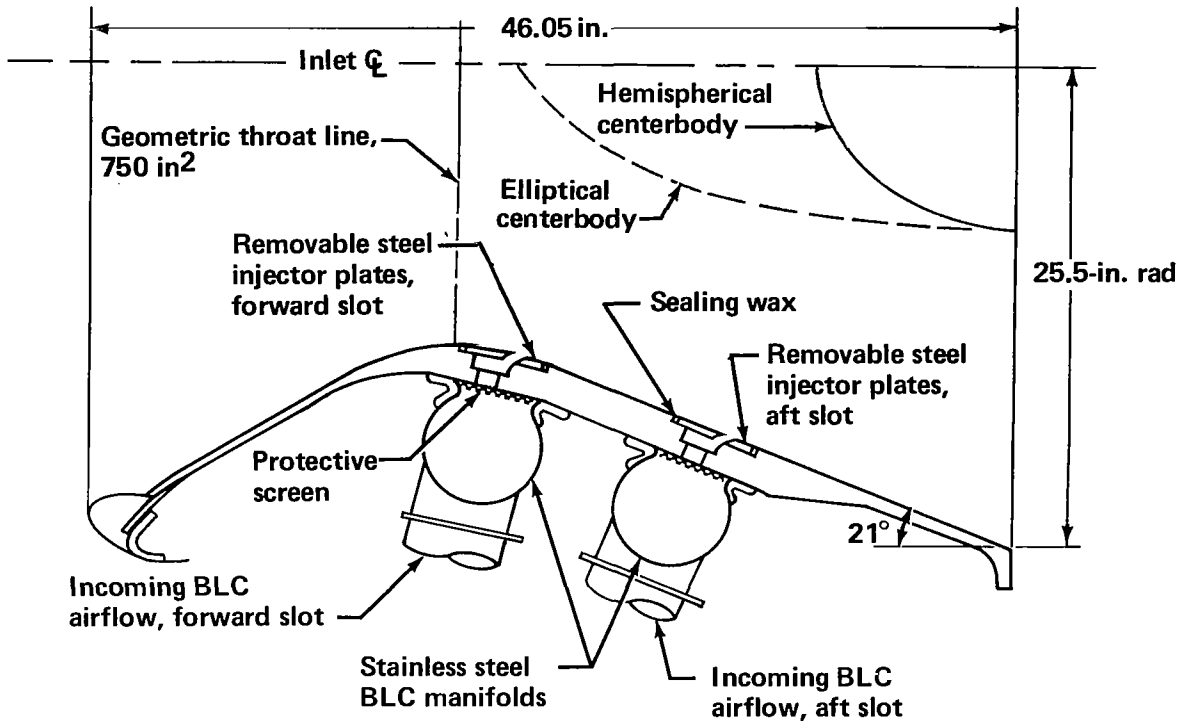

(c) Nonadjustable inlet

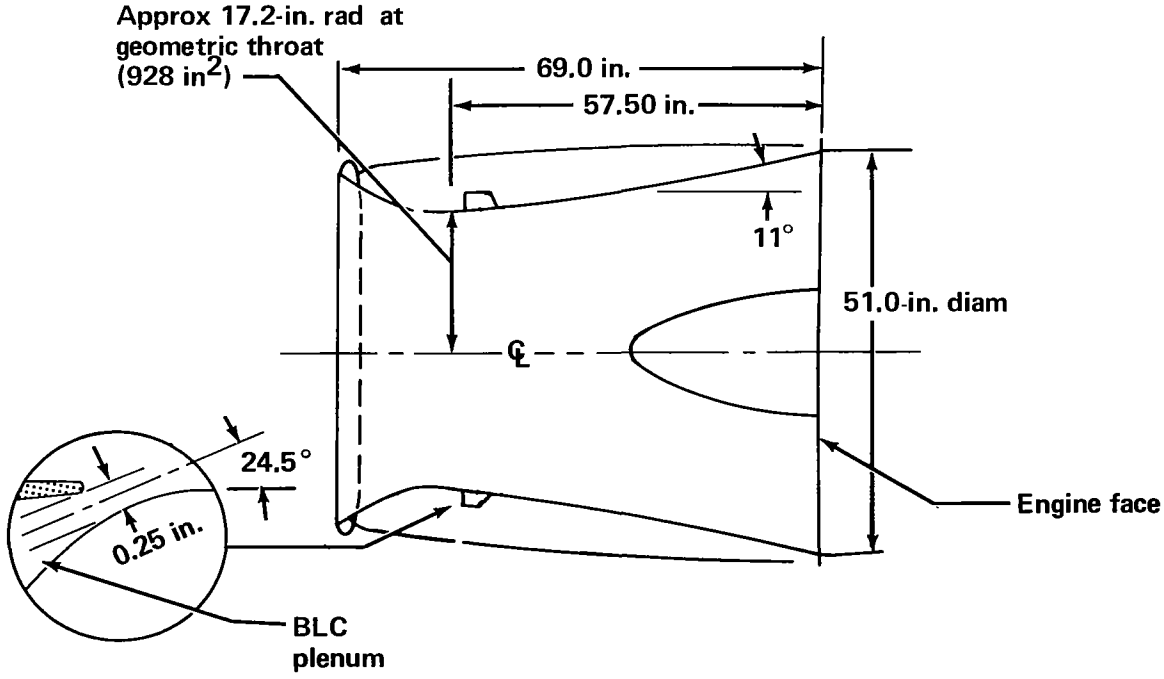

(d) Five-door inlet

FIGURE 8.—CROSS-SECTION SKETCHES OF FULL-SCALE INLETS—Concluded

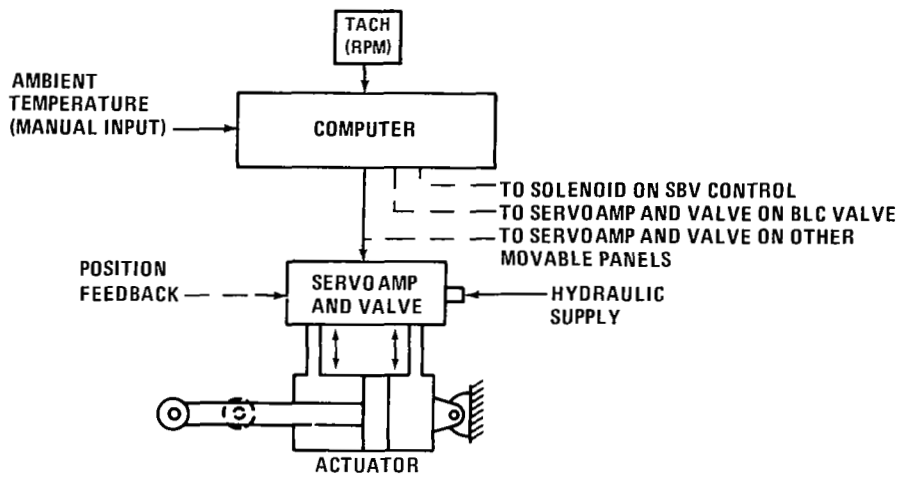

(a) Basic control and actuation system

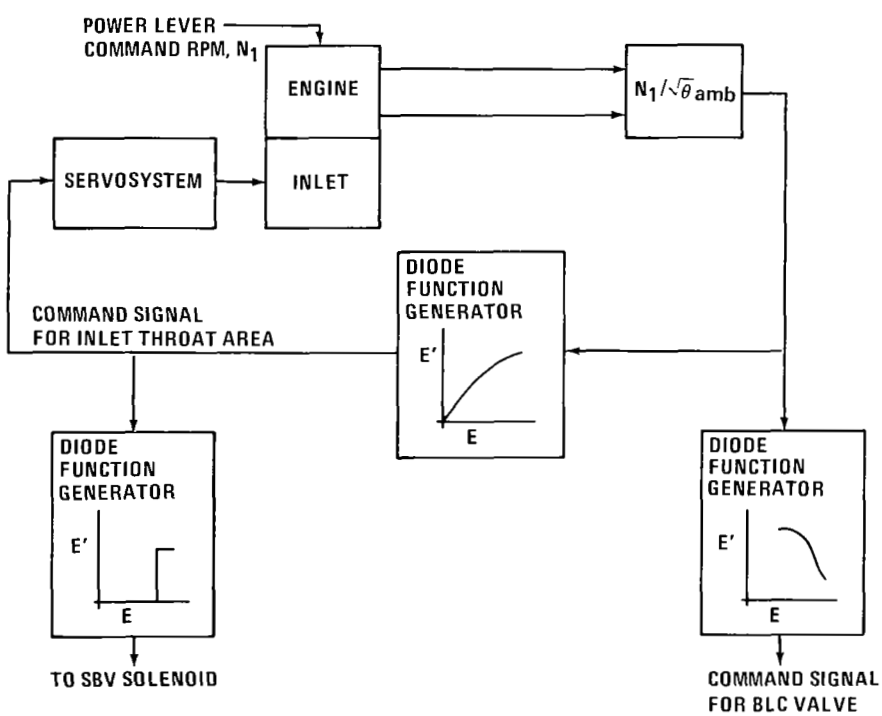

(b) Electrically equivalent basic control system

FIGURE 9.–MECHANIZED INLET CONTROL AND ACTUATION SYSTEM

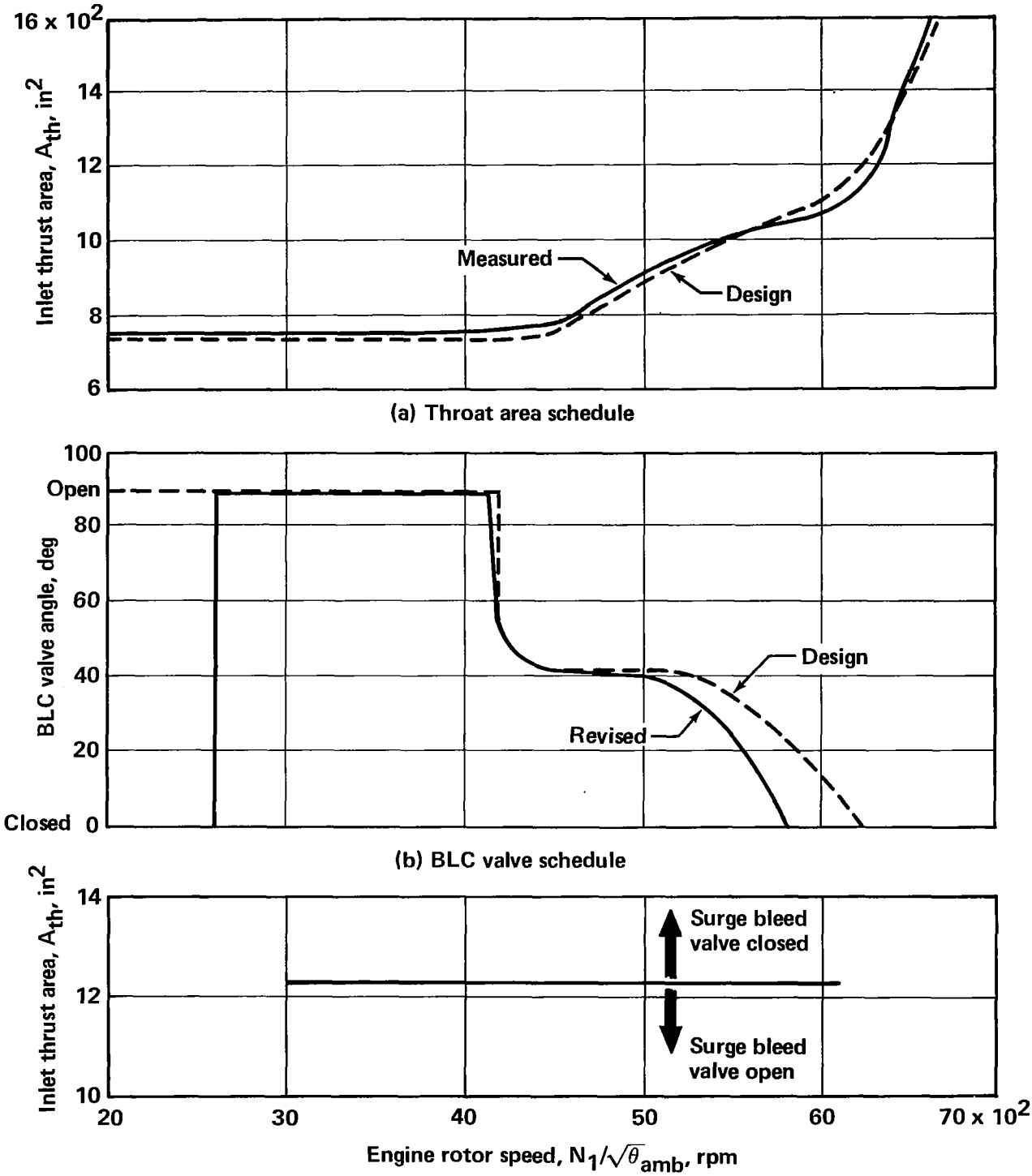

FIGURE 10.–MECHANIZED INLET CONTROL AND ACTUATION SYSTEM SCHEDULES

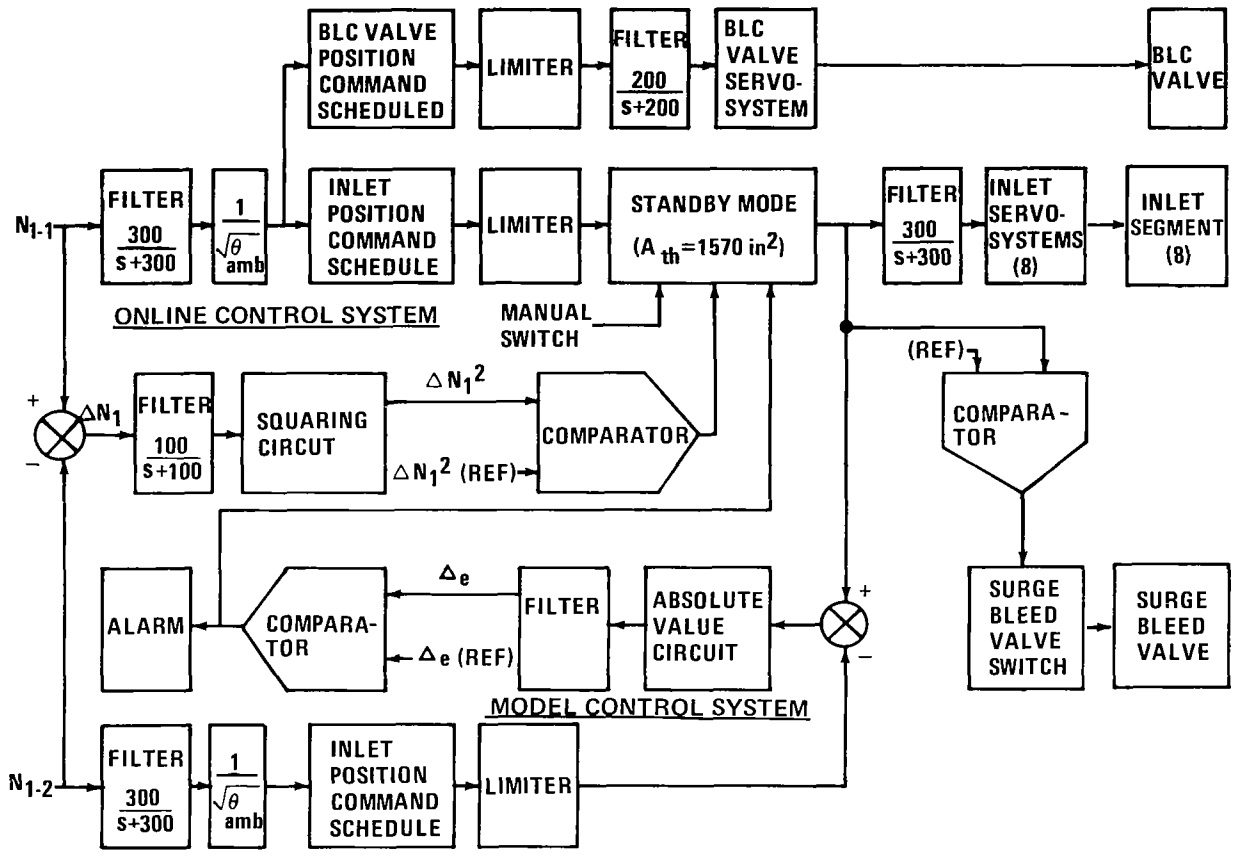

(a) Functional diagram

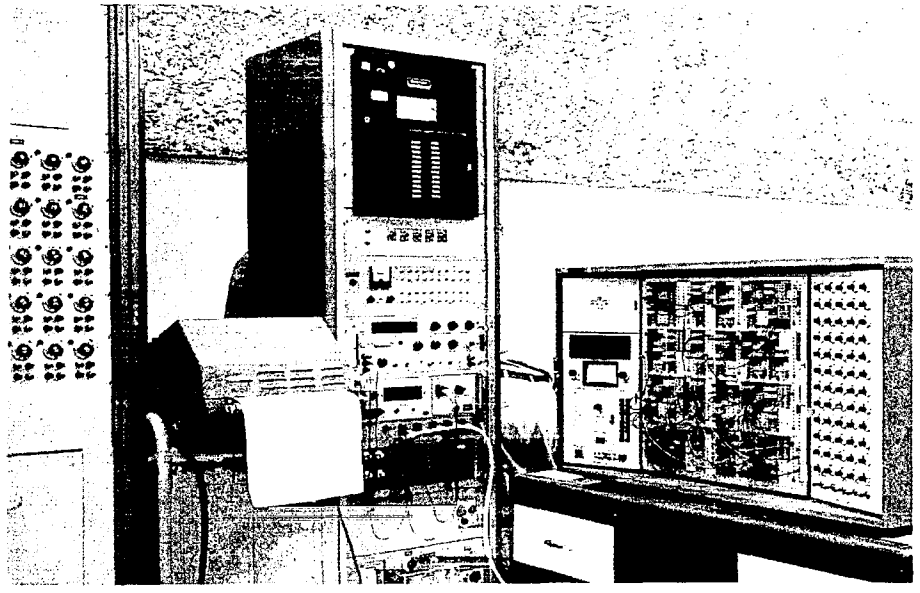

(b) Control and monitoring equipment

FIGURE 11.–FUNCTIONAL CONTROL SYSTEM FOR MECHANIZED INLET

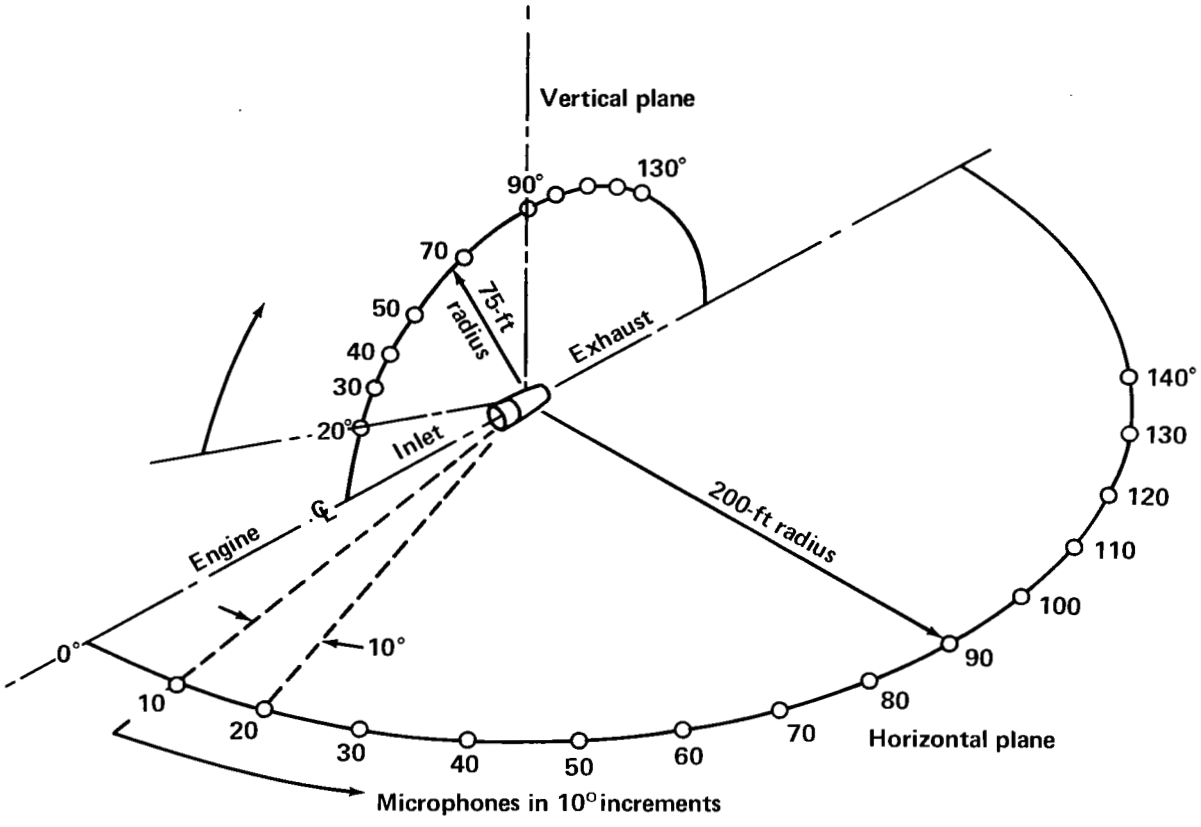

FIGURE 12.—MICROPHONE LOCATIONS

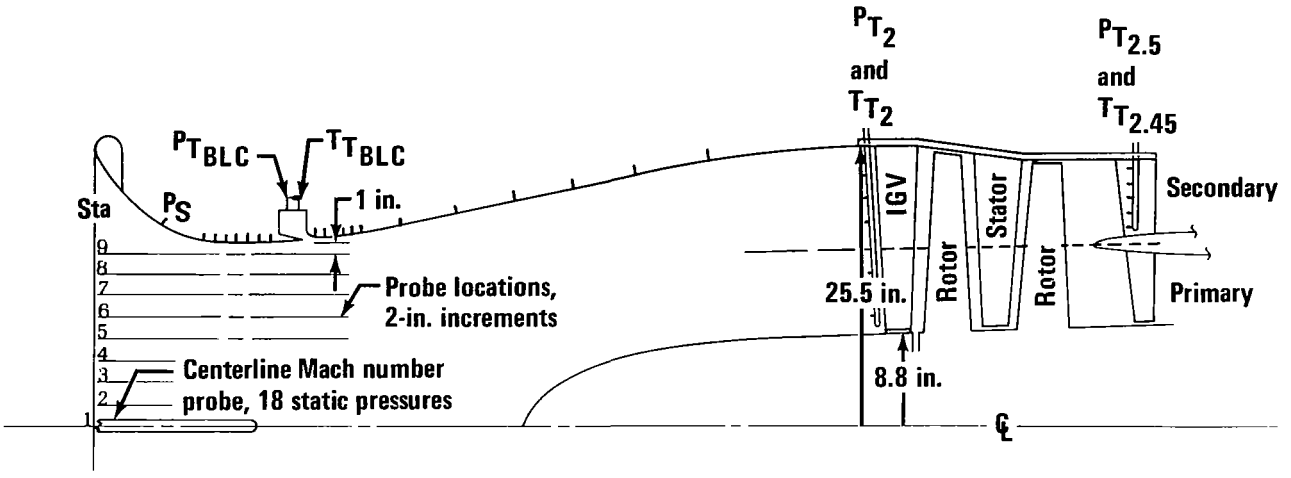

(a) Axial location of inlet and fan instrumentation

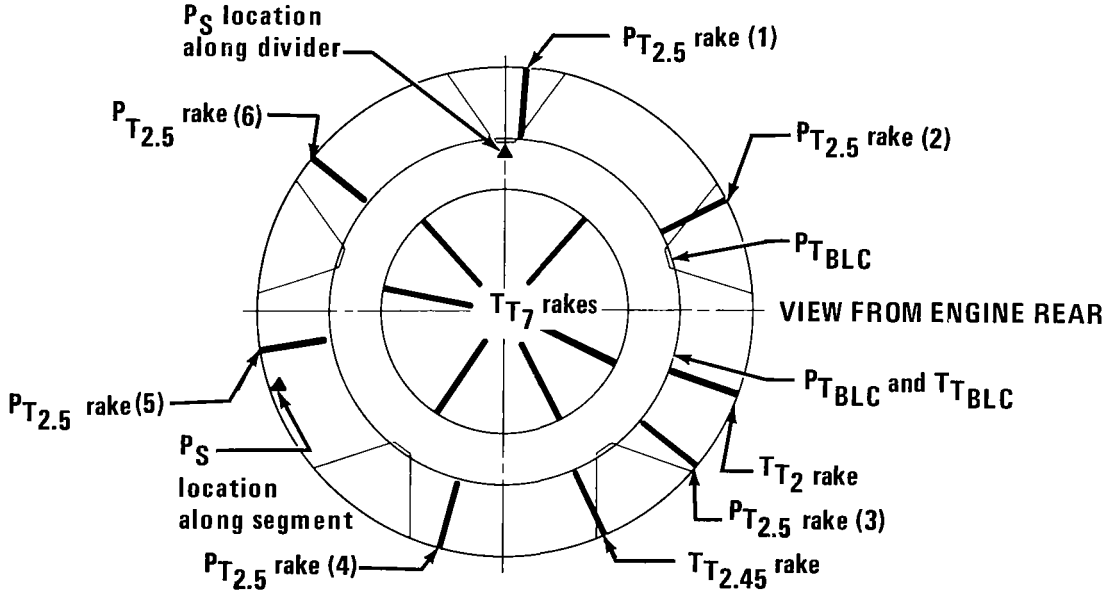

(b) Circumferential location of inlet, fan, and primary nozzle instrumentation

FIGURE 13.–INLET AND ENGINE INSTRUMENTATION

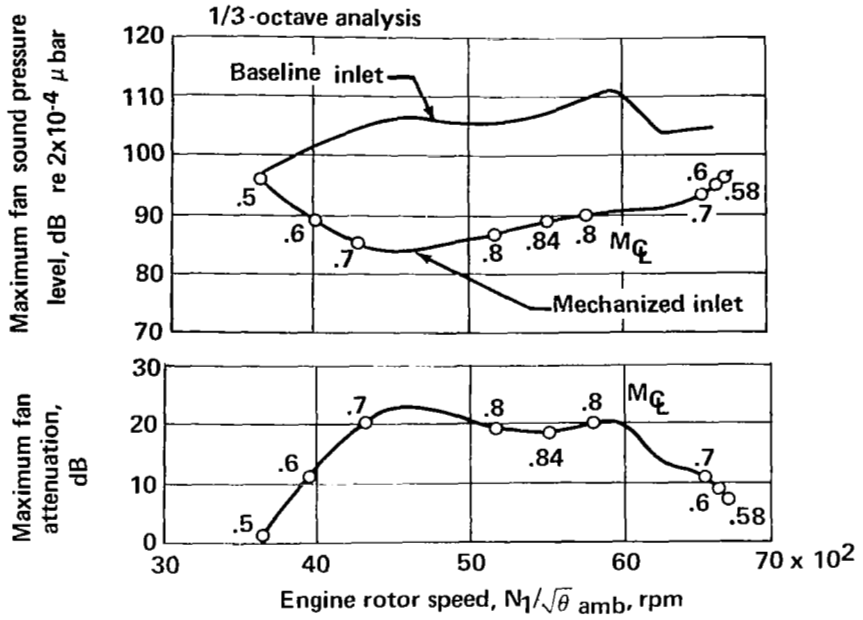

(a) Engine rotor speed

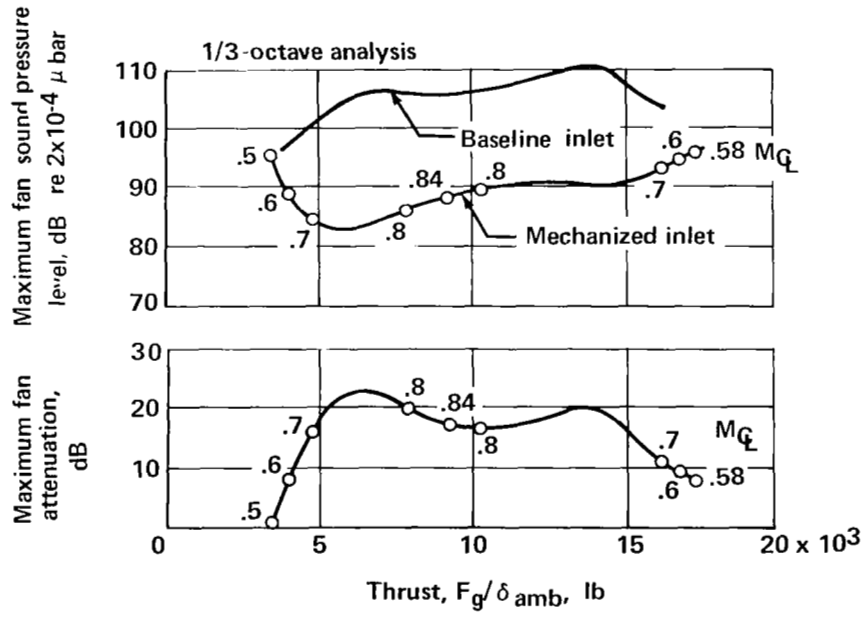

(b) Thrust

FIGURE 14. –SOUND PRESSURE LEVELS AND ATTENUATION FOR THE MECHANIZED INLET AT VARIOUS ENGINE ROTOR SPEEDS AND THRUSTS

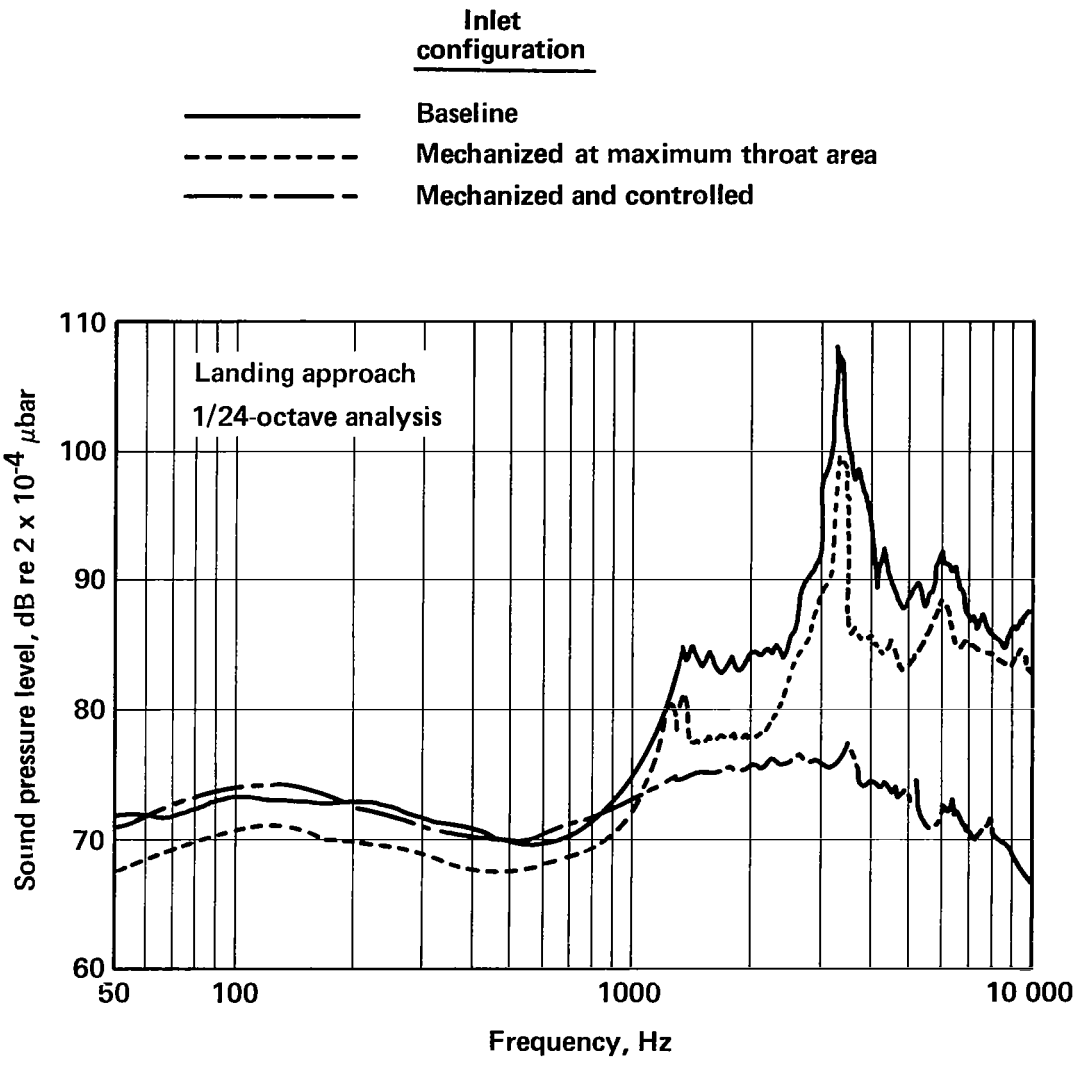

FIGURE 15.—TYPICAL ACOUSTIC SPECTRA FOR THE MECHANIZED INLET

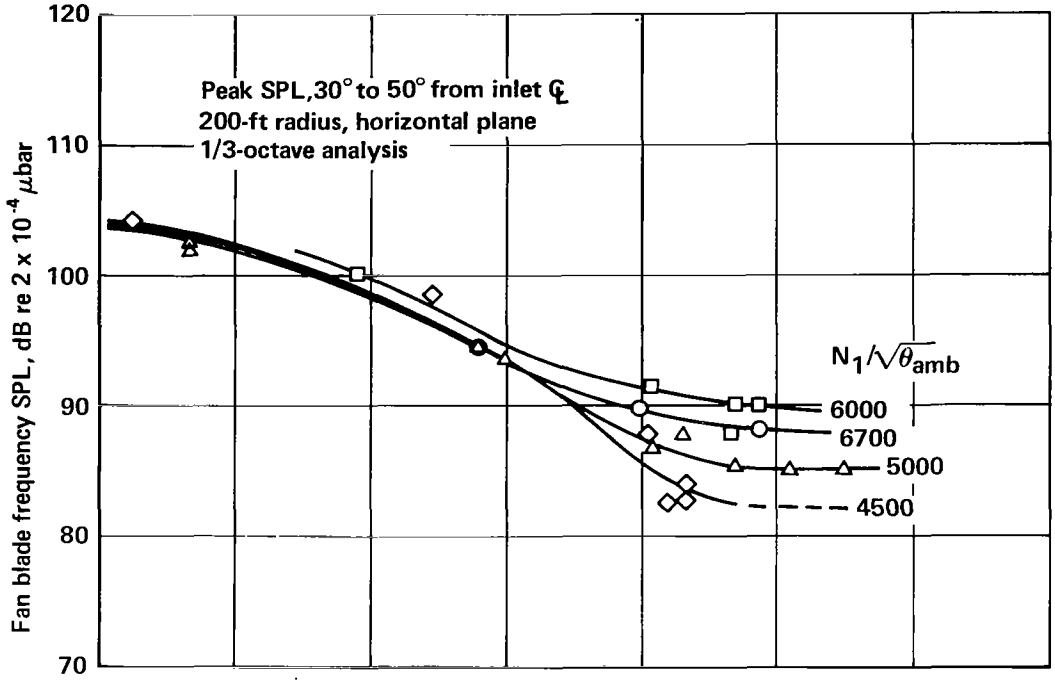

(a) Sound pressure levels

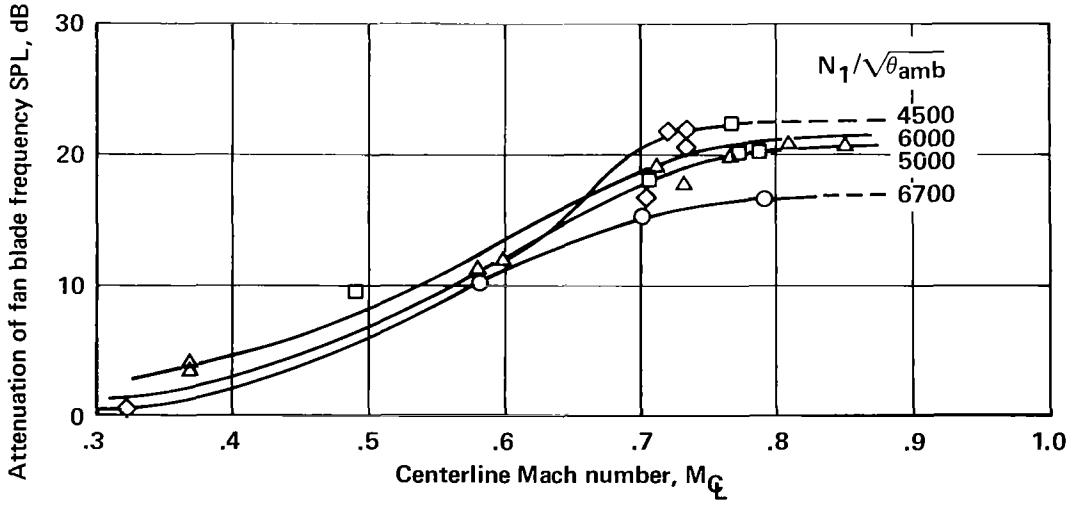

(b) Attenuation

FIGURE 16.—MAXIMUM FAN NOISE LEVELS AND ATTENUATION FOR MECHANIZED INLET

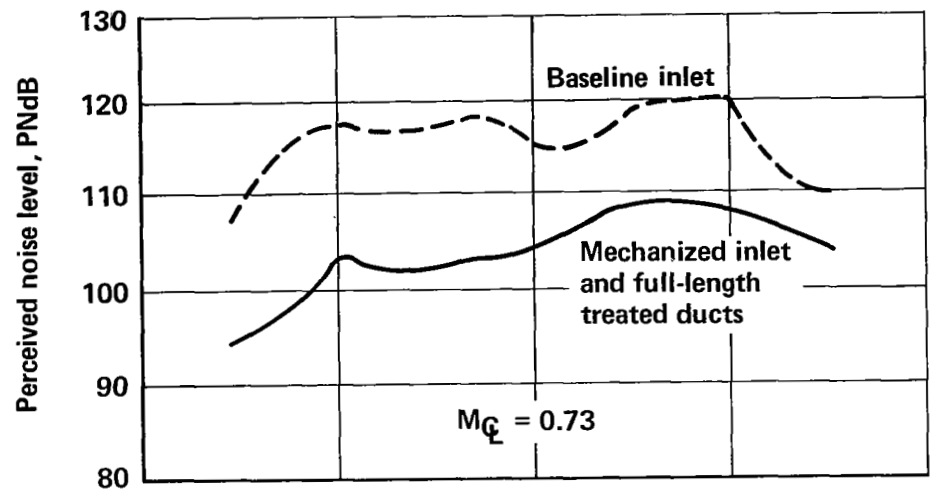

(a) Perceived noise level

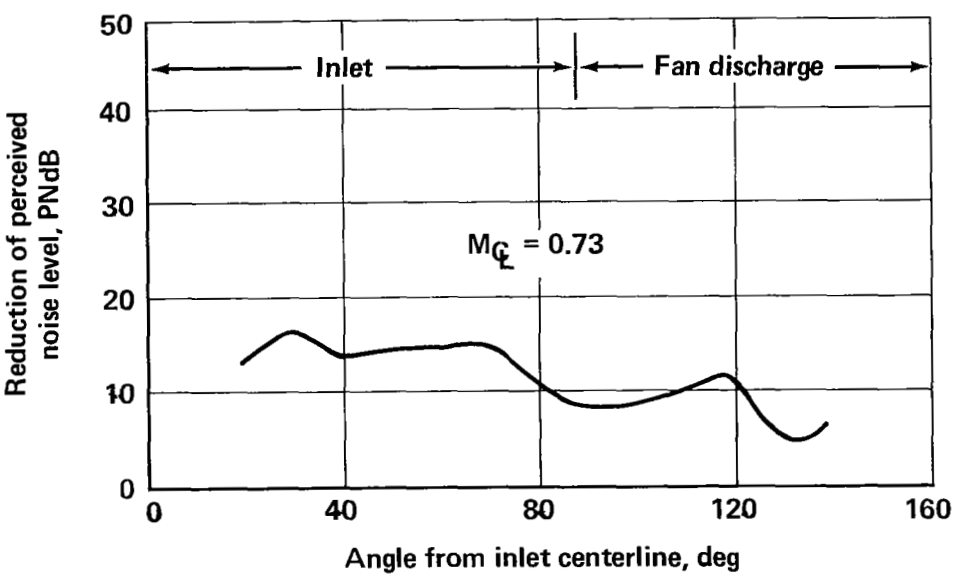

(b) Attenuation

FIGURE 17.–PERCEIVED NOISE LEVELS AND ATTENUATION FOR THE MECHANIZED INLET AT SIMULATED 400-FT AIRPLANE FLYOVER DURING LANDING APPROACH

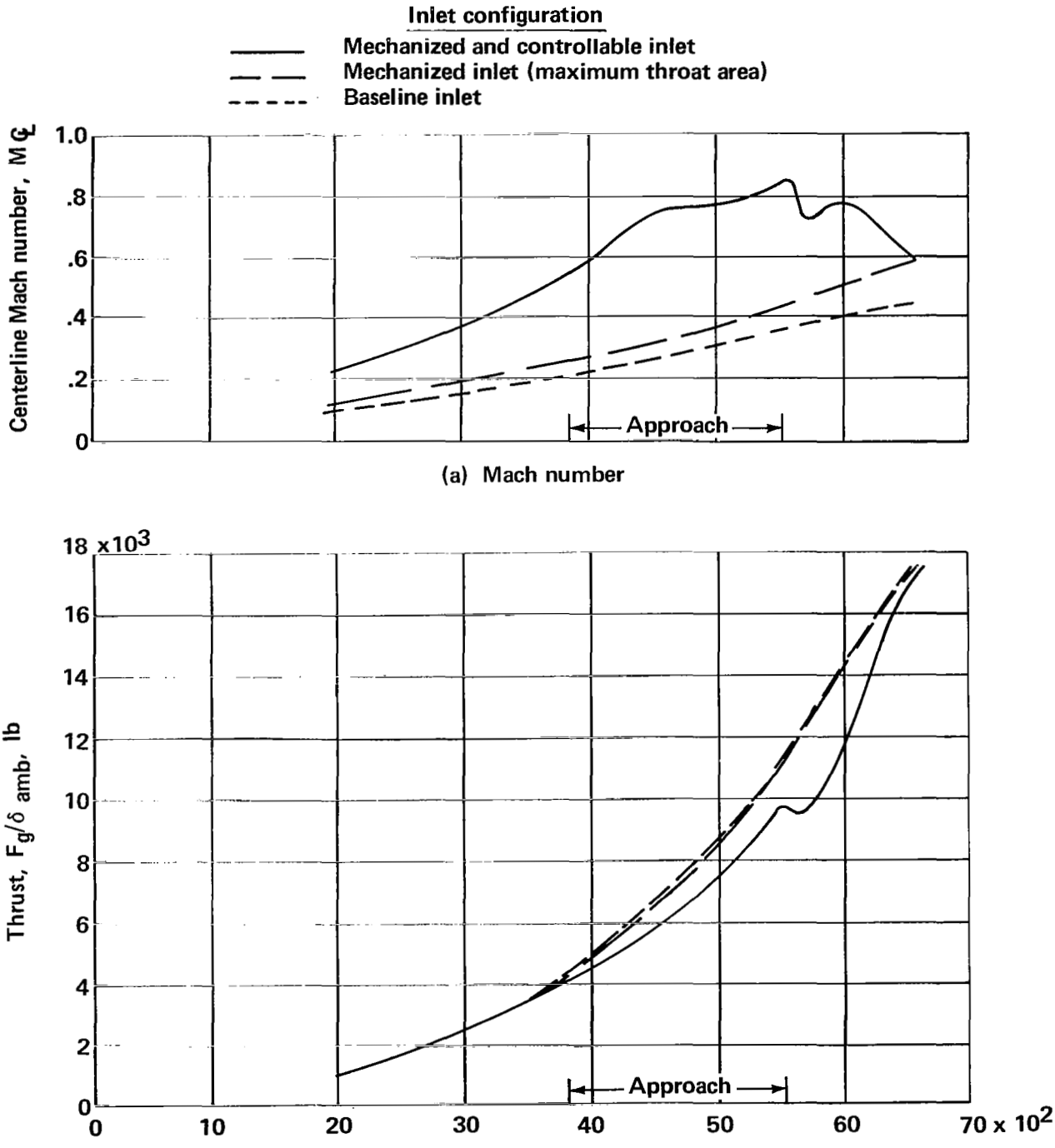

FIGURE 18.—VARIATION OF INLET CENTERLINE MACH NUMBER AND THRUST WITH ENGINE ROTOR SPEED FOR THE MECHANIZED INLET

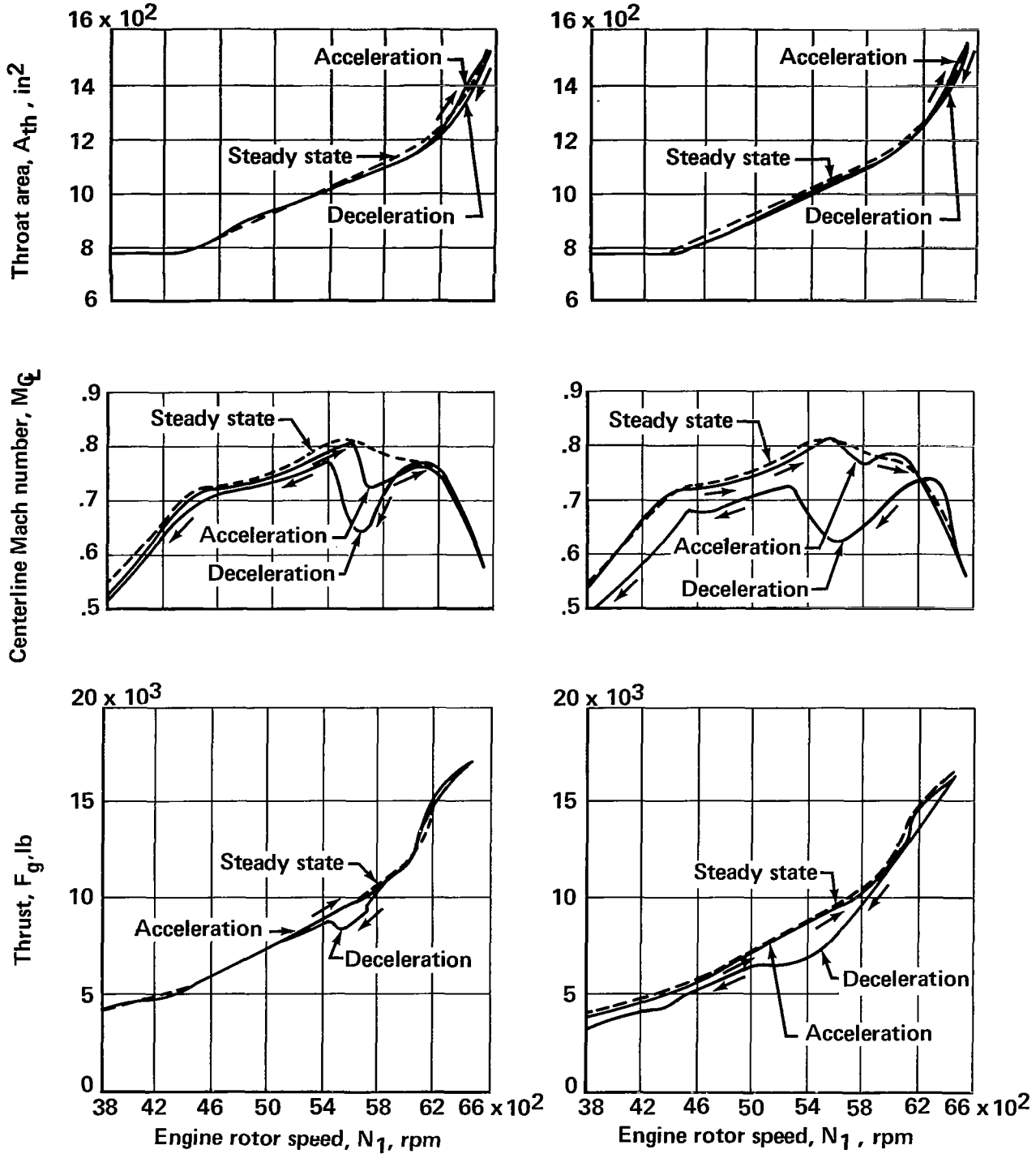

FIGURE 19.– INLET AND ENGINE RESPONSE TO POWER LEVER MOVEMENT FOR THE MECHANIZED INLET IN NOISE SUPPRESSION MODE

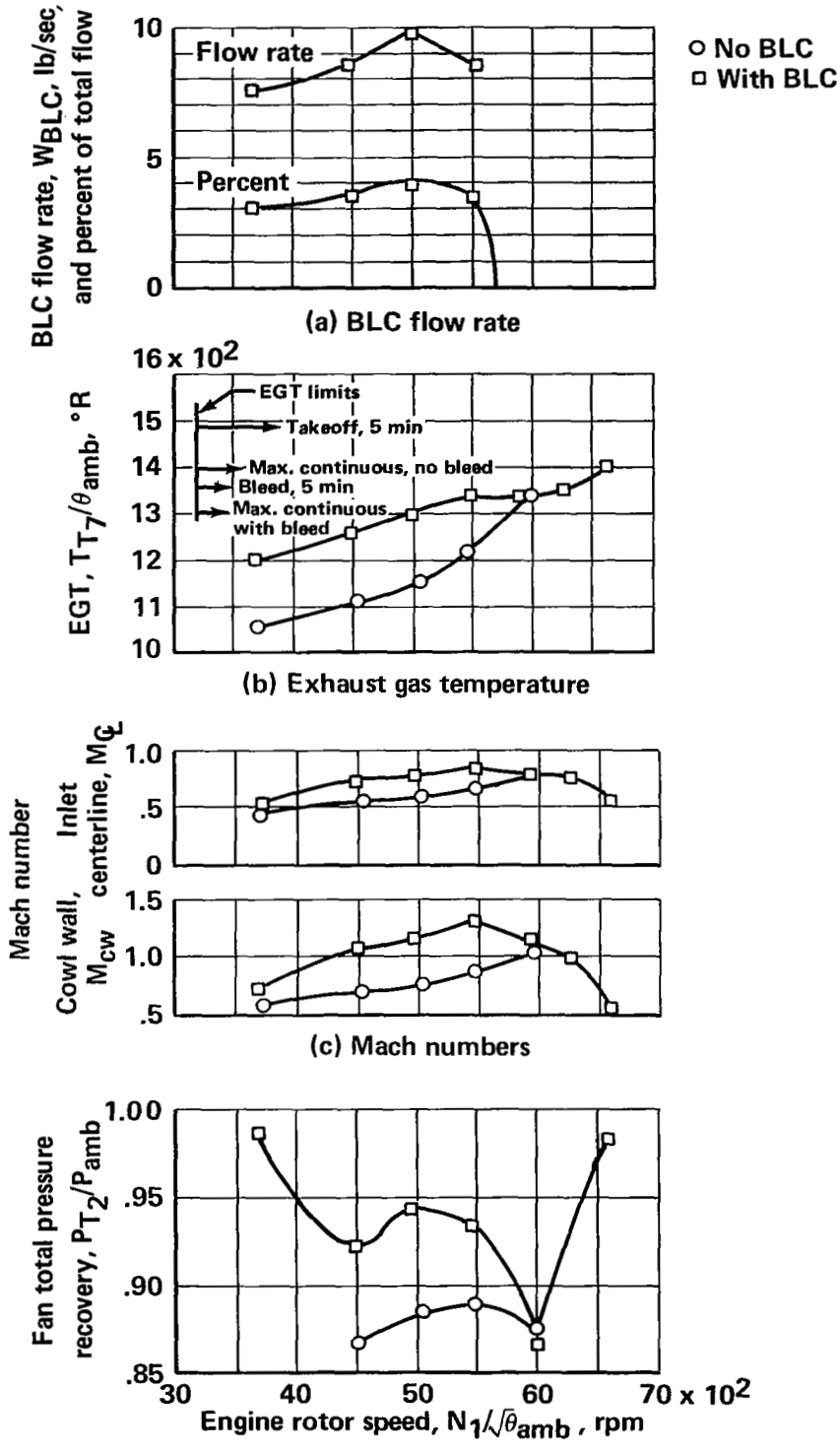

FIGURE 20.— EFFECT OF BOUNDARY LAYER CONTROL BLOWING ON INLET AND ENGINE OPERATING PARAMETERS

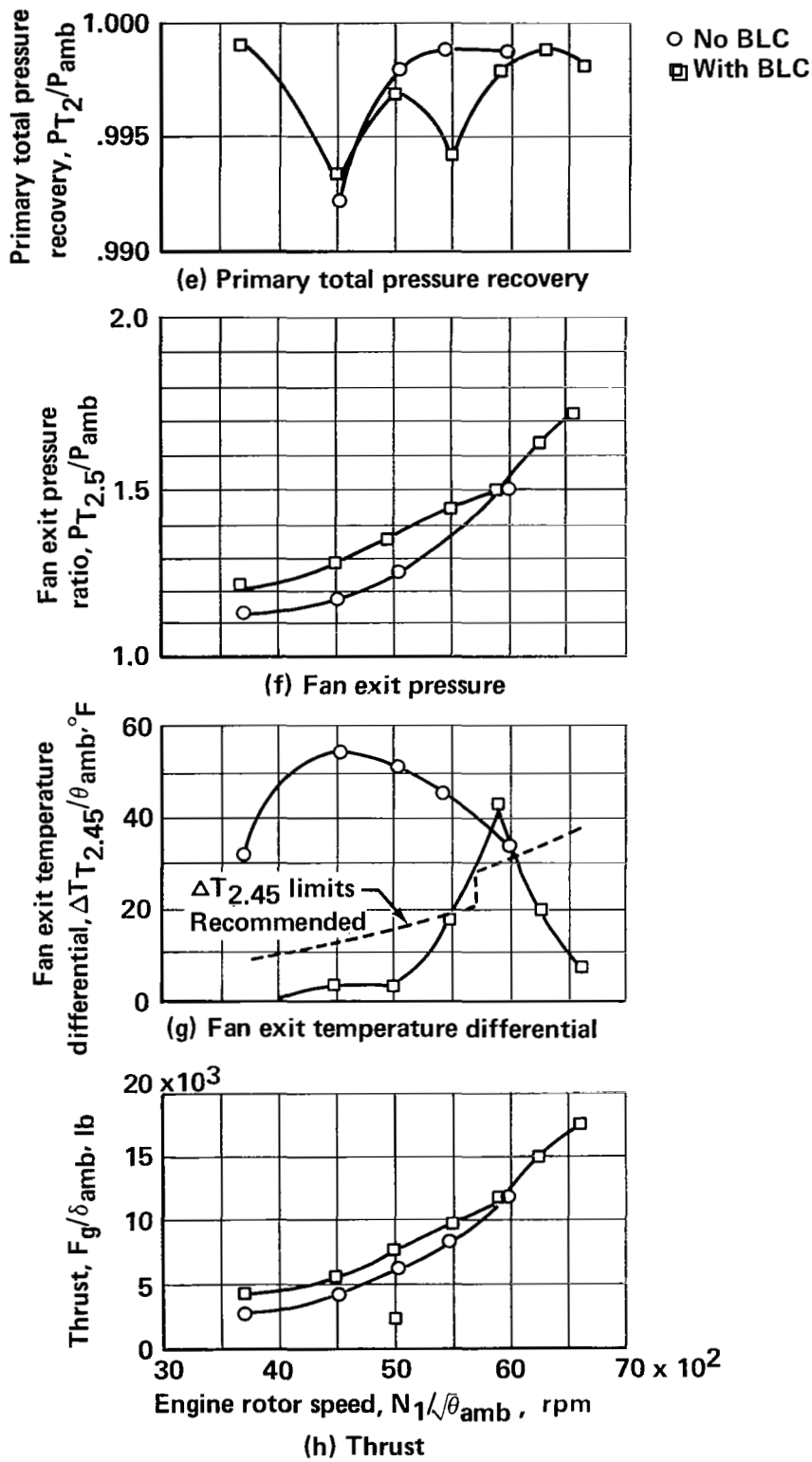

FIGURE 20.–EFFECT OF BOUNDARY LAYER CONTROL BLOWING ON INLET AND ENGINE OPERATING PARAMETERS–Concluded

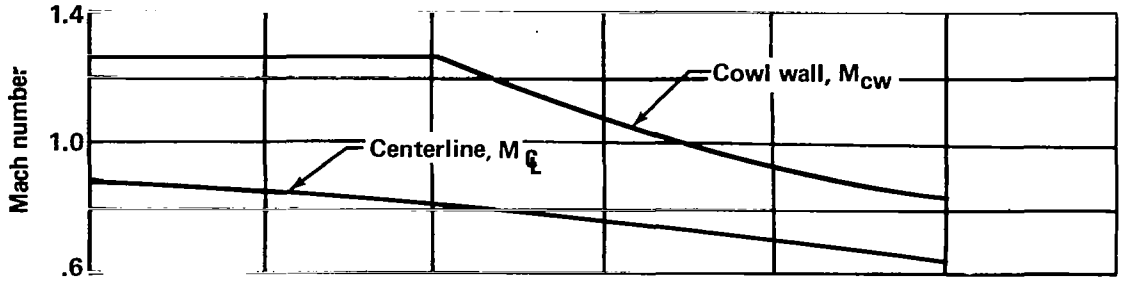

(a) Mach number

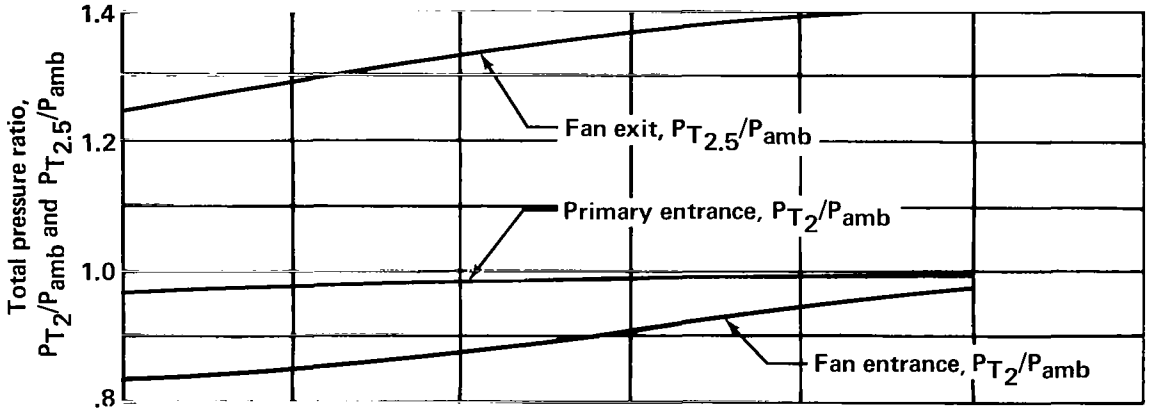

(b) Total pressure ratios

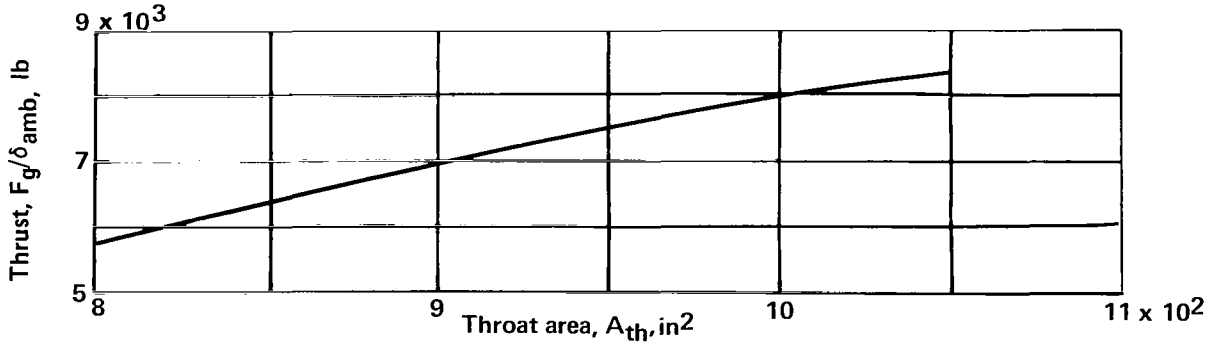

(c) Thrust

FIGURE 21.– EFFECT OF VARIATION OF INLET THROAT AREA FOR THE MECHANIZED INLET AT CONSTANT APPROACH ENGINE ROTOR SPEED

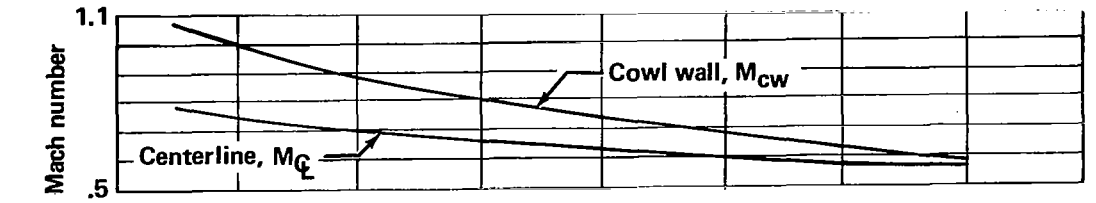

(a) Mach number

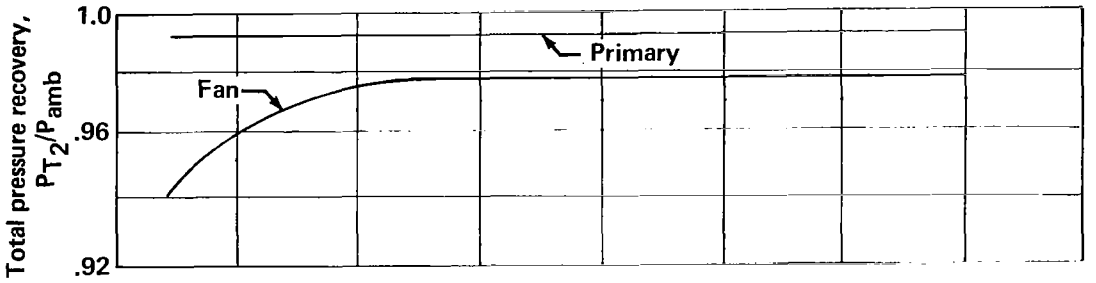

(b) Total pressure recovery

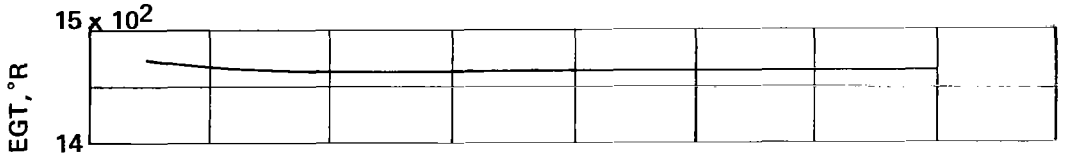

(c) Exhaust gas temperature

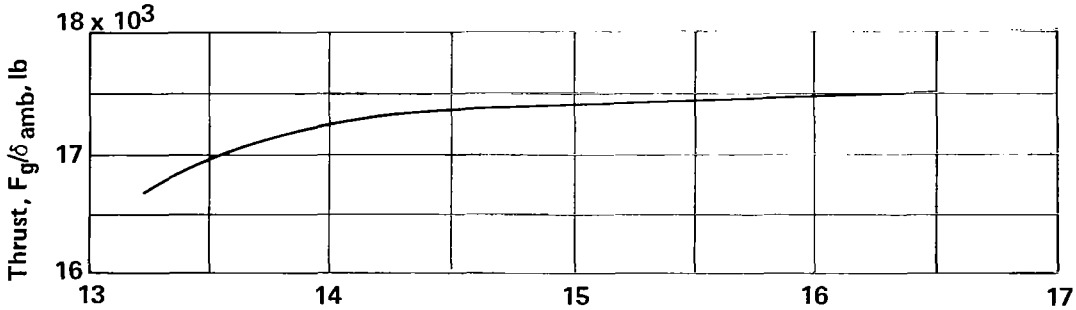

(d) Thrust

FIGURE 22.– EFFECT OF VARIATION OF INLET THROAT AREA FOR THE MECHANIZED INLET AT CONSTANT TAKEOFF ENGINE ROTOR SPEED

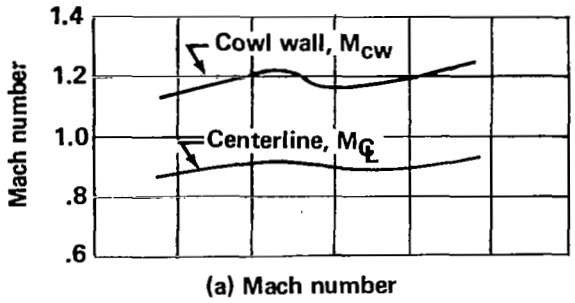

(a) Mach number

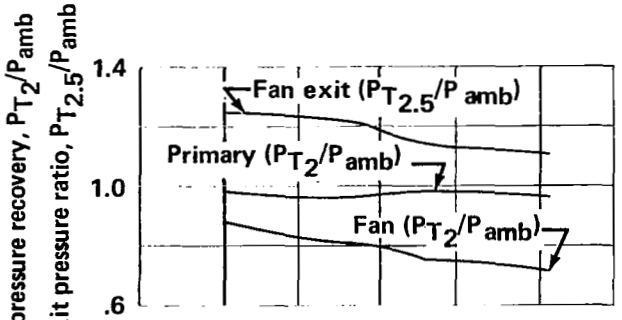

(b) Total pressure ratios

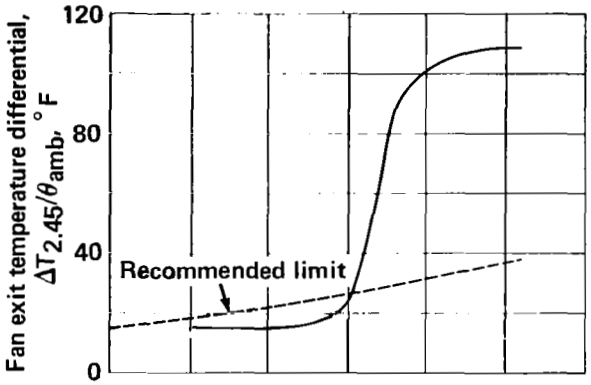

(c) Fan exit temperatures

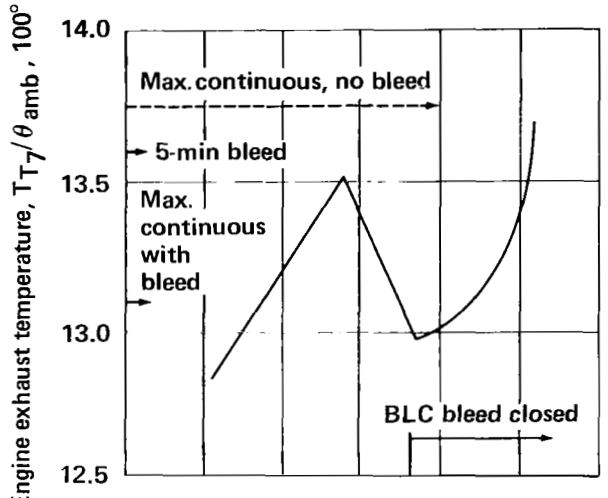

(d) Exhaust gas temperature

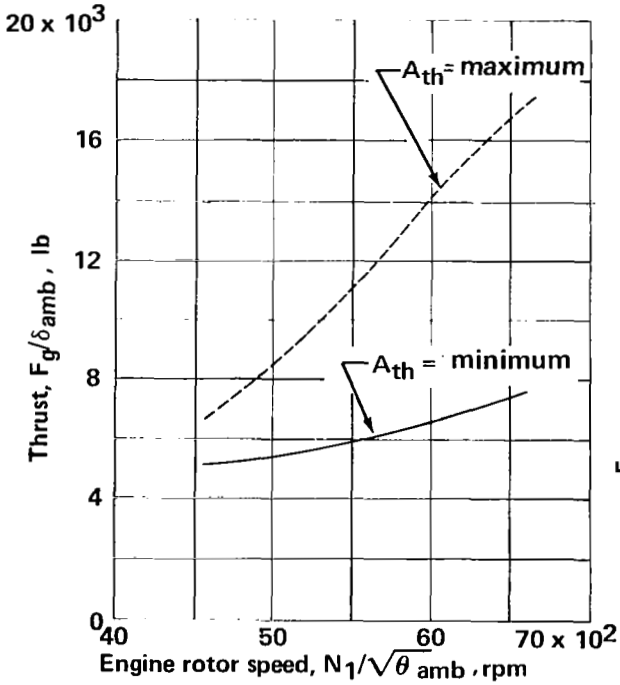

(e) Thrust

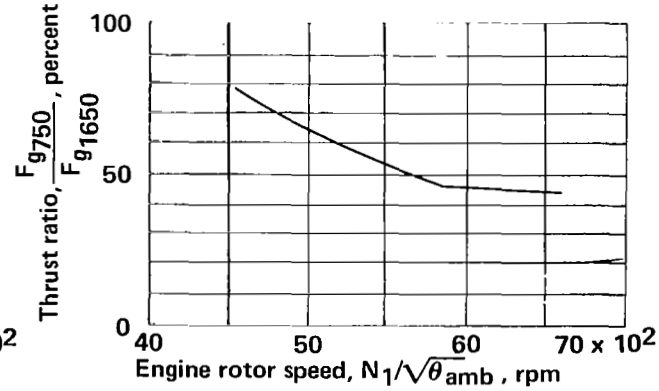

(f) Thrust ratio

FIGURE 23.—INLET AND ENGINE OPERATION WITH THE INLET IN MINIMUM THROAT AREA POSITION

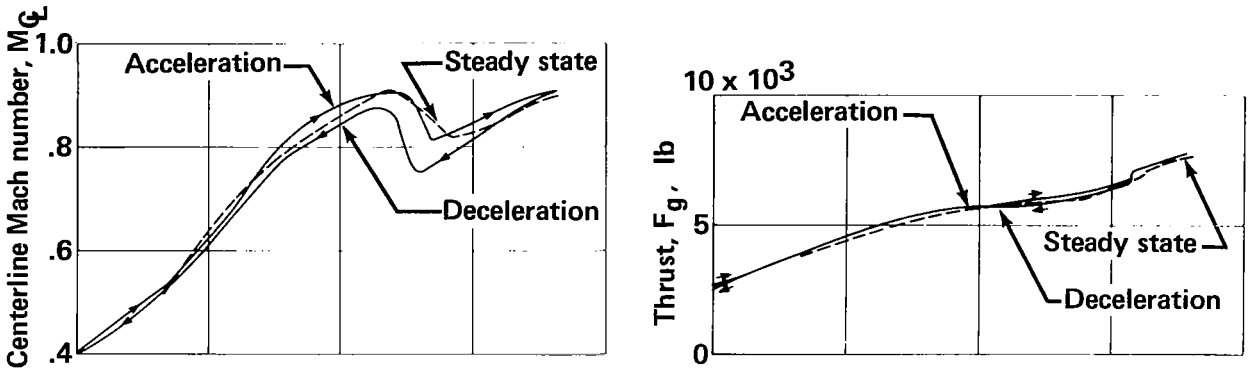

(a) 60-sec movement

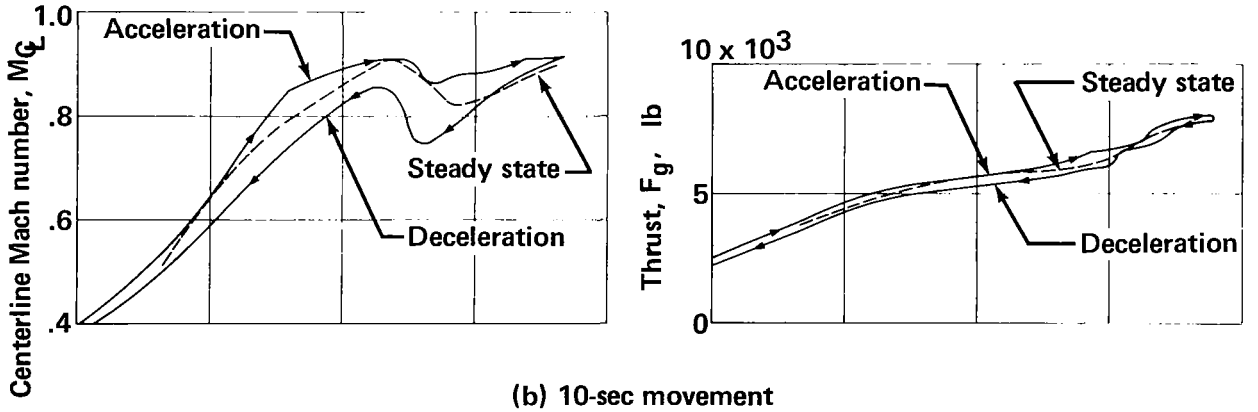

(b) 10-sec movement

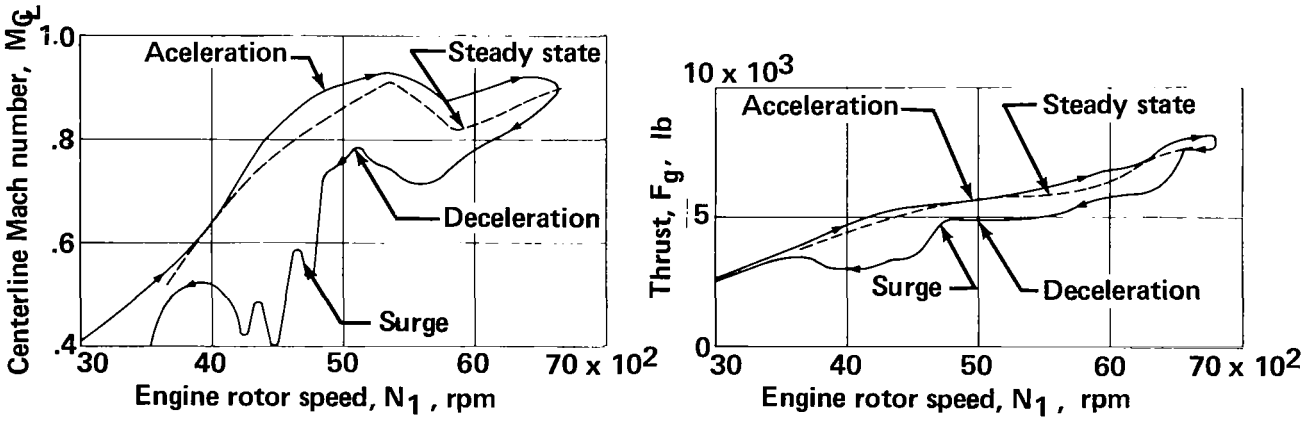

(c) 1-sec "snap" movement

FIGURE 24.– INLET AND ENGINE RESPONSE TO POWER LEVER MOVEMENT WITH CONSTANT MINIMUM INLET THROAT AREA

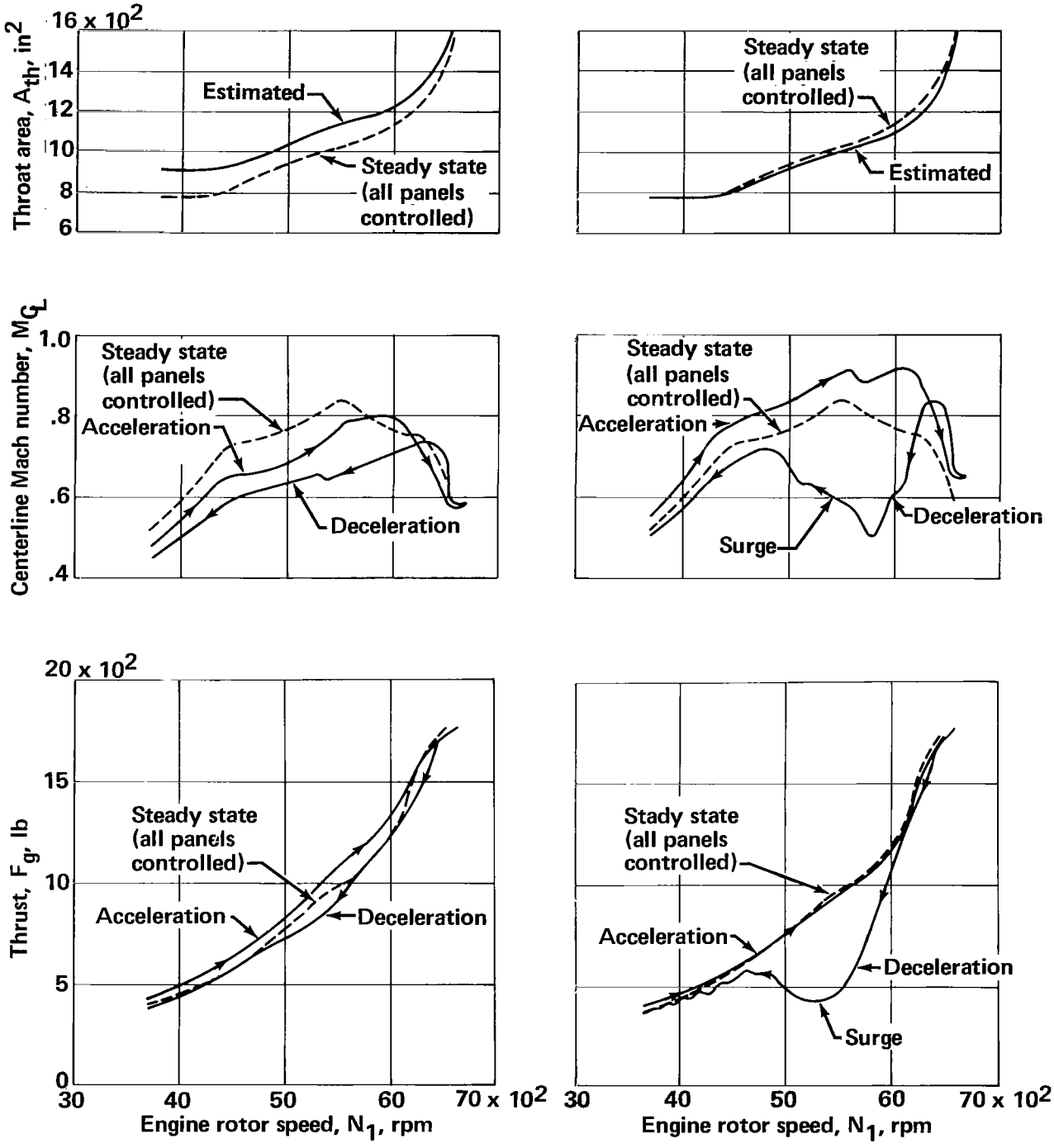

(a) Maximum throat area position

(b) Minimum throat area position

FIGURE 25.—INLET AND ENGINE RESPONSE WITH ONE SEGMENT AT EITHER MINIMUM OR MAXIMUM THROAT AREA POSITION (1-SEC POWER LEVER MOMENT)

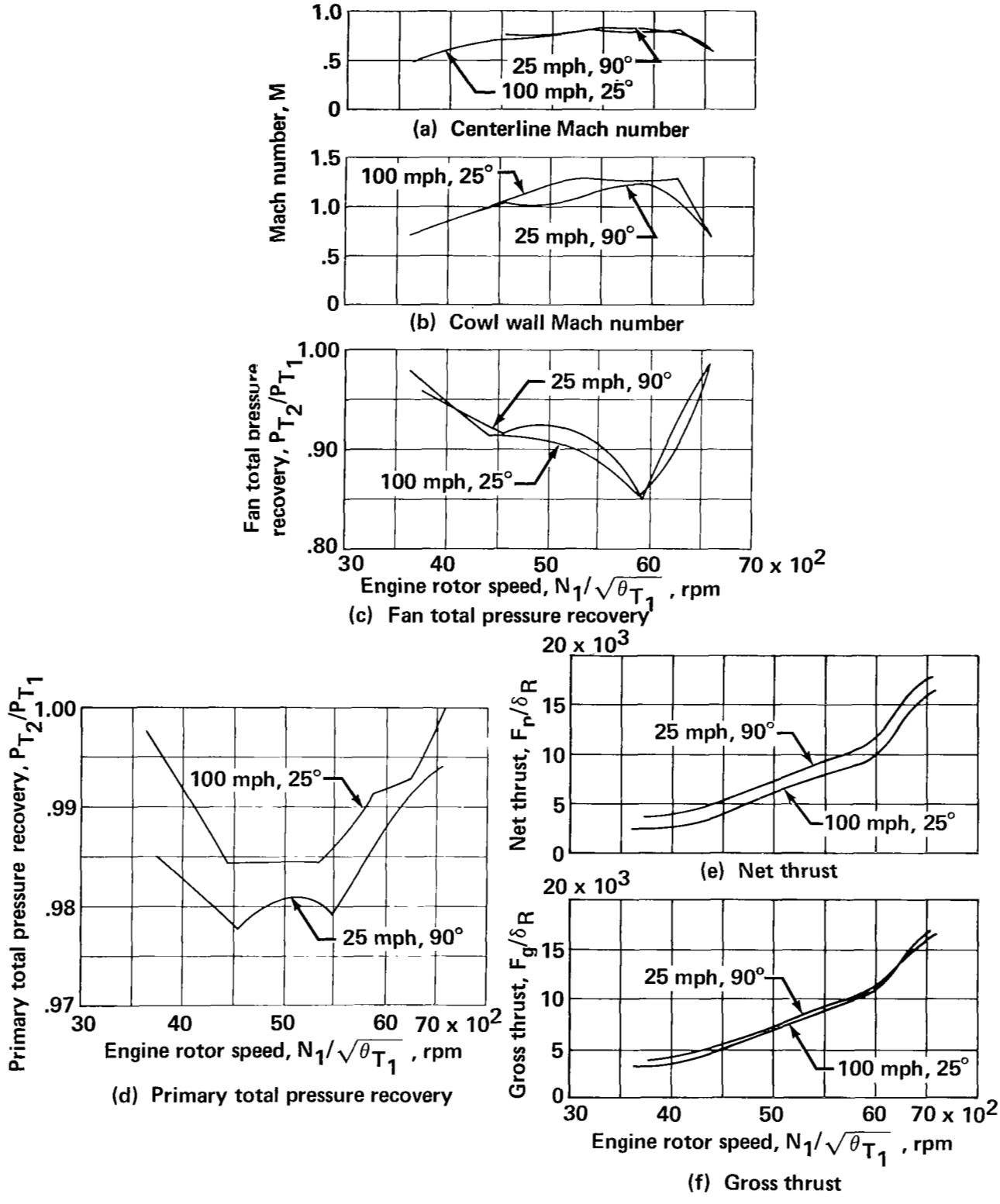

FIGURE 26.–EFFECT OF CROSSWIND ON MACH NUMBER, TOTAL PRESSURE RECOVERY, AND THRUST OF MECHANIZED INLET IN NOISE SUPPRESSION MODE

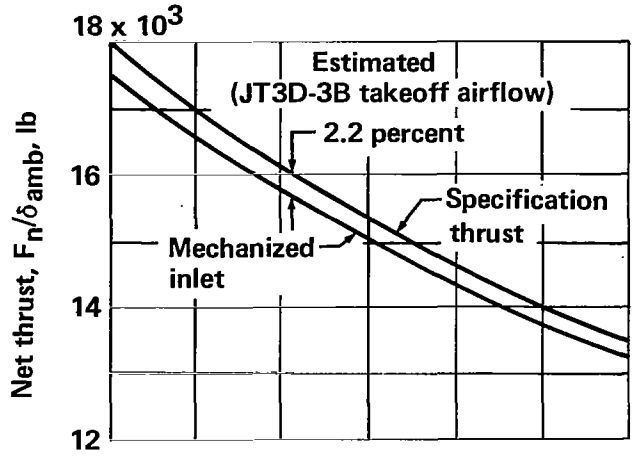

(a) Takeoff thrust

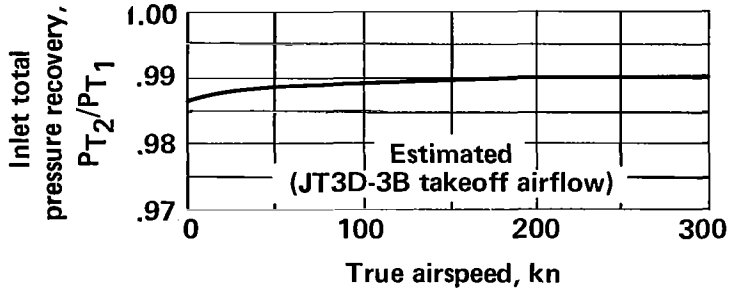

(b) Total pressure recovery at takeoff

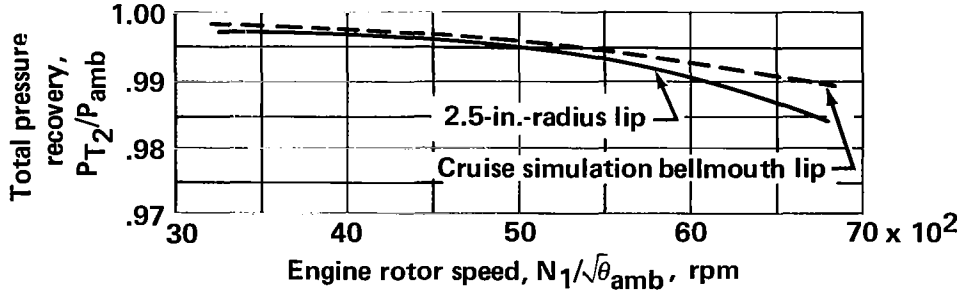

(c) Total pressure recovery, 0 kn

FIGURE 27.– THRUST AND TOTAL PRESSURE RECOVERY FOR MECHANIZED INLET IN TAKEOFF CONFIGURATION

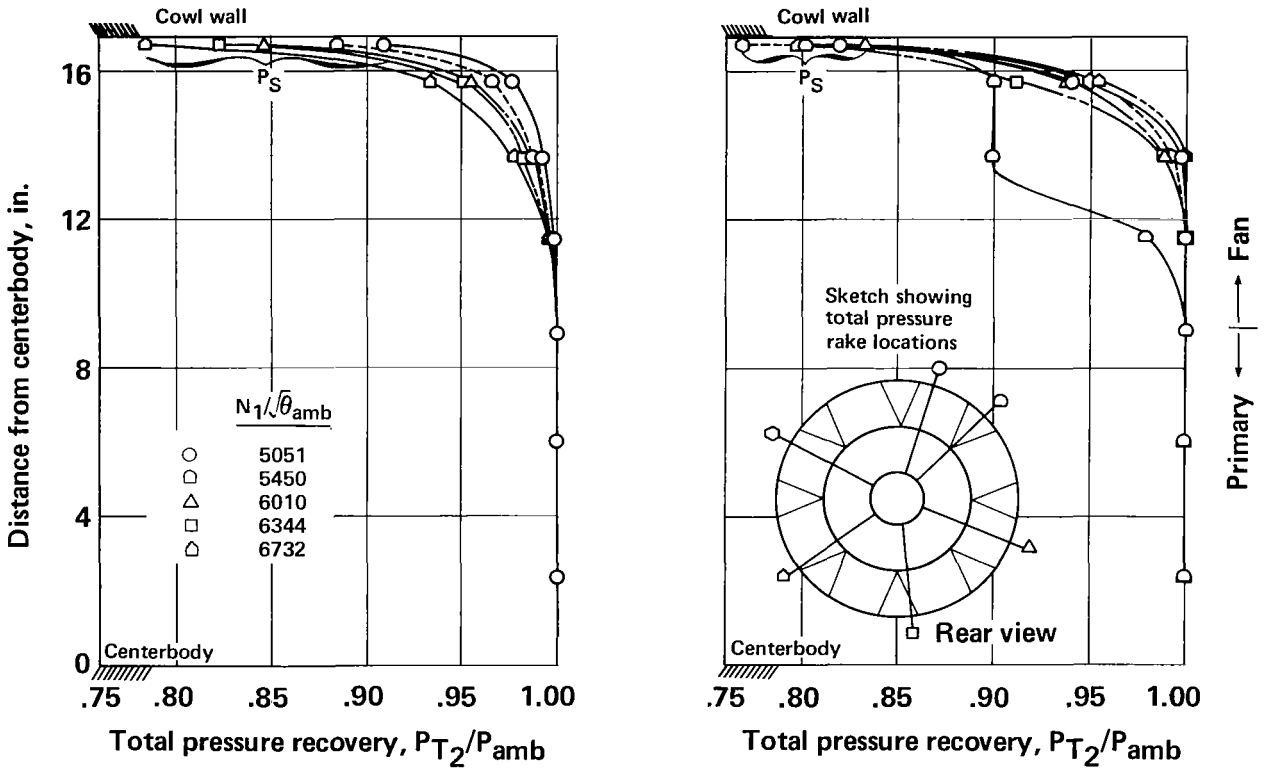

(d) Effect of varying rotor speed

(e) Circumferential pressure distributions

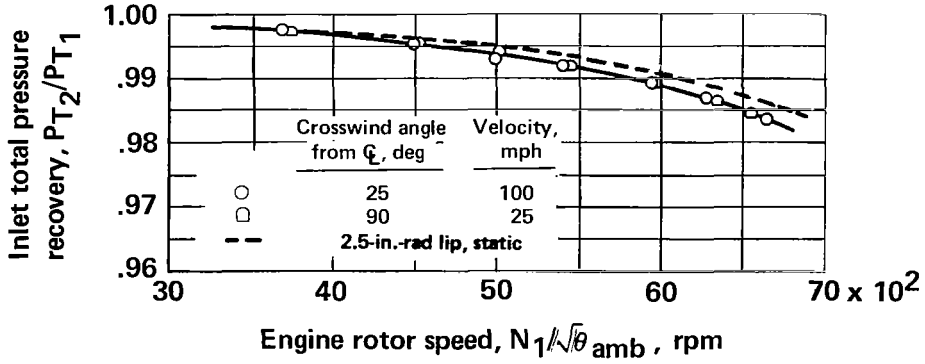

(f) Effect of crosswinds

FIGURE 27.–THRUST AND TOTAL PRESSURE RECOVERY FOR MECHANIZED INLET IN TAKEOFFF CONFIGURATION– Concluded

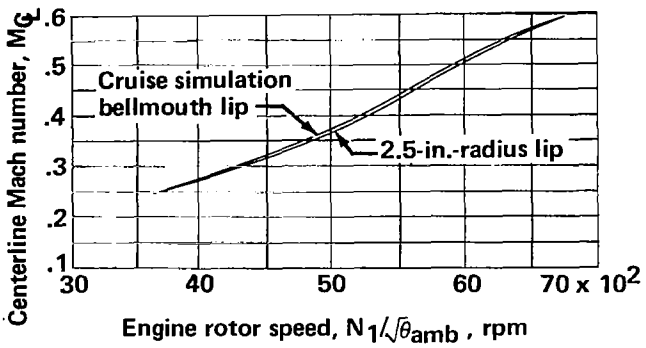

(a) Center Mach numbers, unsuppressed mode

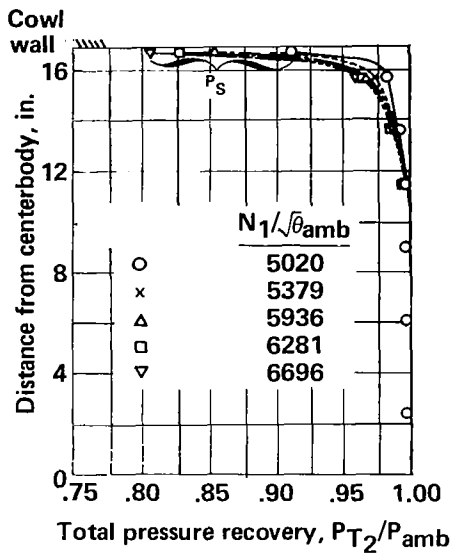

(b) Effect of varying rotor speed

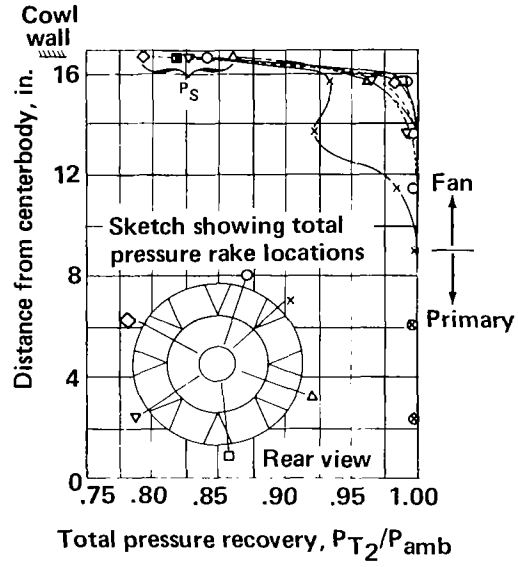

(c) Circumferential pressure distribution

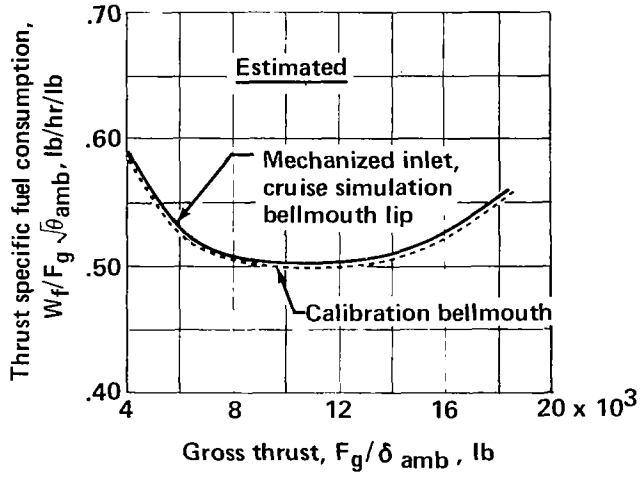

(d) Thrust specific fuel consumption

FIGURE 28.– TSFC, PRESSURE RECOVERY, AND MACH NUMBERS FOR CRUISE SIMULATION

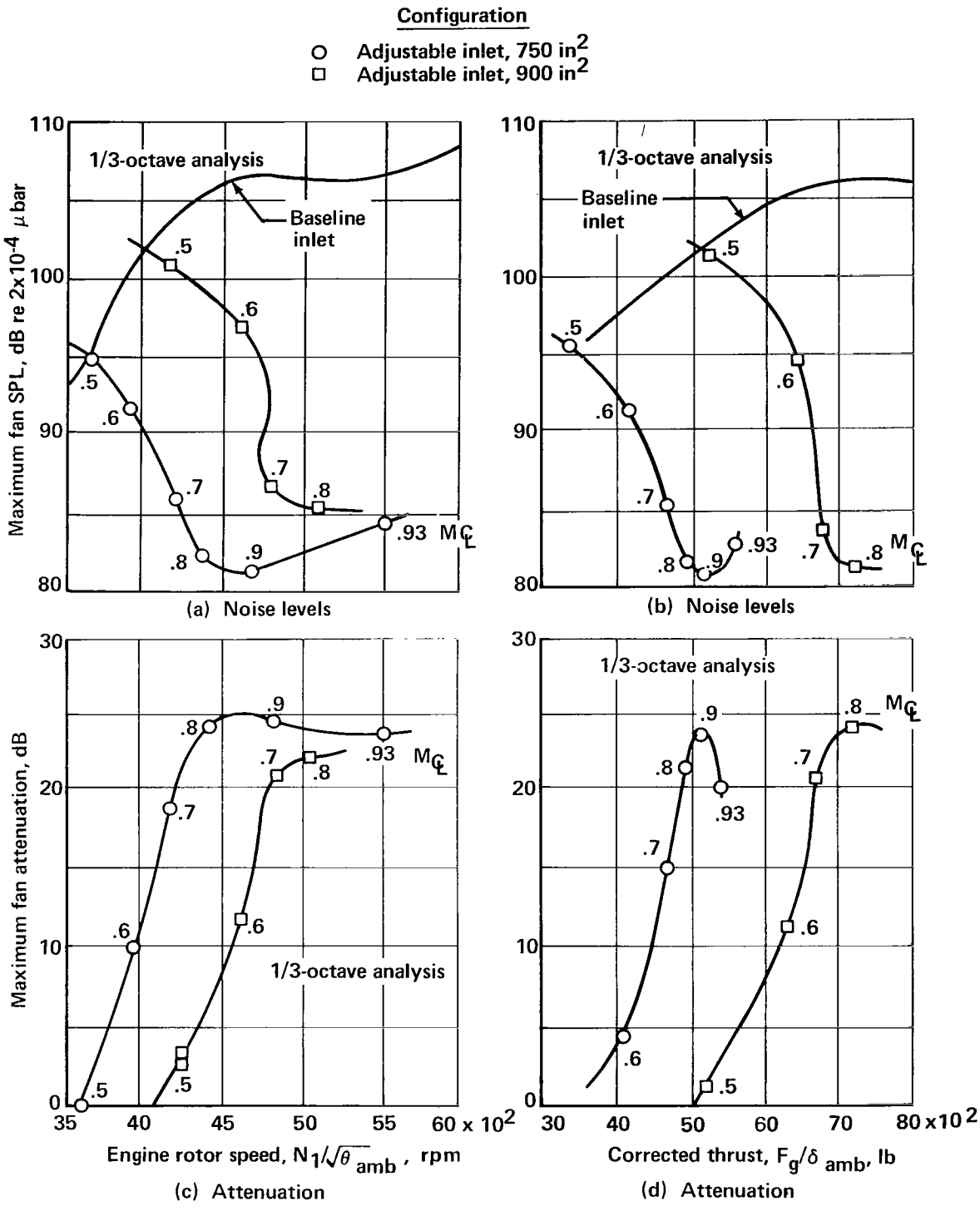

FIGURE 29.—NOISE LEVELS AND ATTENUATION FOR ADJUSTABLE INLET

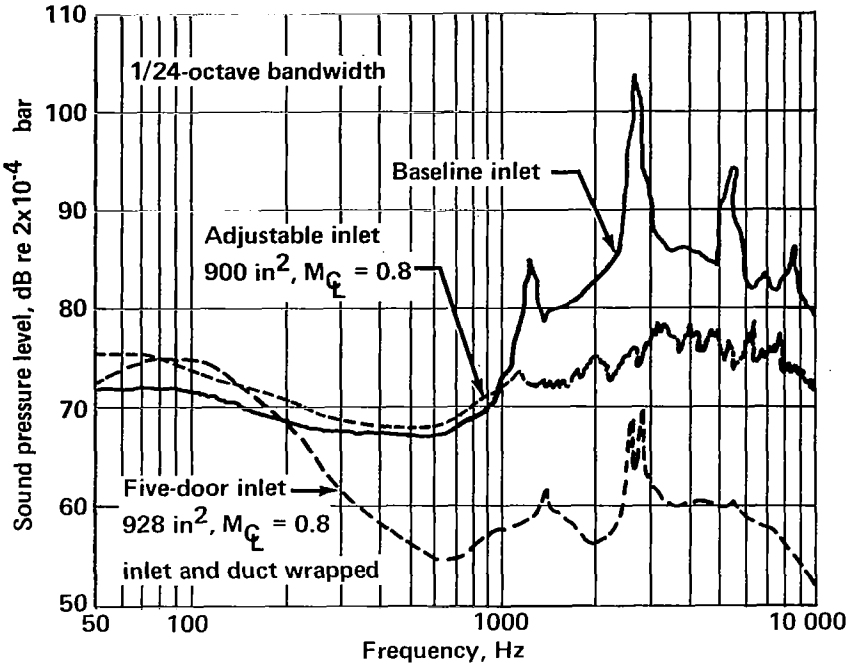

(a) Typical Spectra at landing approach

One engine, 200 ft flyover, M_{C_L} = 0.8

○ Adjustable inlet, 750 in^2

□ Adjustable inlet, 900 in^2

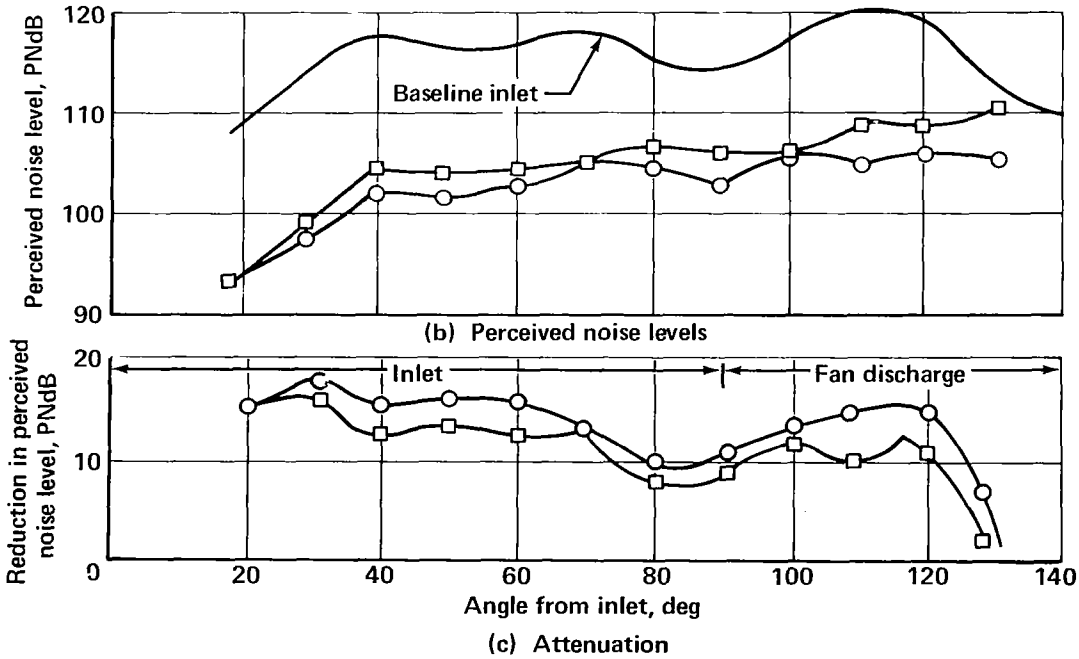

(b) Perceived noise levels

(c) Attenuation

FIGURE 30.—ACOUSTIC SPECTRA, PERCEIVED NOISE LEVELS, AND ATTENUATION FOR ADJUSTABLE INLET

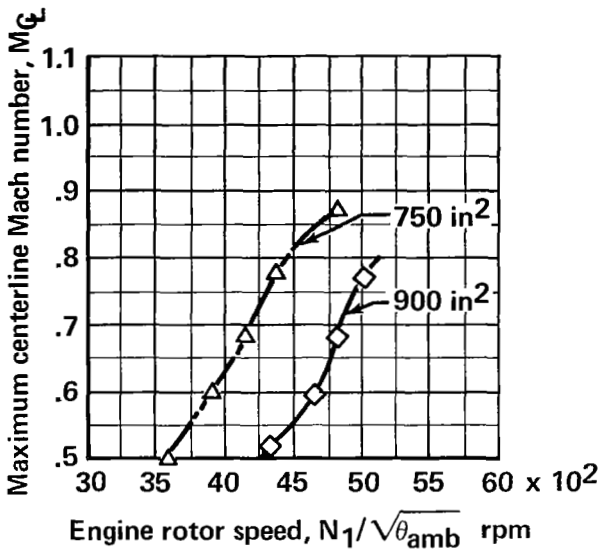

(a) Centerline Mach number

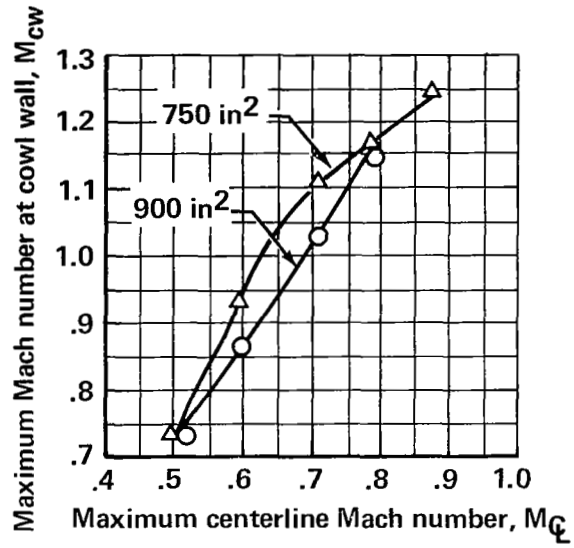

(b) Mach number at cowl wall

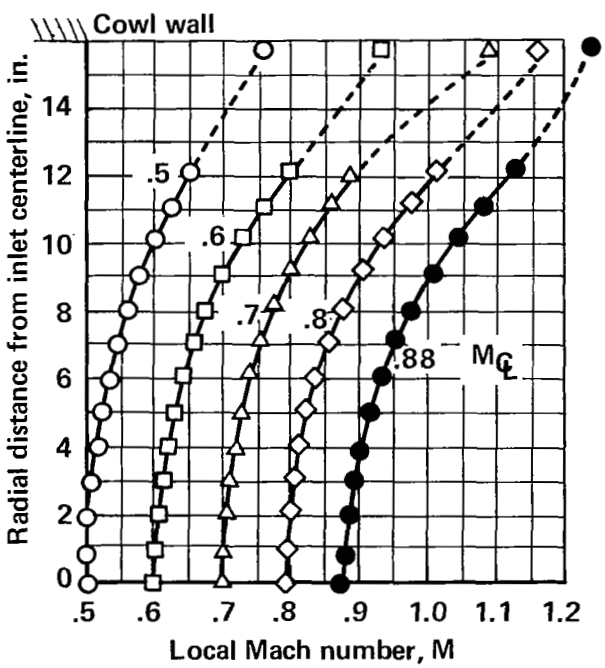

(c) Throat area–750 in^2

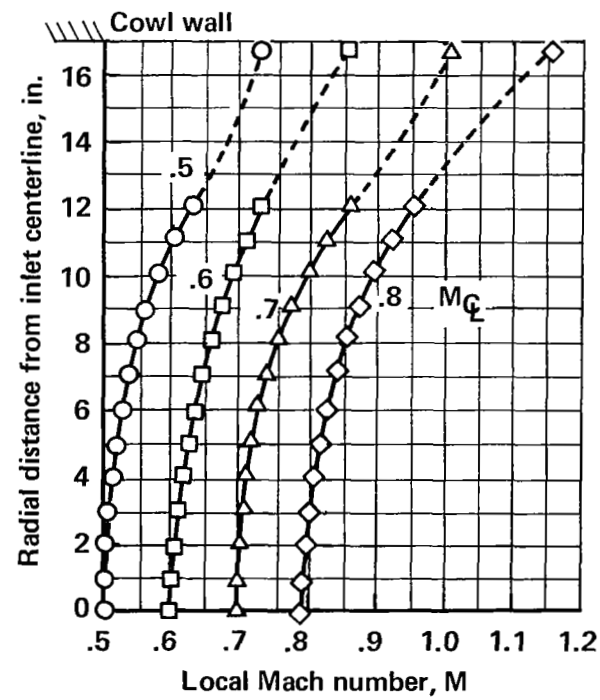

(d) Throat area–900 in^2

FIGURE 31–CENTERLINE, COWL WALL, AND LOCAL MACH NUMBERS IN THE THROAT REGION OF THE ADJUSTABLE INLET WITH FORWARD SLOT BLC FLOWING

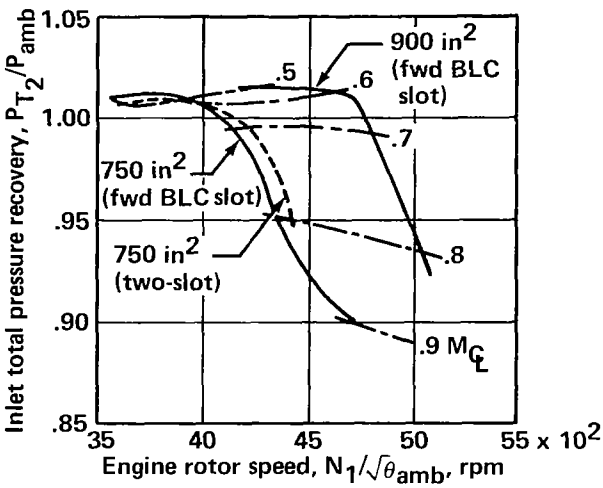

(a) Engine rotor speed

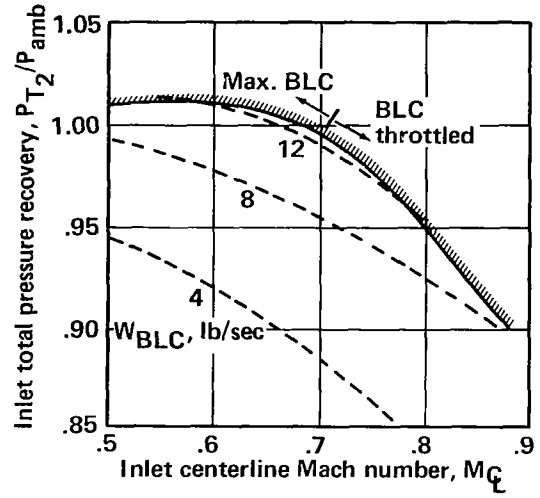

(b) Centerline Mach number, forward slot BLC, 750-in^2 throat area

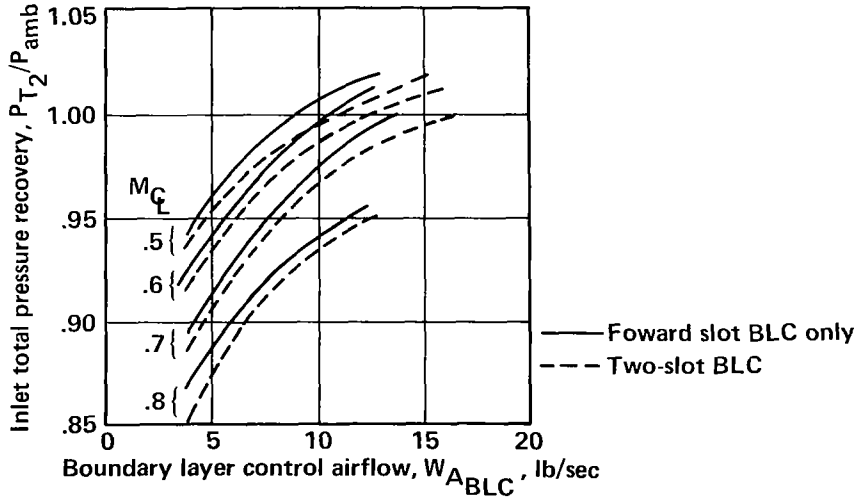

(c) BLC airflow, 750-in^2 throat area

FIGURE 32.—EFFECT OF ENGINE ROTOR SPEED, CENTERLINE MACH NUMBER, AND BLC AIRFLOW ON TOTAL PRESSURE RECOVERY FOR THE ADJUSTABLE INLET

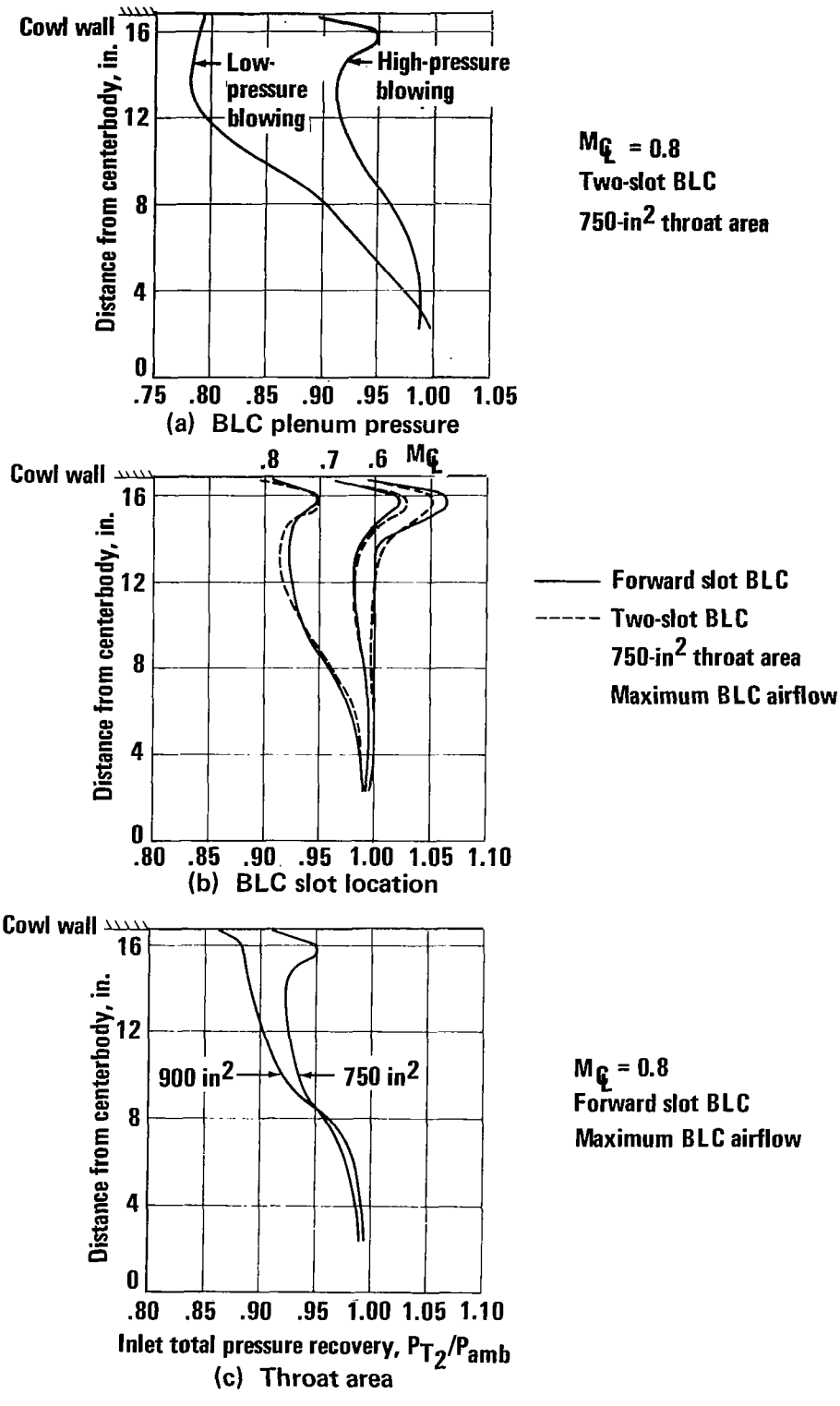

FIGURE 33.–EFFECT OF BLC PRESSURE, SLOT LOCATION, AND INLET THROAT AREA ON RADIAL TOTAL PRESSURE RECOVERY PROFILES FOR ADJUSTABLE INLET

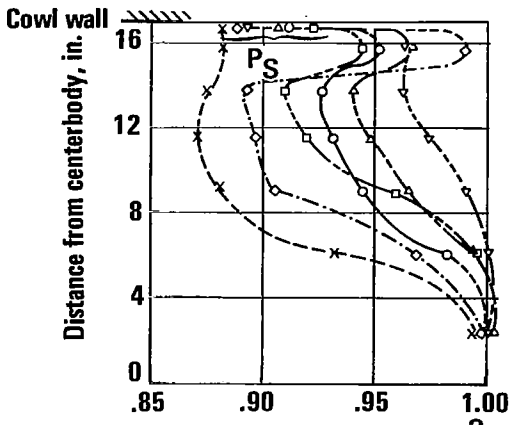

(a) Two-slot BLC, 750 in^2

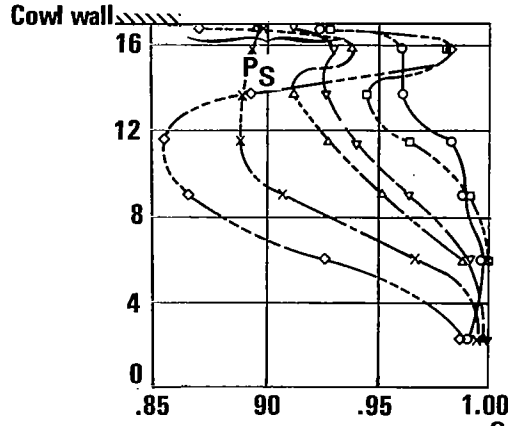

(b) Forward slot BLC, 750 in^2

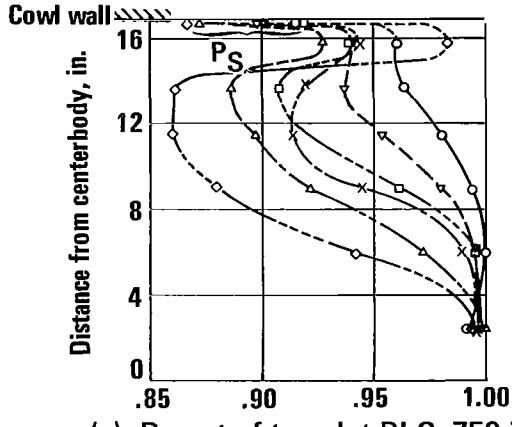

(c) Repeat of two-slot BLC, 750 in^2

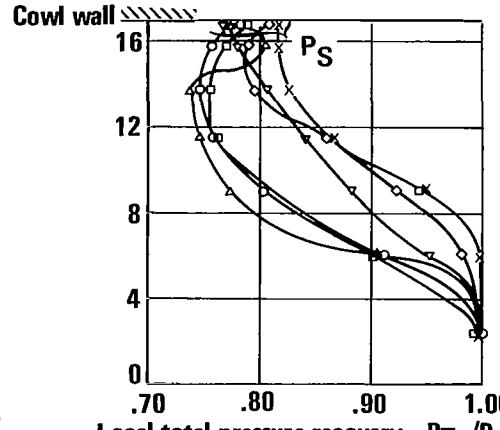

(d) Two-slot, low-pressure BLC, 750 in^2

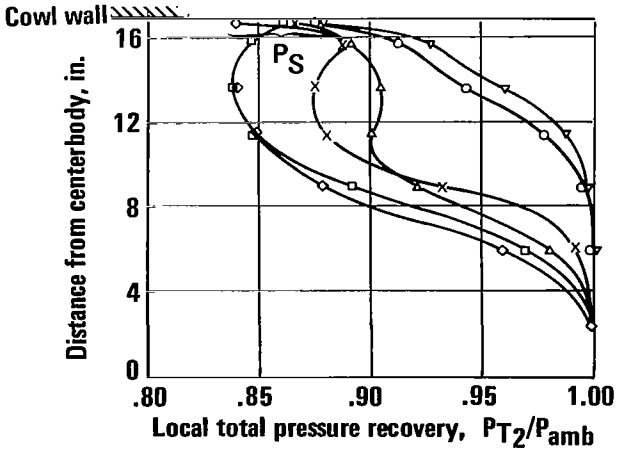

(e) Forward slot BLC, 900 in^2

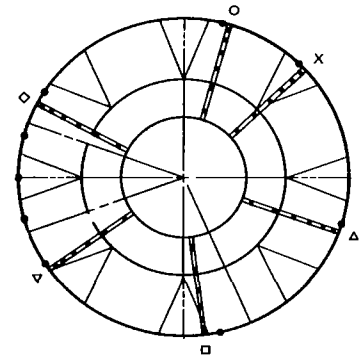

Rear view of inlet showing rake locations

FIGURE 34.—TOTAL PRESSURE RECOVERY BY INDIVIDUAL PROBE FOR ADJUSTABLE INLET AT 0.8 CENTERLINE MACH NUMBER

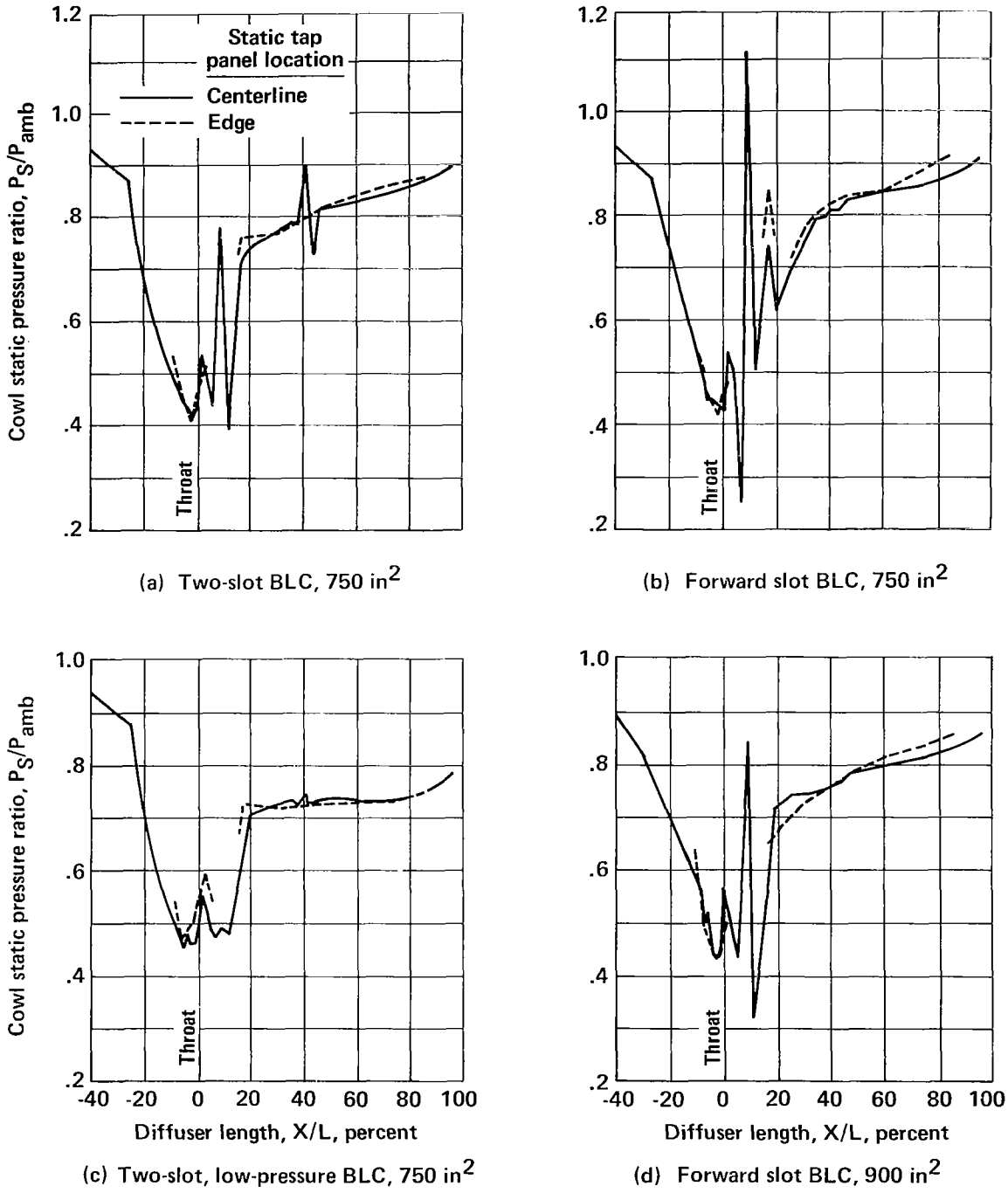

FIGURE 35.—AXIAL DISTRIBUTION OF COWL WALL STATIC PRESSURES WITH VARIOUS BLC CONFIGURATIONS AND INLET THROAT AREAS FOR ADJUSTABLE INLET

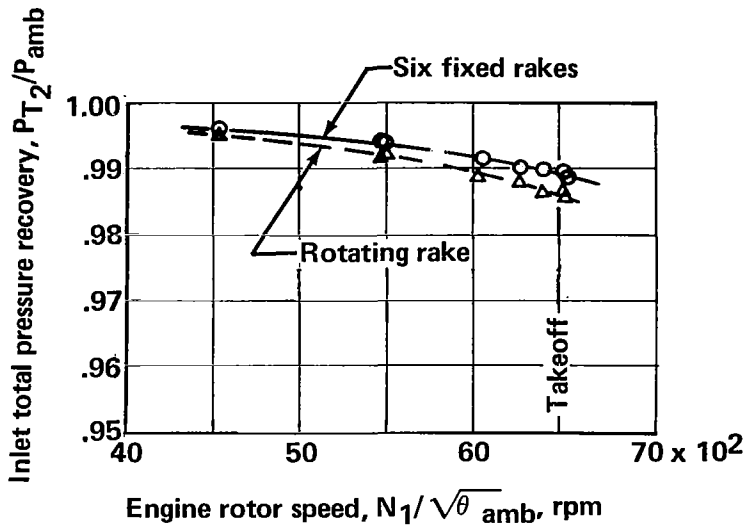

(a) Average recovery

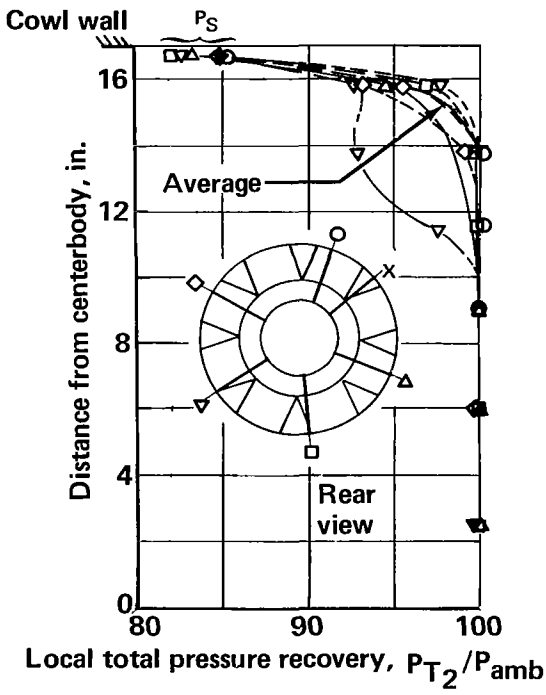

(b) Fixed rakes

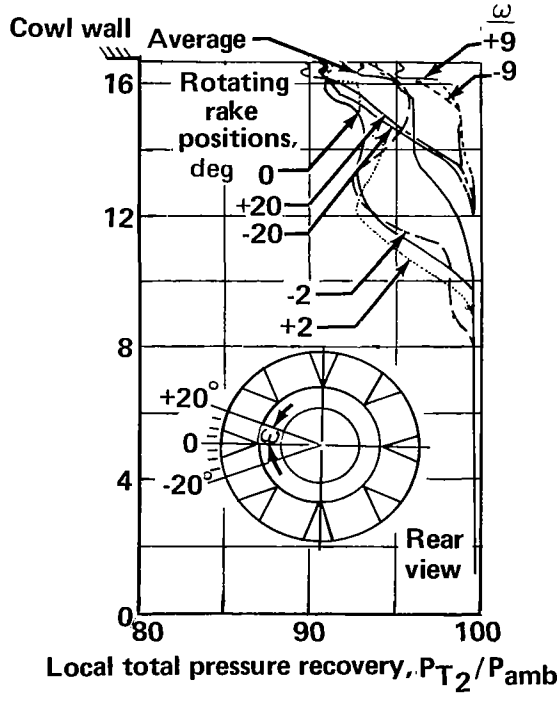

(c) Rotating rake

FIGURE 36.—TOTAL PRESSURE RECOVERY OF ADJUSTABLE INLET, TAKEOFF CONFIGURATION

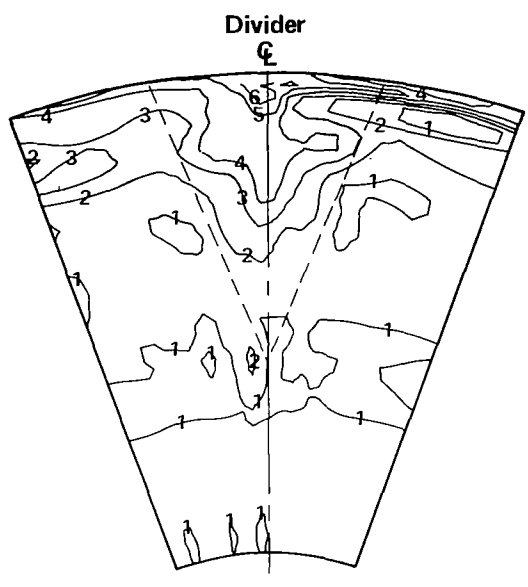

$M_{℄} = 0.13$, $N_1/\sqrt{\theta_{amb}} = 1982$

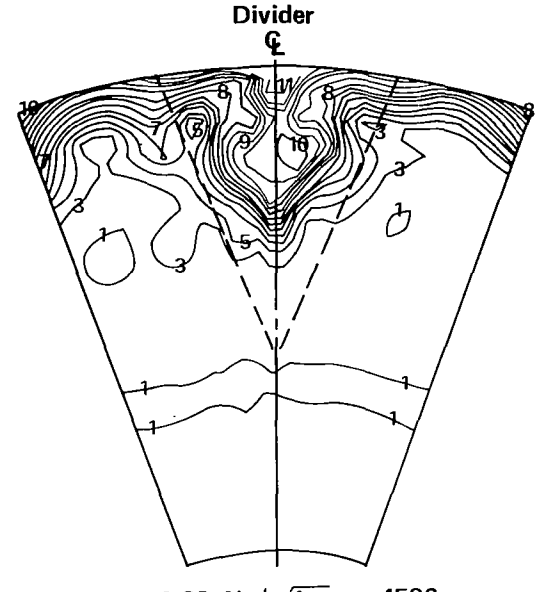

$M_{℄} = 0.32$, $N_1/\sqrt{\theta_{amb}} = 4526$

	Total pressure recovery, P_{T_2}/P_{amb}
1	1.000
2	0.999
3	0.998
4	0.997
5	0.996
6	0.995
7	0.990

	Total pressure recovery, P_{T_2}/P_{amb}
8	0.985
9	0.980
10	0.975
11	0.974
12	0.965
13	0.950
14	0.940

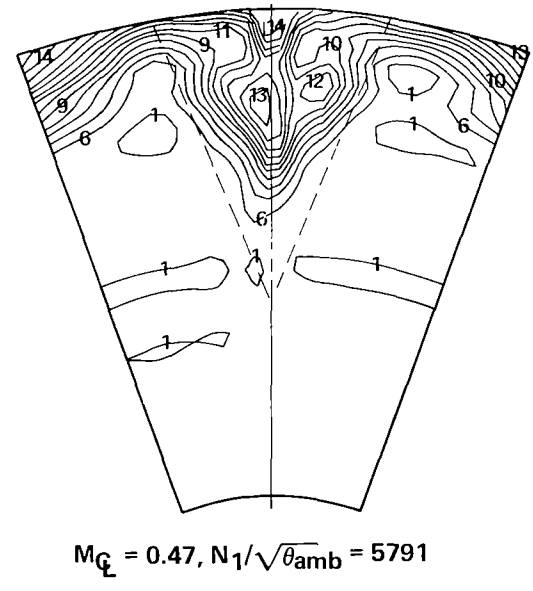

$M_{℄} = 0.47$, $N_1/\sqrt{\theta_{amb}} = 5791$

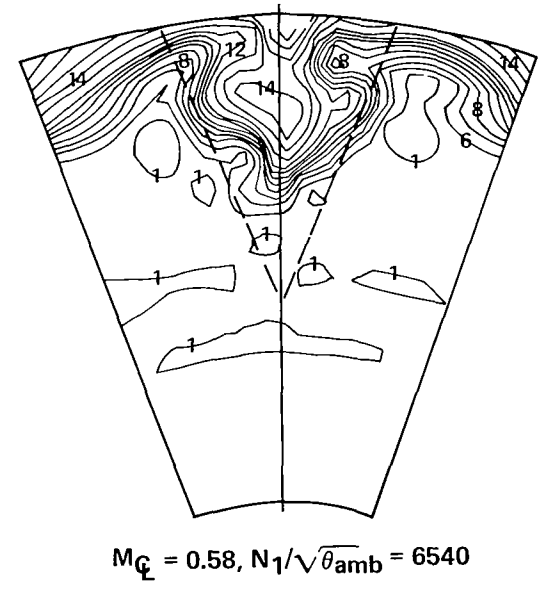

$M_{℄} = 0.58$, $N_1/\sqrt{\theta_{amb}} = 6540$

FIGURE 37.–TOTAL PRESSURE DISTRIBUTION BEHIND A DIVIDER FOR THE ADJUSTABLE INLET AT VARIOUS ENGINE ROTOR SPEEDS AND CENTERLINE MACH NUMBERS (A_{th} = 1570 IN^2)

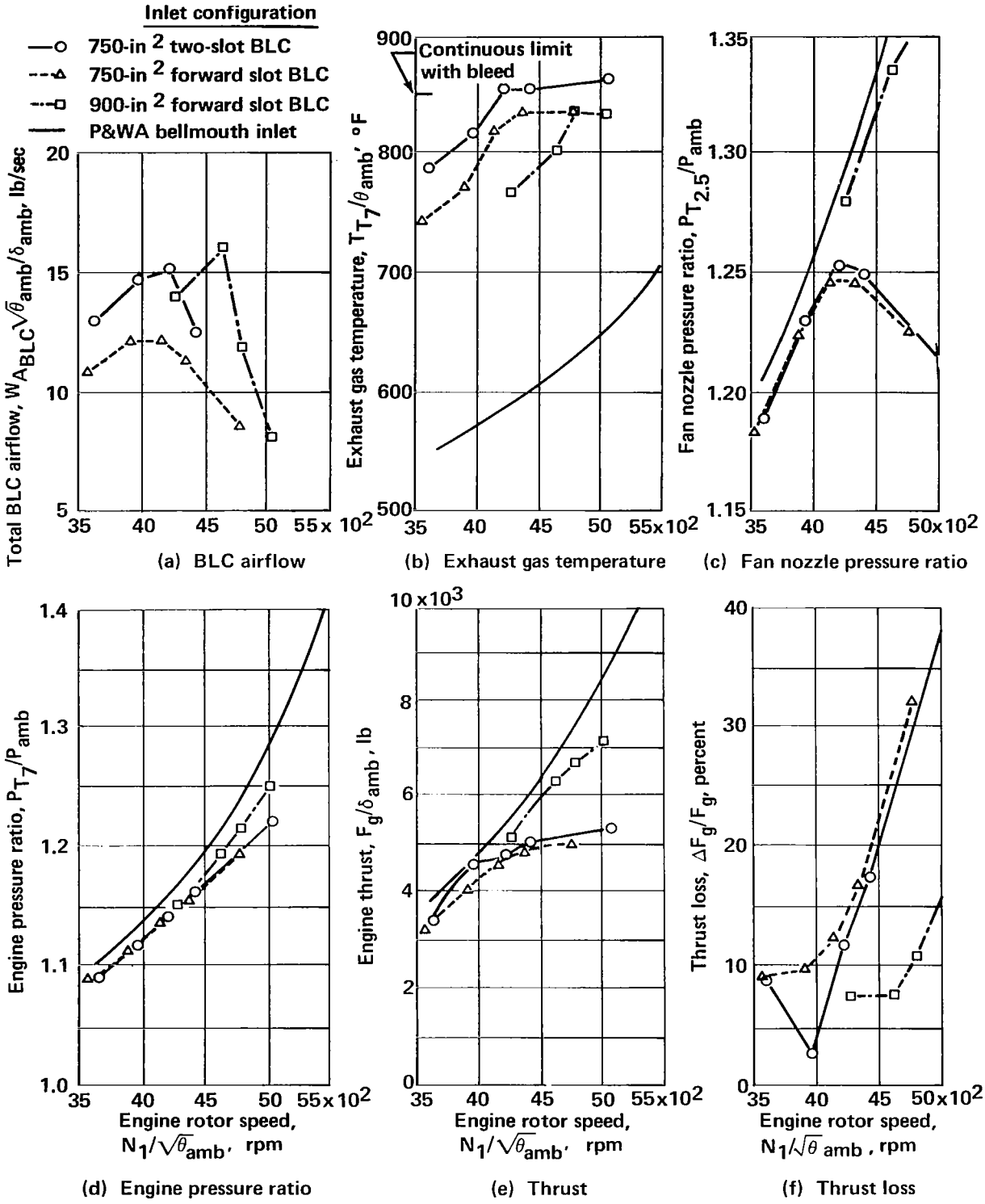

FIGURE 38.—ENGINE OPERATING PARAMETERS, NOISE-SUPPRESSED MODE, ADJUSTABLE INLET

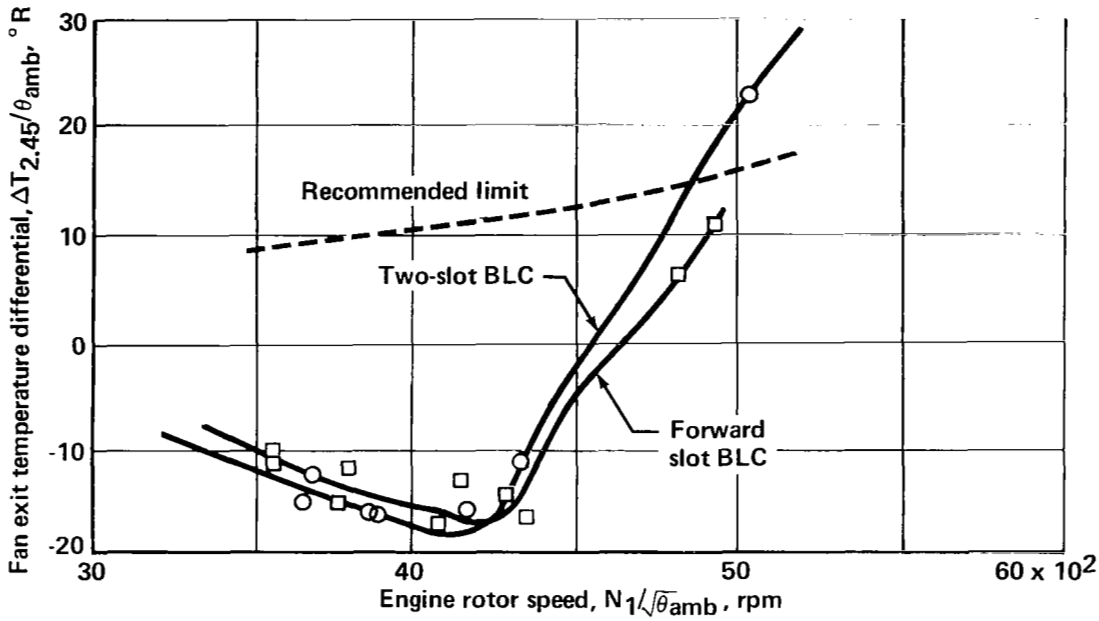

(g) Fan exit temperature differential

FIGURE 38.—ENGINE OPERATING PARAMETERS, NOISE-SUPPRESSED MODE, ADJUSTABLE INLET—Concluded

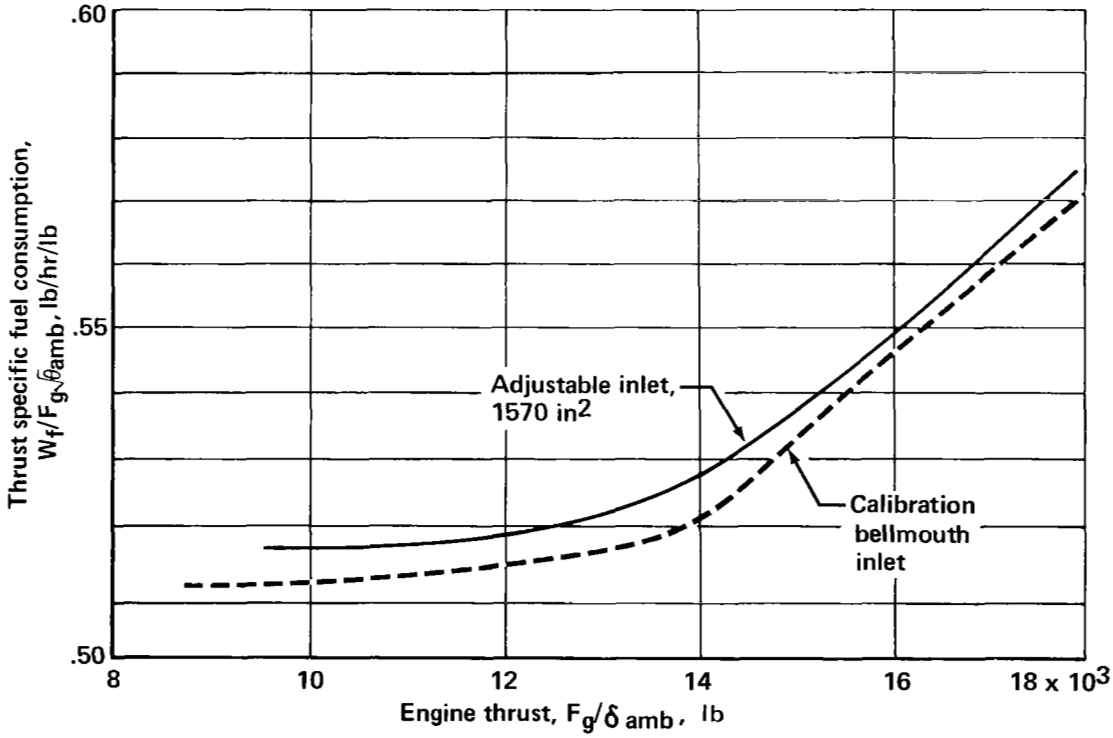

FIGURE 39.— THRUST SPECIFIC FUEL CONSUMPTION FOR ADJUSTABLE INLET IN TAKEOFF CONFIGURATION

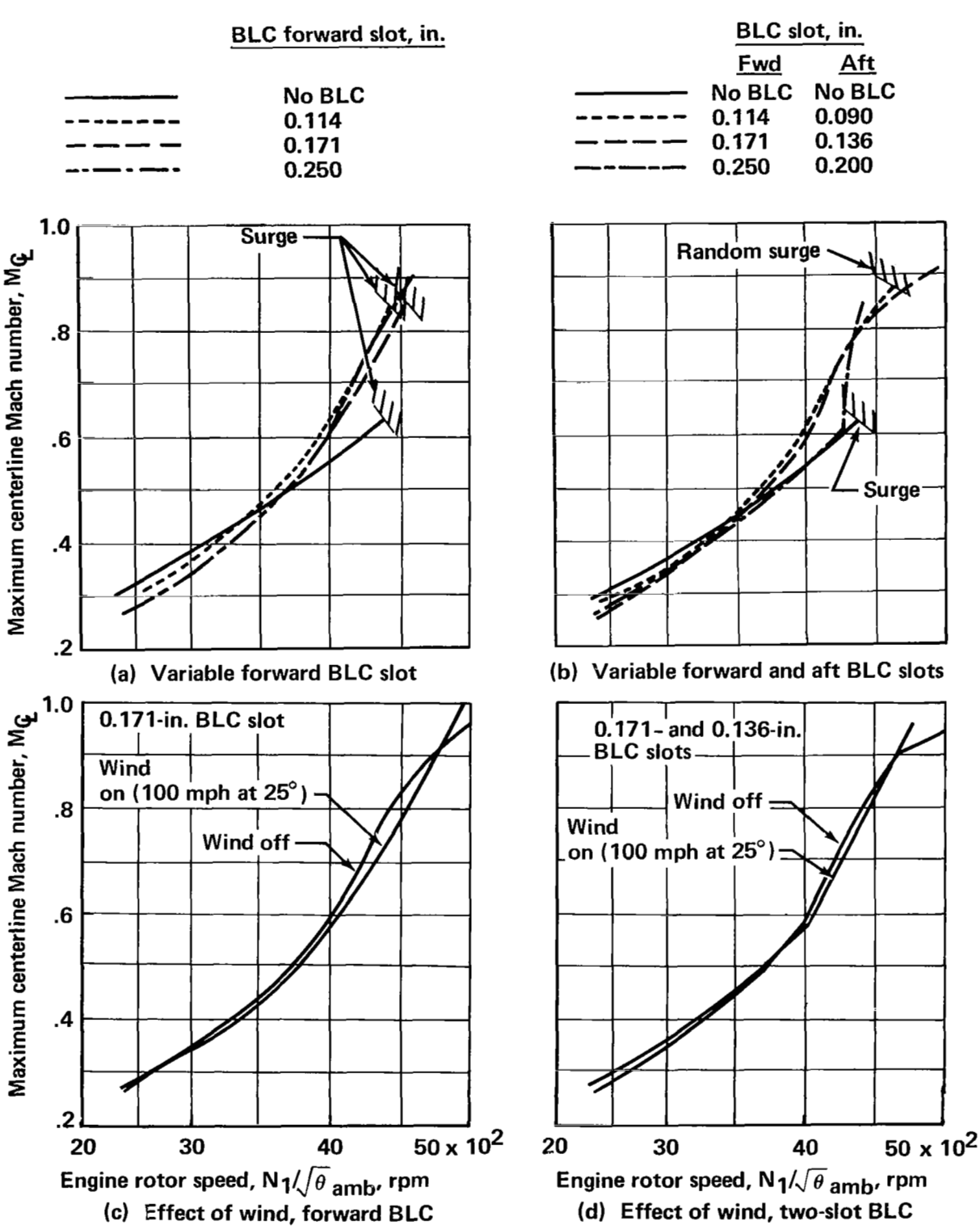

FIGURE 40.—EFFECT OF BLC SLOT CONFIGURATION AND WIND ON MAXIMUM CENTERLINE MACH NUMBERS OF NONADJUSTABLE INLET

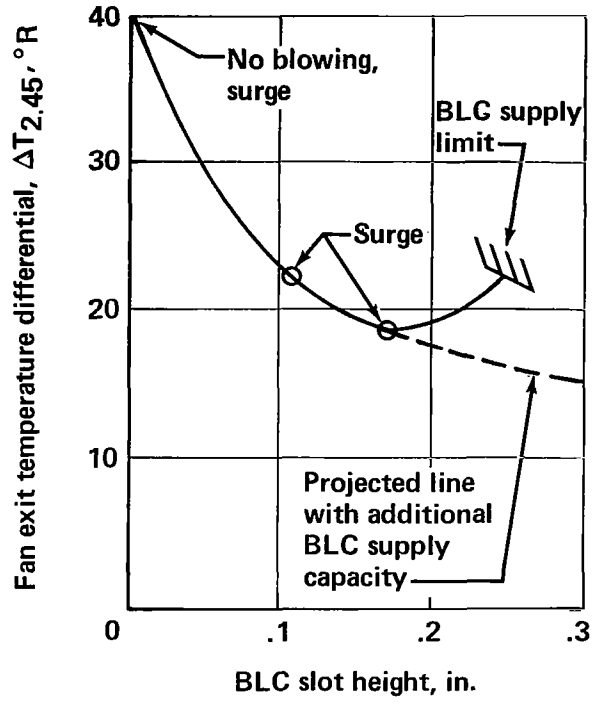

(a) Fan temperature differential

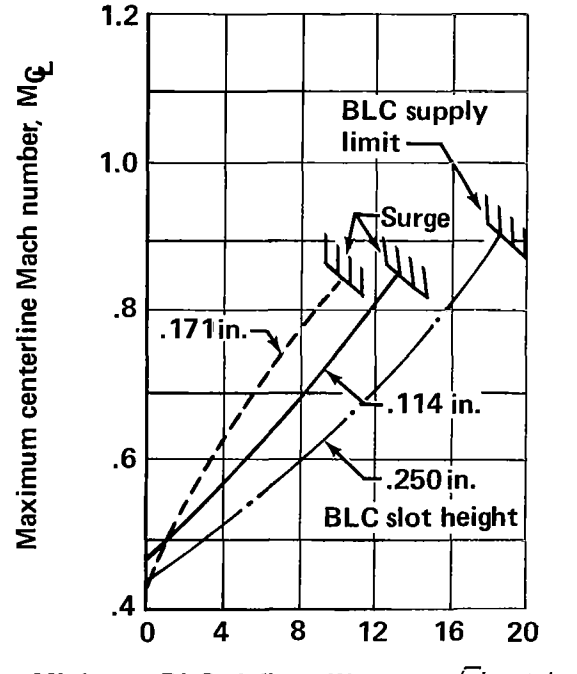

(b) Centerline Mach number

FIGURE 41.–EFFECT OF FORWARD BLC SLOT HEIGHT ON FAN EXIT TEMPERATURE DIFFERENTIALS, MACH NUMBERS, AND SURGE

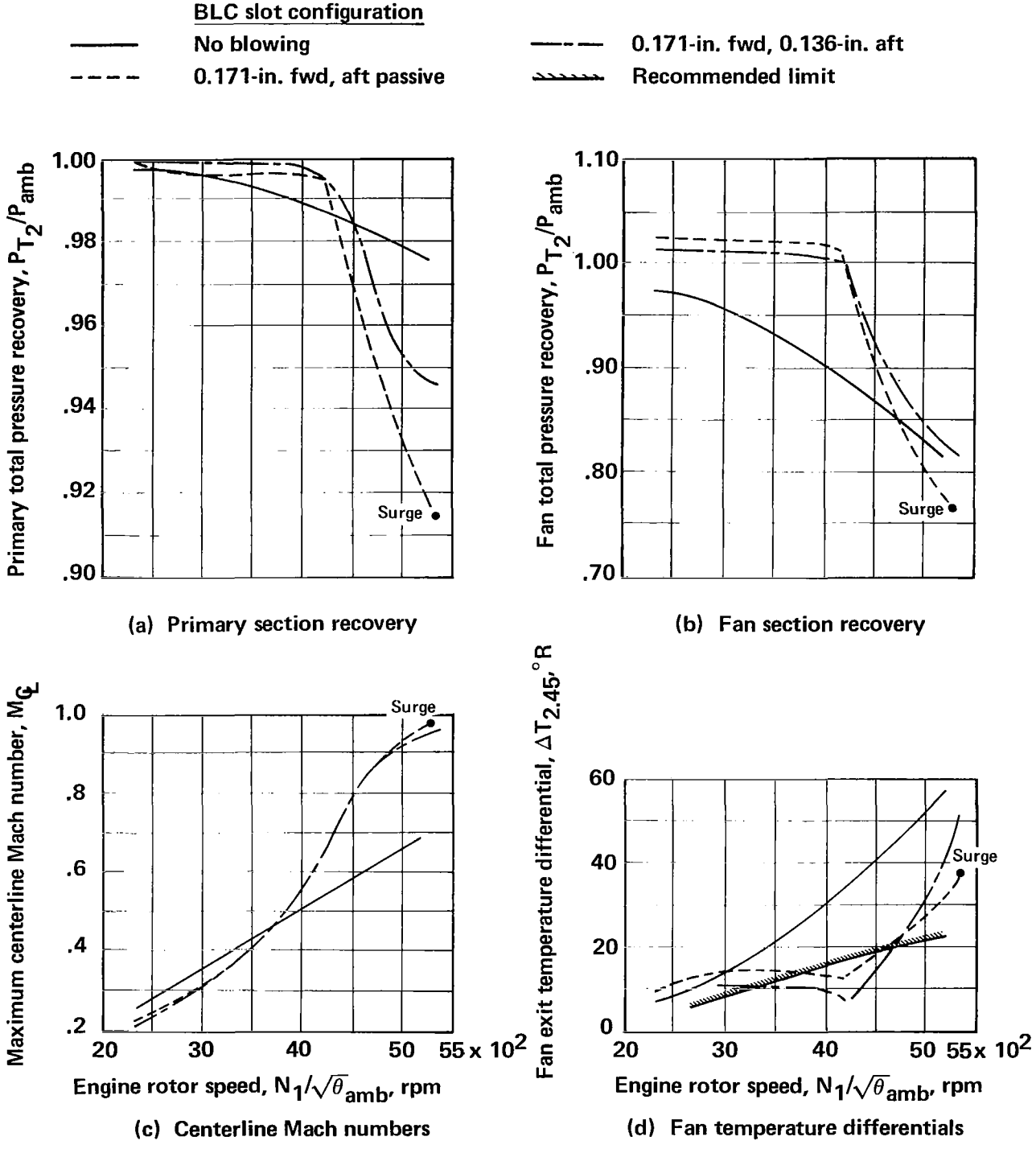

FIGURE 42.—EFFECT OF BLC SLOT LOCATION ON PRESSURE RECOVERY, MACH NUMBERS, FAN TEMPERATURE DIFFERENTIALS, AND SURGE (RESTRICTOR REMOVED)

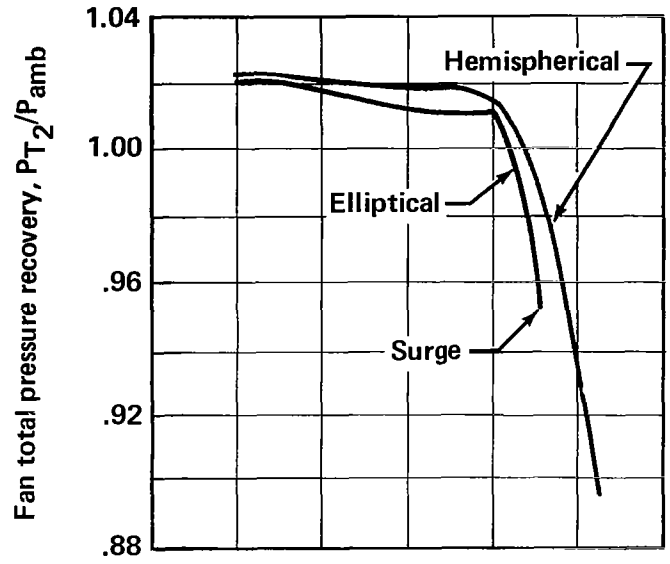

(a) Fan section recovery

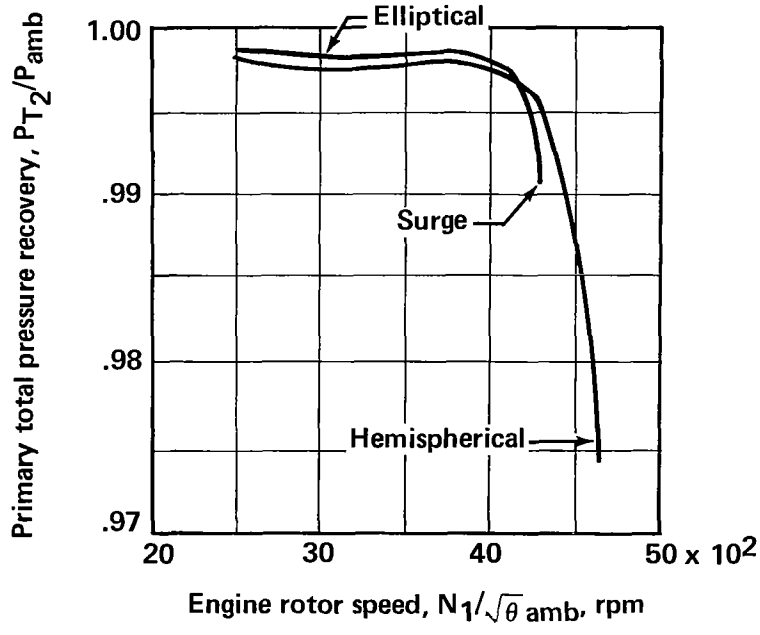

(b) Primary section recovery

FIGURE 43.—EFFECT OF CENTERBODY CONFIGURATION ON PRESSURE RECOVERY AND SURGE

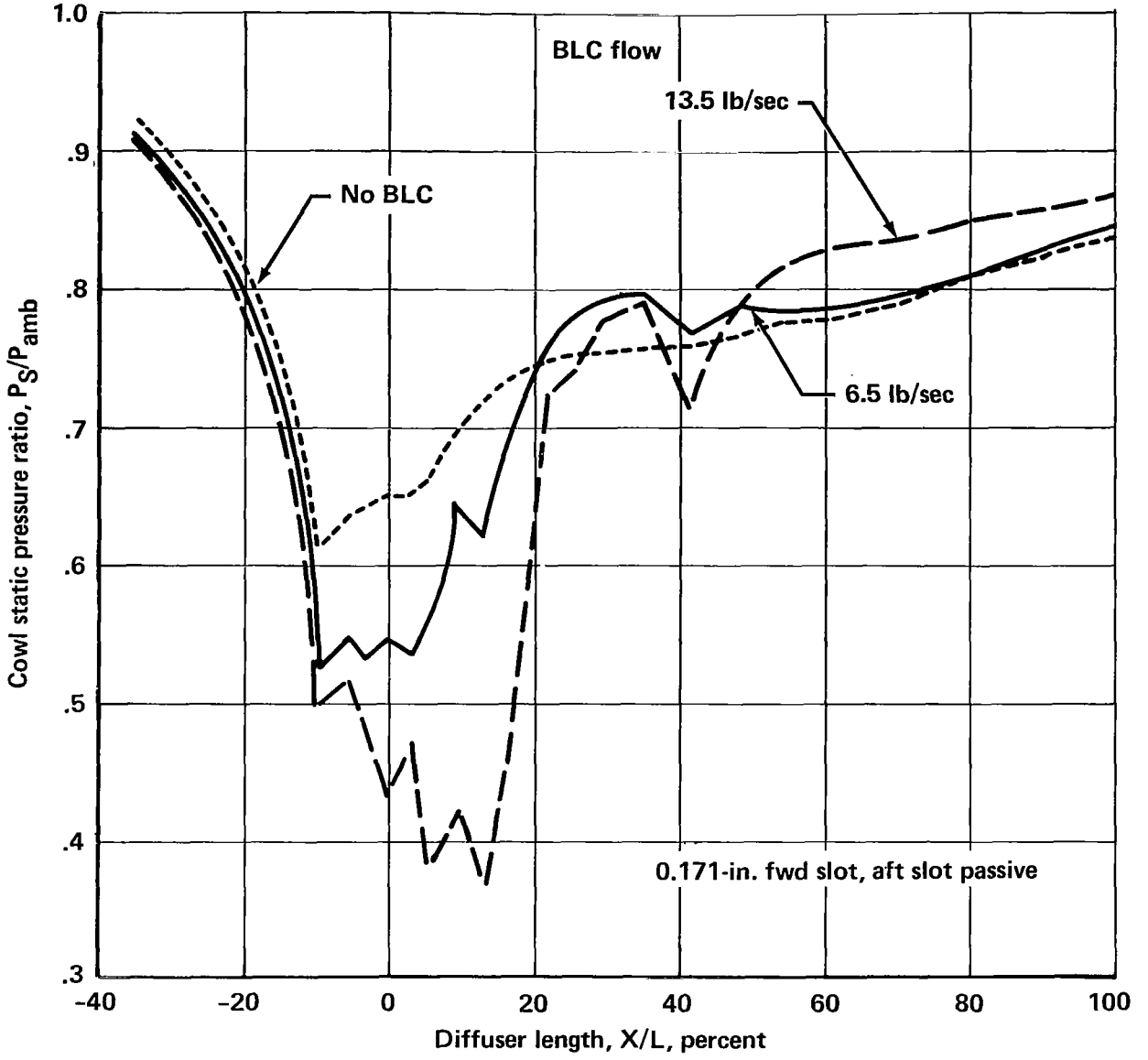

FIGURE 44.–STATIC PRESSURE RECOVERY FOR NONADJUSTABLE INLET, FORWARD BLC ONLY

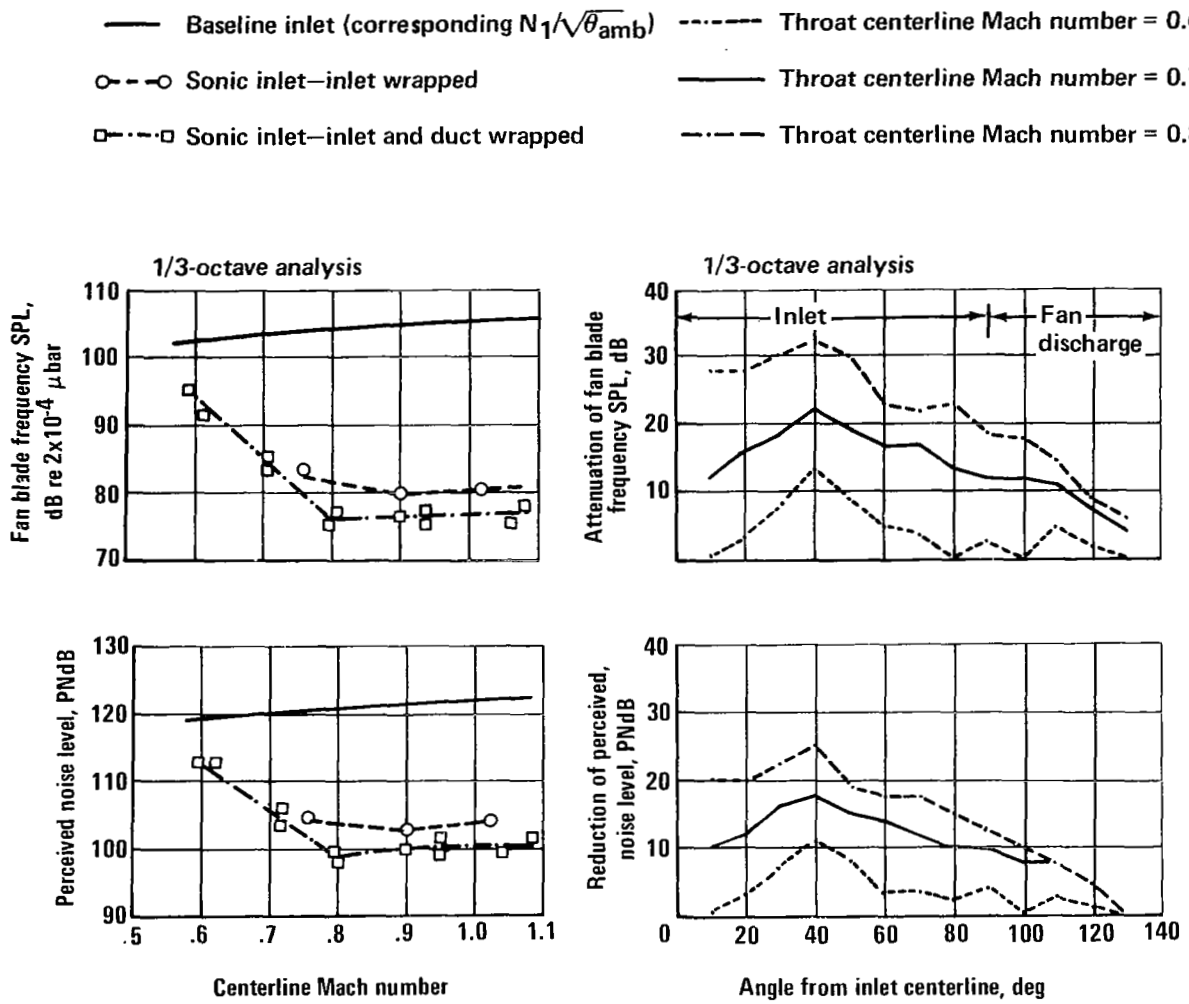

(a) Noise levels at 200-ft radius, 30° to inlet centerline, horizontal plane

(b) Attenuation of noise levels at 200-ft radius, inlet and duct wrapped

FIGURE 45.—ACOUSTIC CHARACTERISTICS OF FIVE-DOOR INLET IN LANDING APPROACH CONFIGURATION (928-IN^2 THROAT AREA)

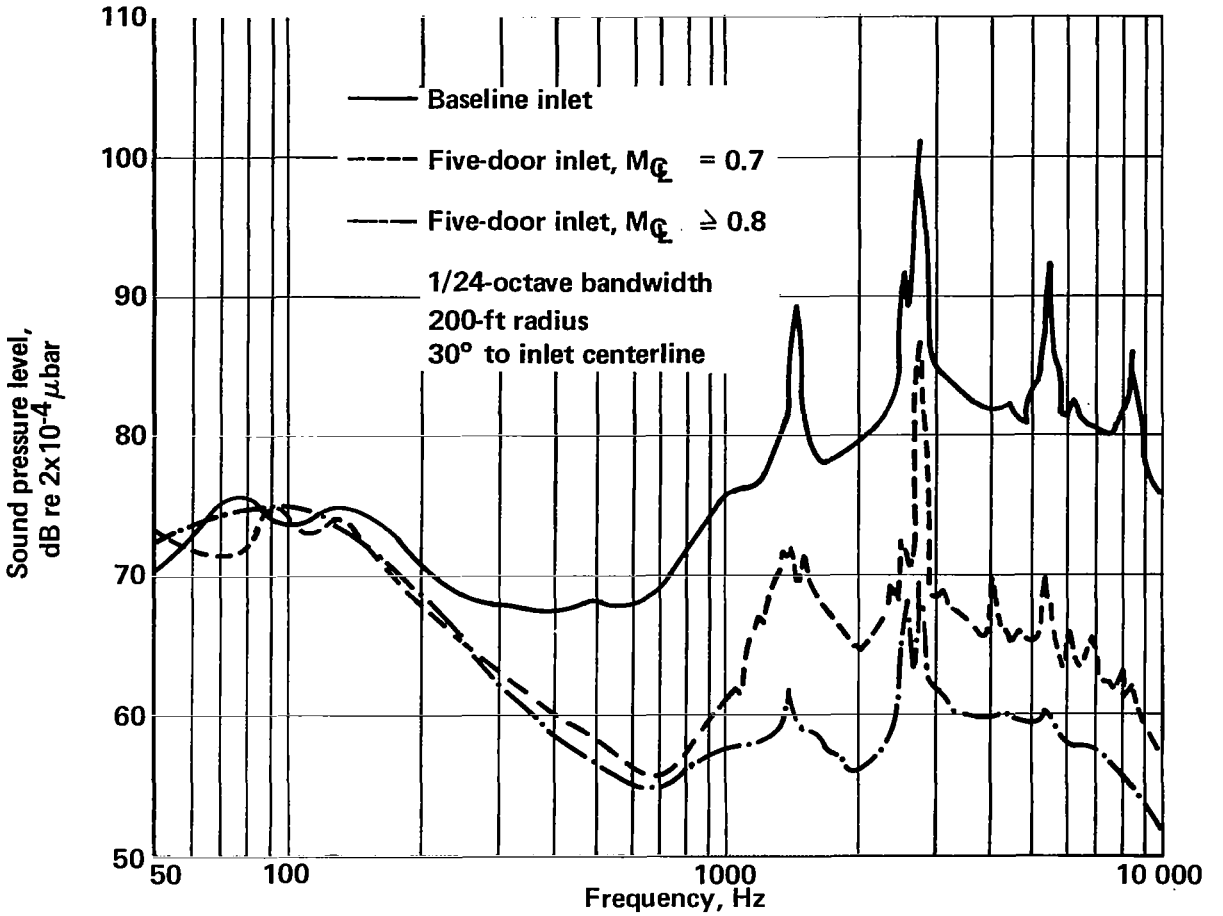

FIGURE 46.—ACOUSTIC SPECTRA OF FIVE-DOOR INLET IN LANDING APPROACH CONFIGURATION (928-IN^2 THROAT AREA)

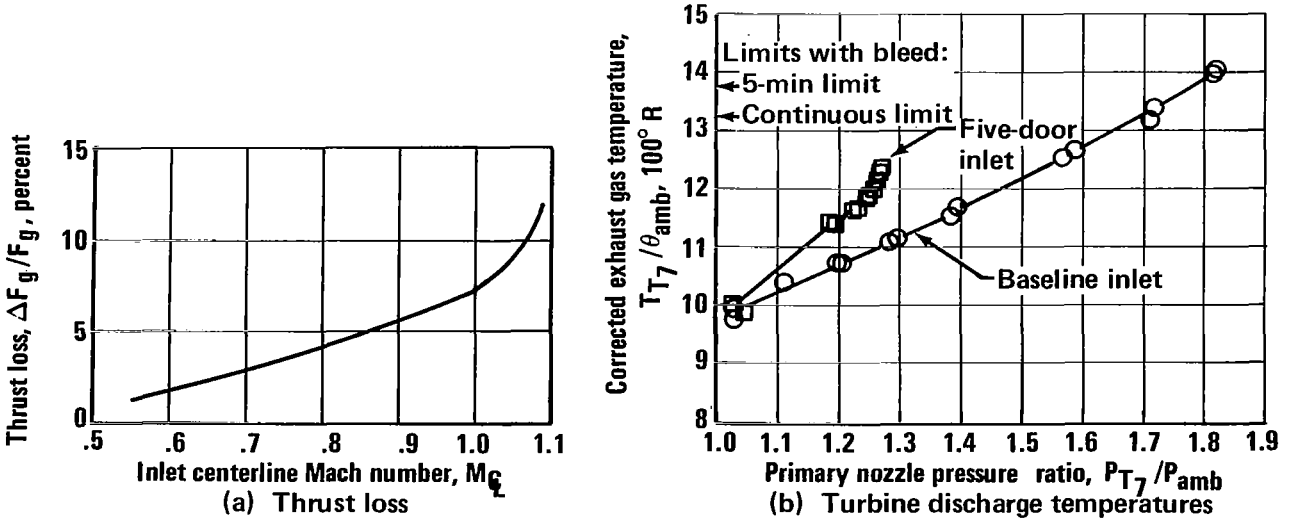

FIGURE 47.—THRUST AND TURBINE DISCHARGE TEMPERATURES FOR FIVE-DOOR INLET IN LANDING APPROACH CONFIGURATION (928-IN^2 THROAT AREA)

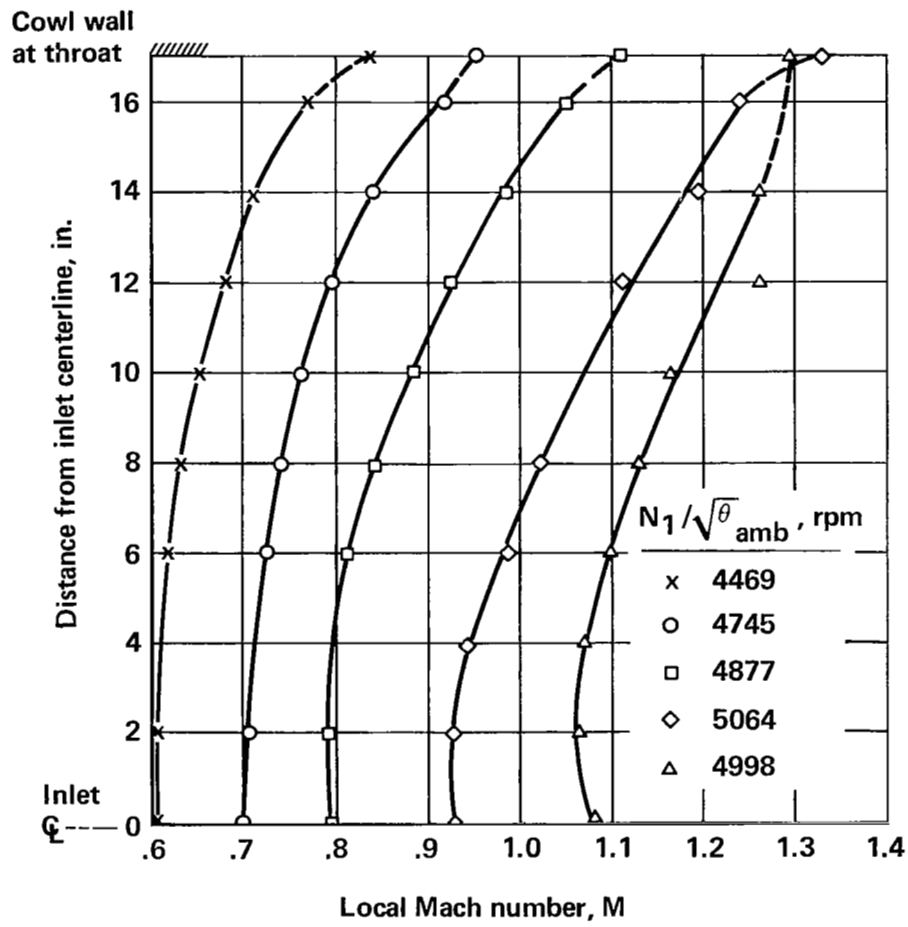

FIGURE 48.—RADIAL DISTRIBUTION OF MACH NUMBERS IN THE THROAT OF THE FIVE-DOOR INLET (928-IN^2 THROAT AREA)

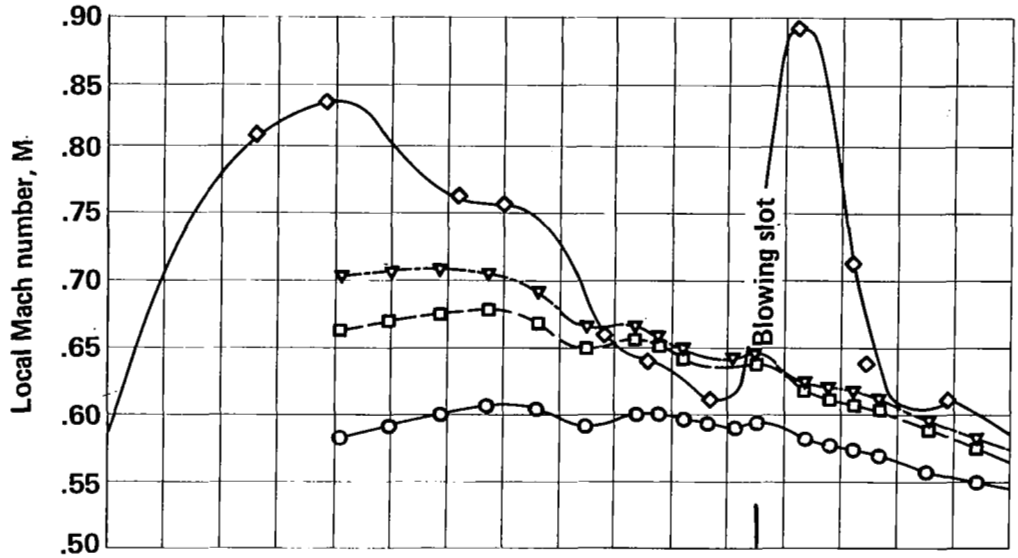

(a) Centerline Mach number of approximately 0.6

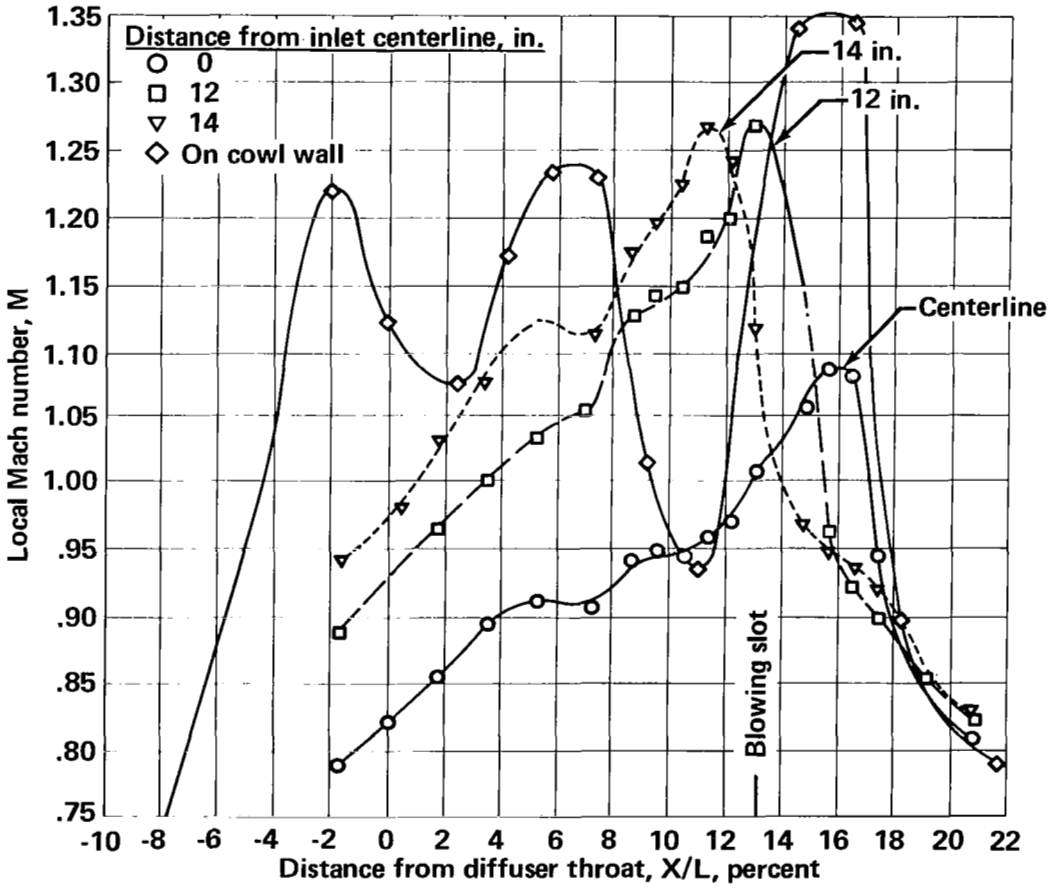

(b) Centerline Mach number of approximately 1.0

FIGURE 49.—AXIAL MACH NUMBER DISTRIBUTION IN THE THROAT OF THE FIVE-DOOR INLET (928-IN^2 THROAT AREA)

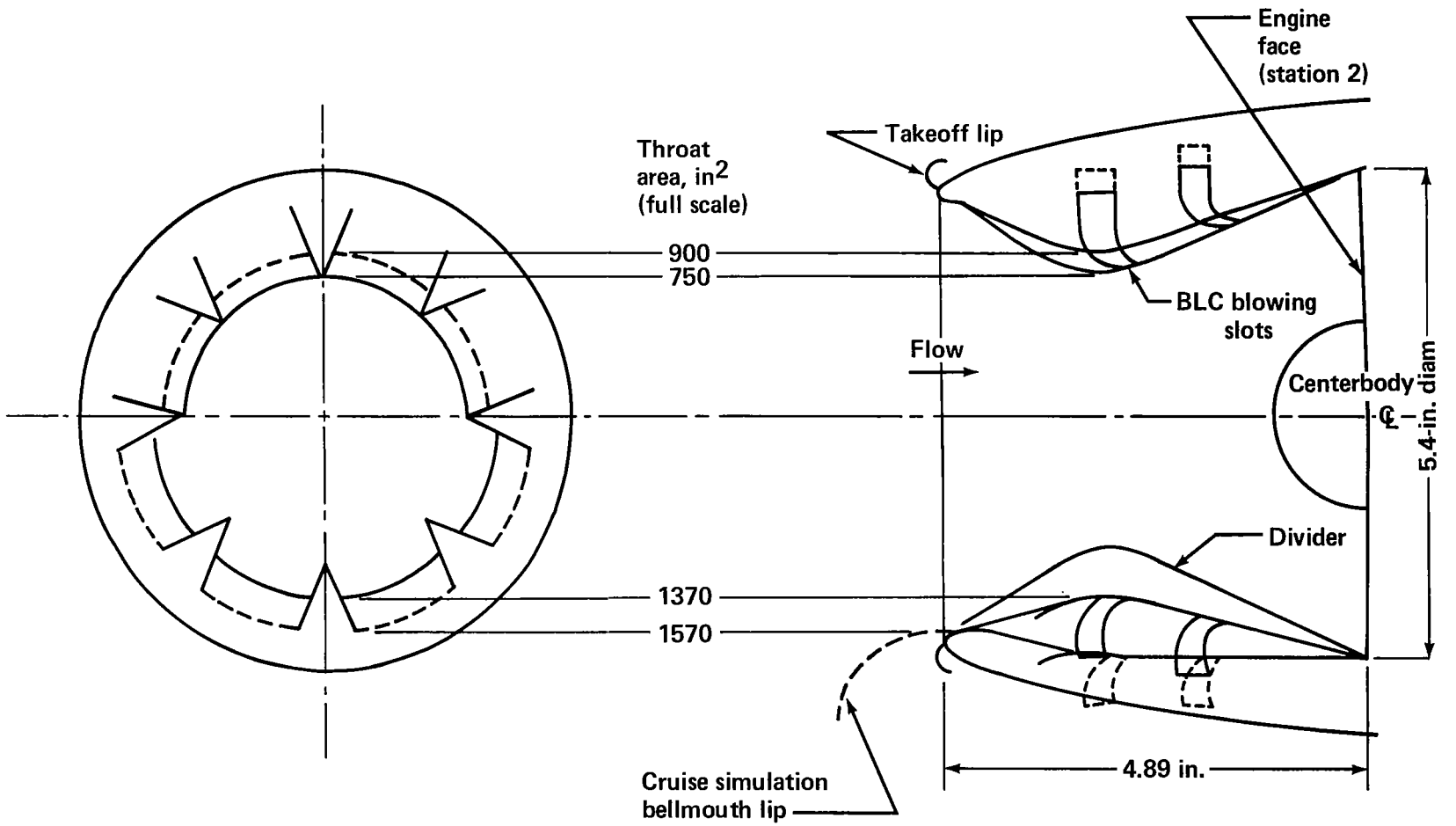

(a) Model cross sections

FIGURE A-1.– 1/9-SCALE ADJUSTABLE INLET MODELS

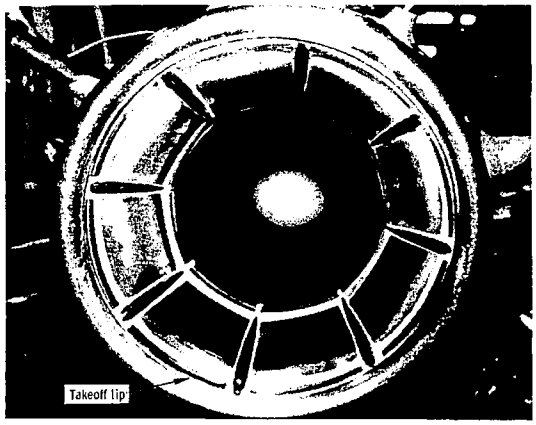

(b) Landing approach (750 in^2 full scale)

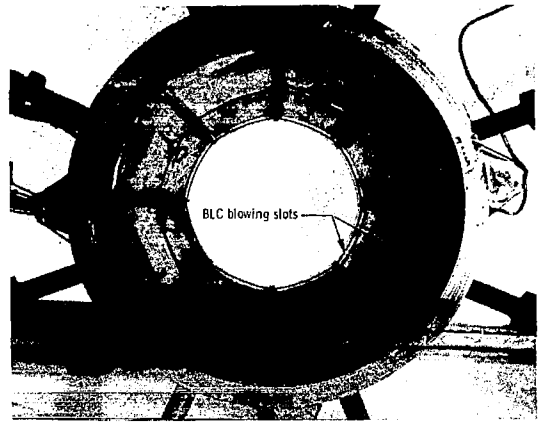

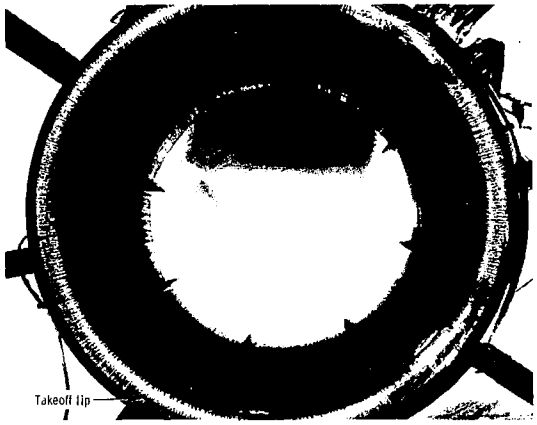

(c) Landing approach (900 in^2 full scale)

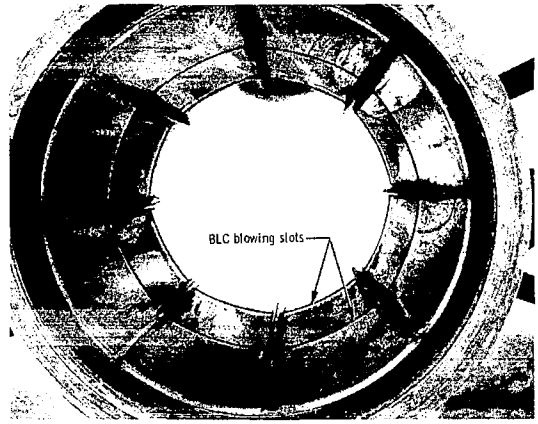

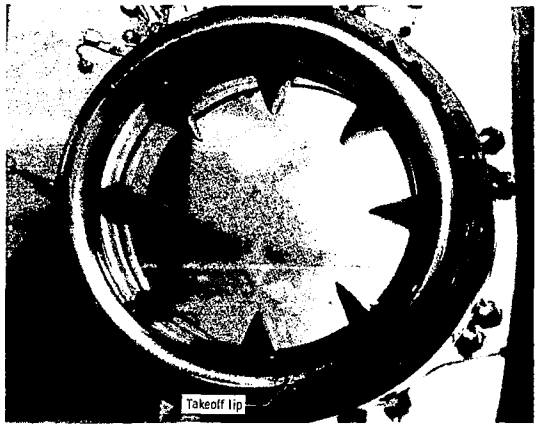

(d) Takeoff model (1370 in^2 full scale)

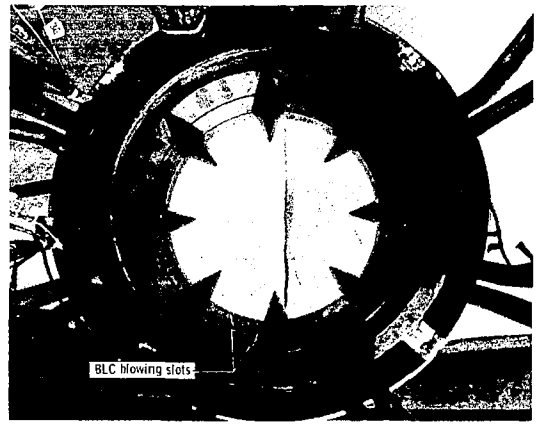

FRONT VIEWS *REAR VIEWS*

FIGURE A-1.– 1/9-SCALE ADJUSTABLE INLET MODELS–Continued

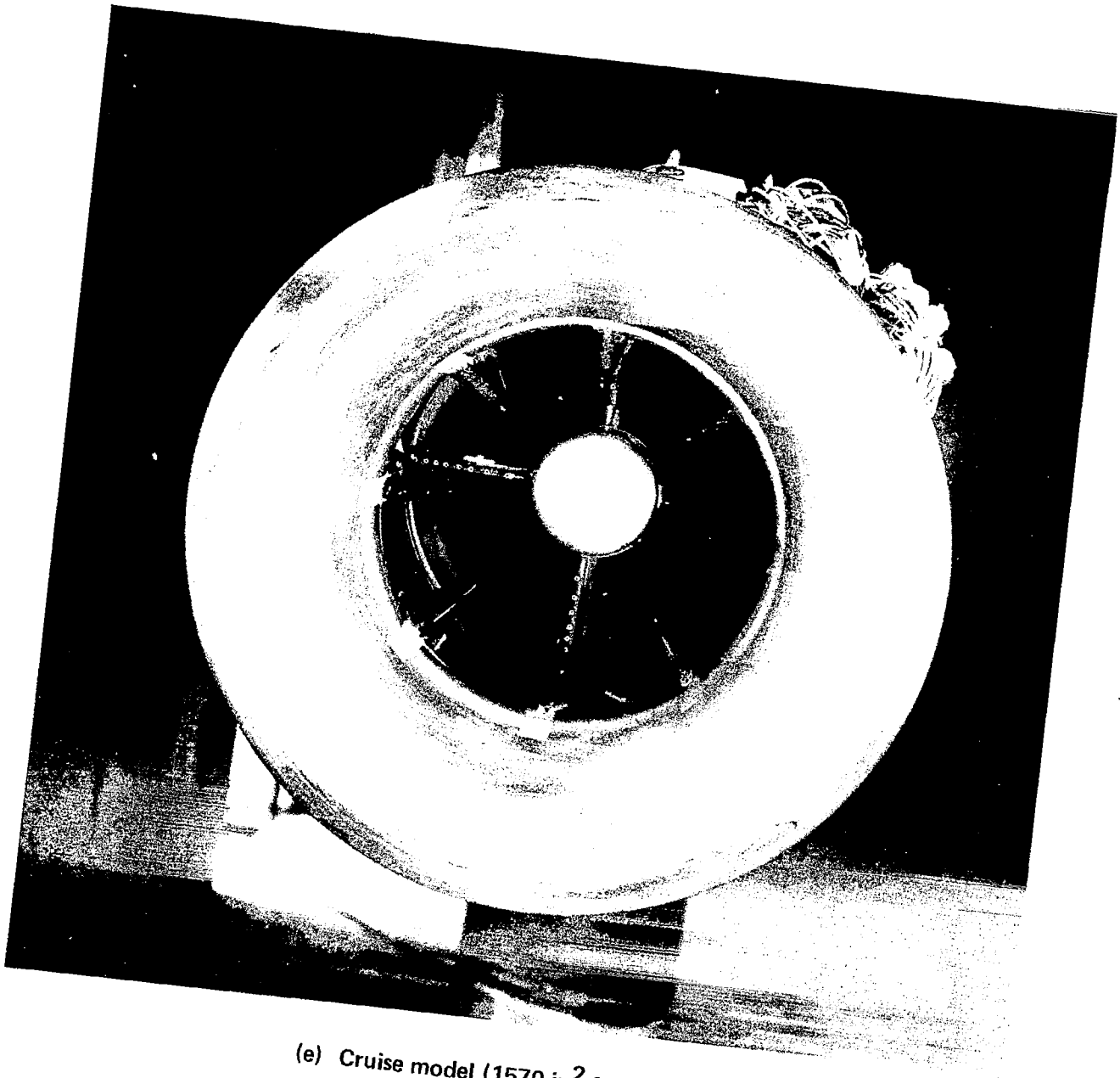

(e) Cruise model (1570 in^2 full scale)

FIGURE A-1.– 1/9-SCALE ADJUSTABLE INLET MODELS–Concluded

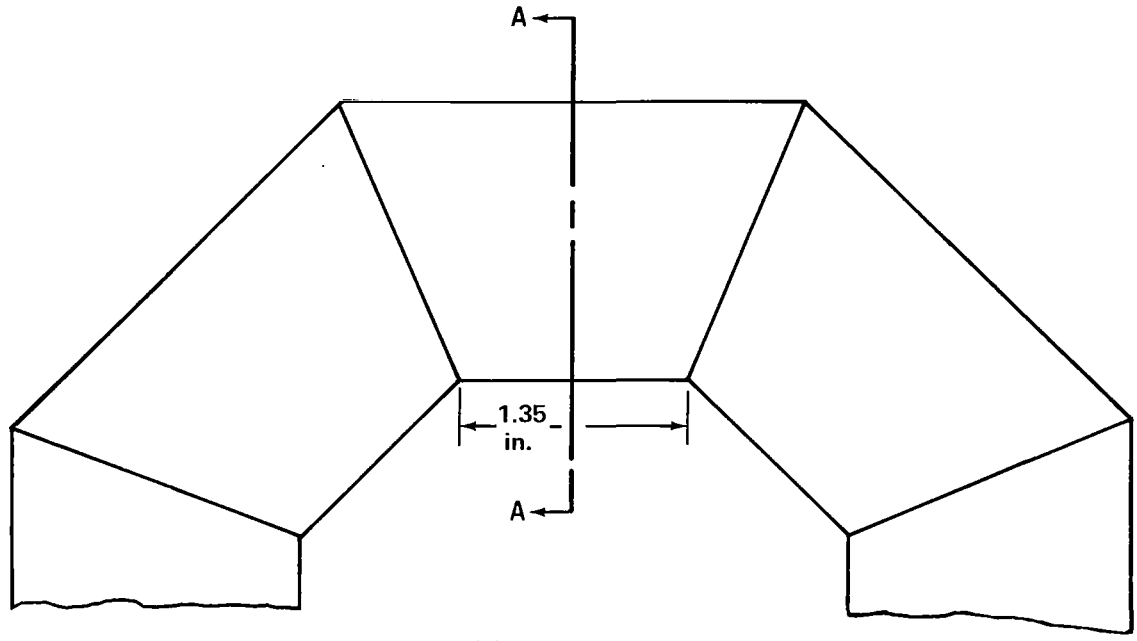

(a) Looking aft

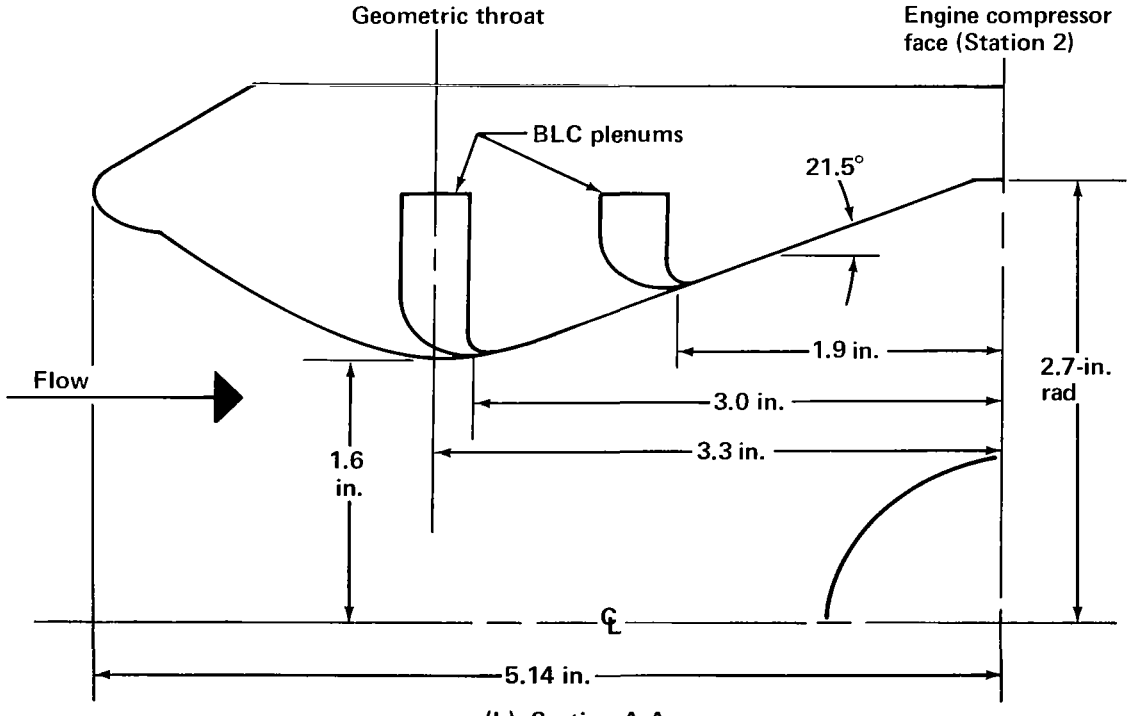

(b) Section A-A

FIGURE A-2.–1/9-SCALE NONADJUSTABLE INLET MODEL

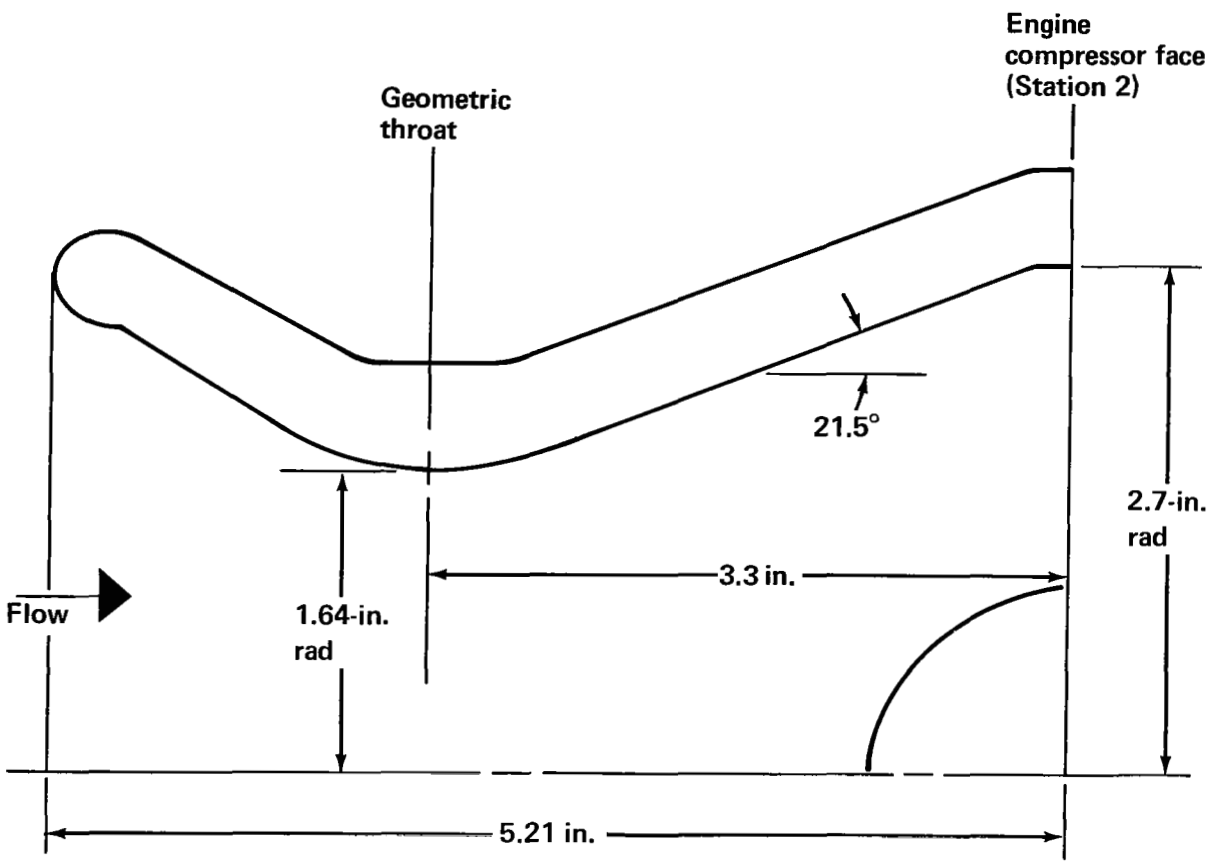

FIGURE A-3.—1/9-SCALE NON-BLC INLET MODEL

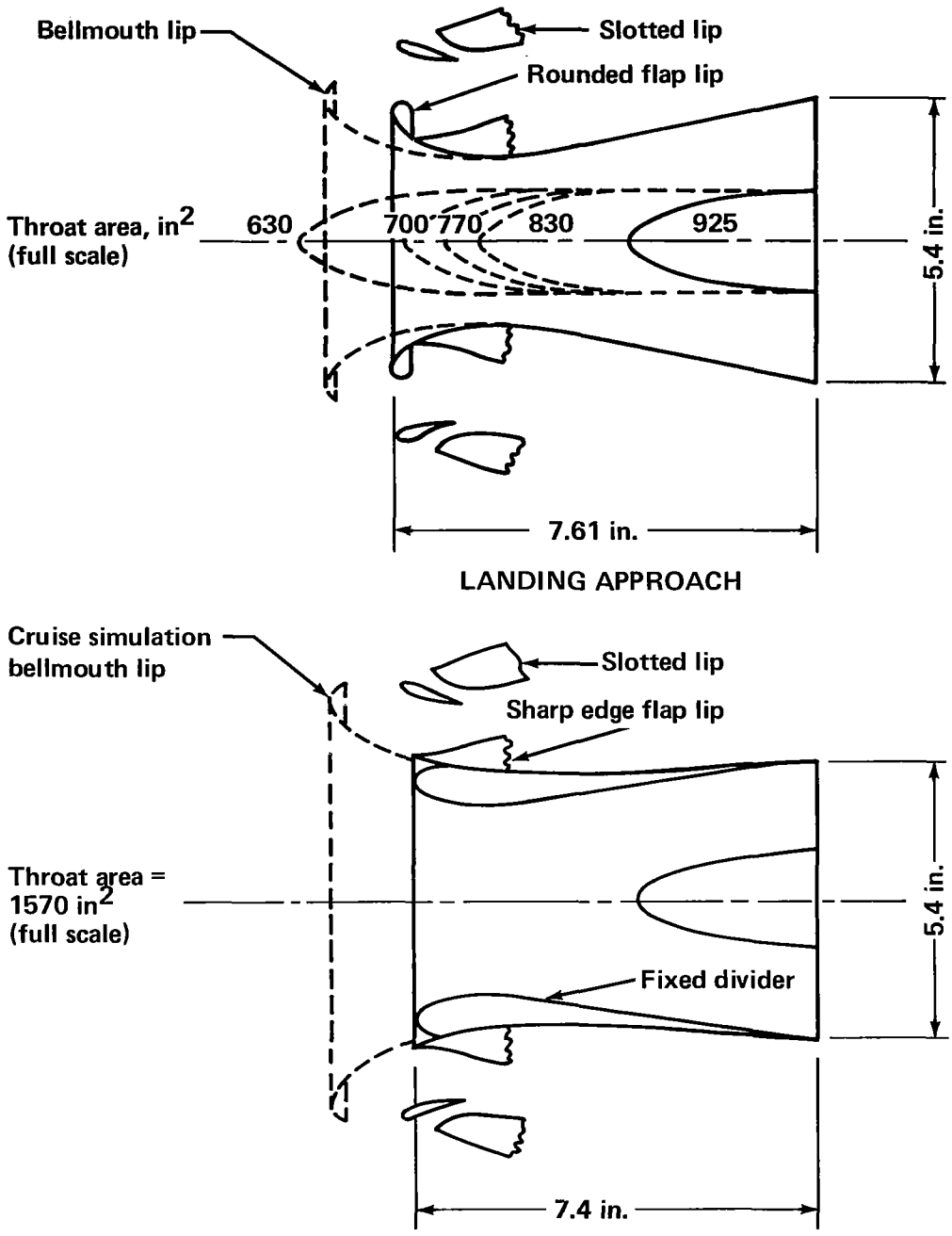

(a) Model cross sections

FIGURE A-4.—1/9-SCALE FIVE-DOOR INLET MODELS

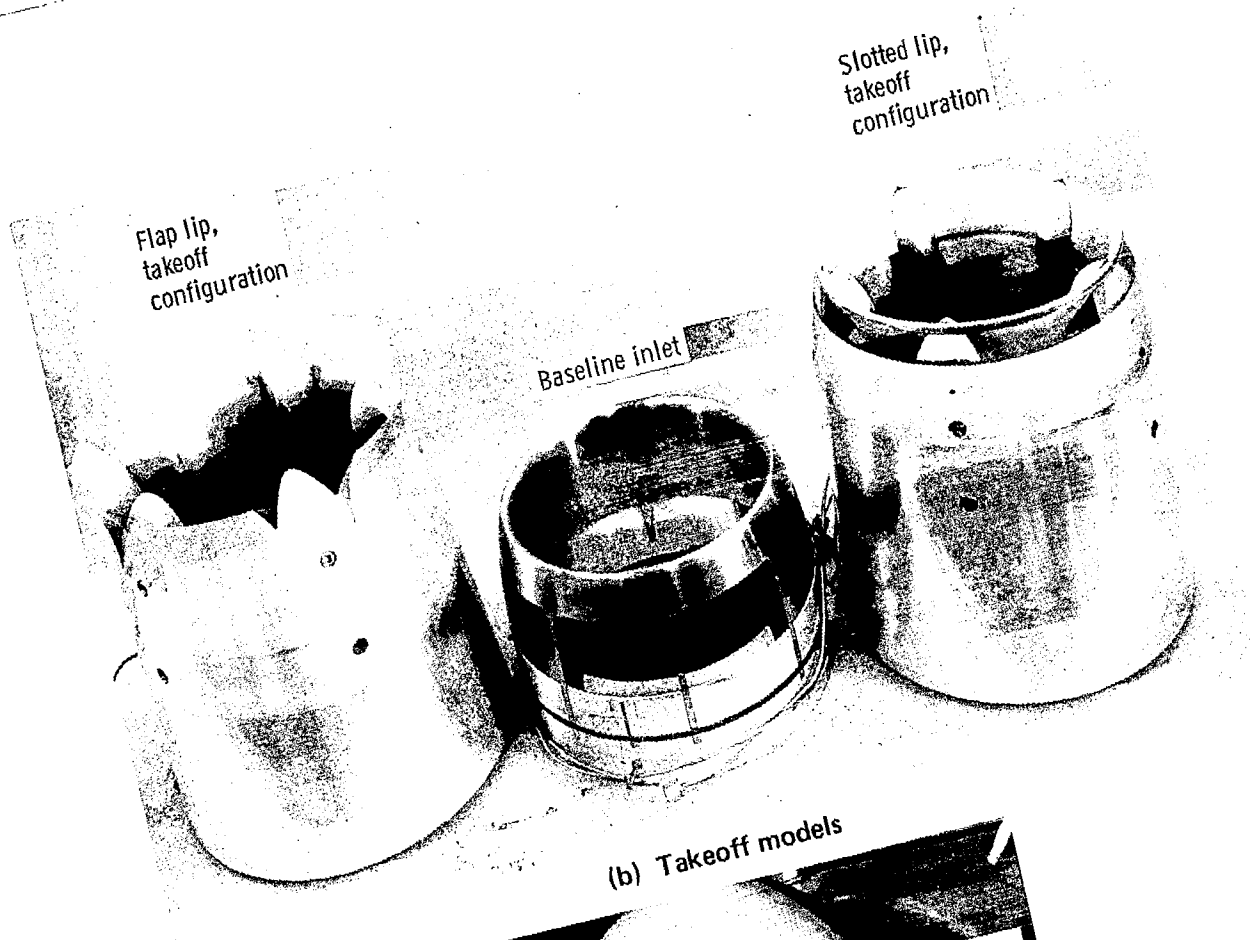

(b) Takeoff models

...nd centerbody

...ODELS—Concluded

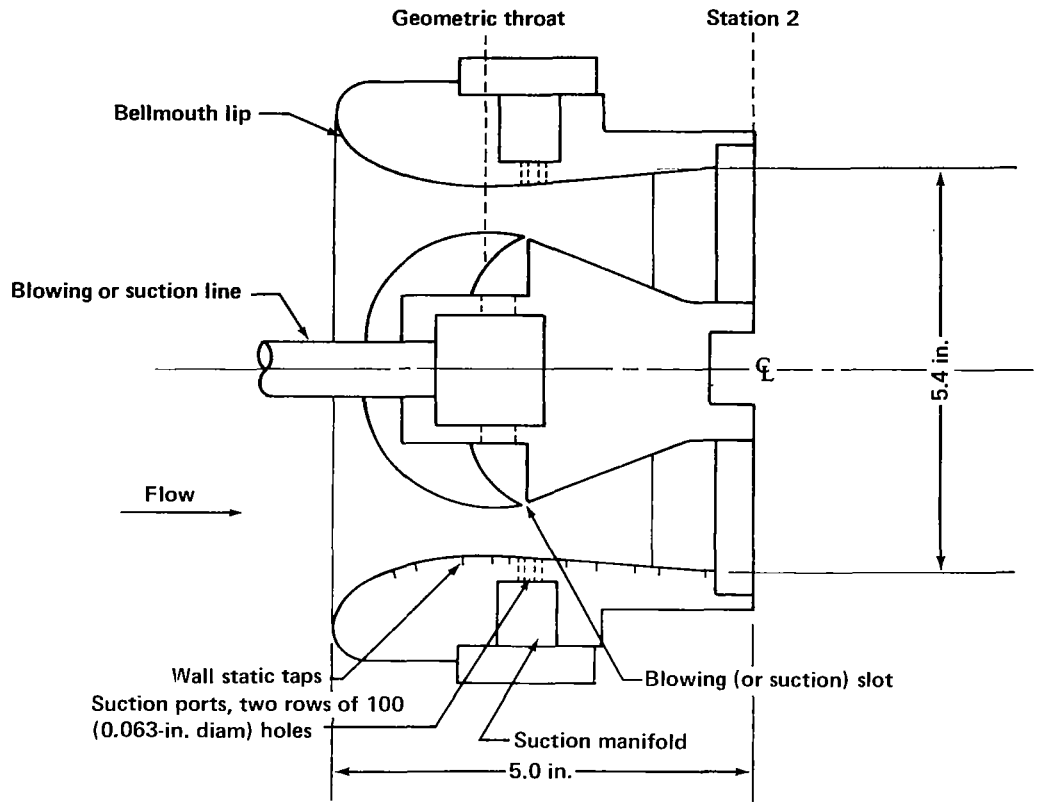

FIGURE A-5.–1/9-SCALE EXPANDING CENTERBODY INLET MODEL

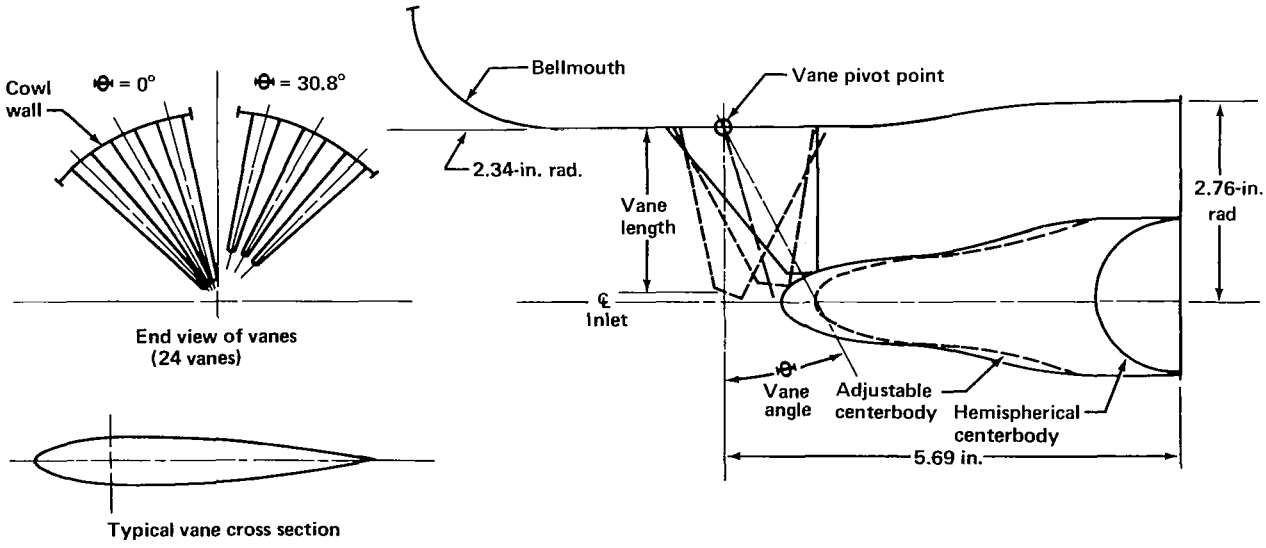

FIGURE A-6.–1/9-SCALE RADIAL VANE INLET MODEL

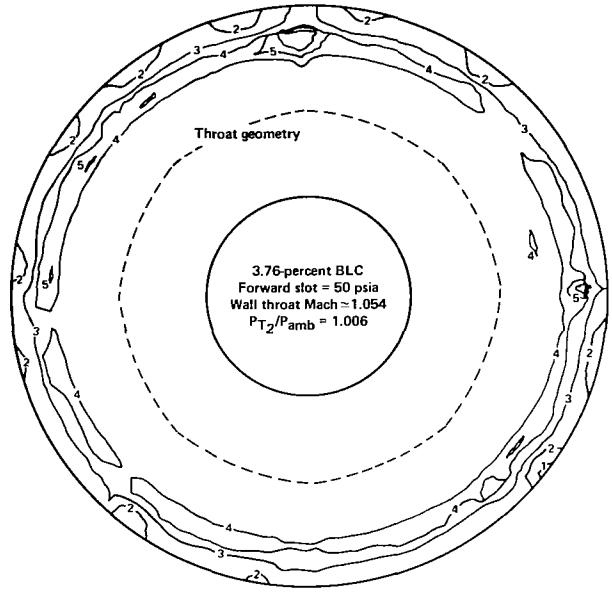

	Pressure recovery
1	1.10
2	1.06
3	1.02
4	0.998
5	0.994

(a) Diffuser exit total pressure distribution, with BLC

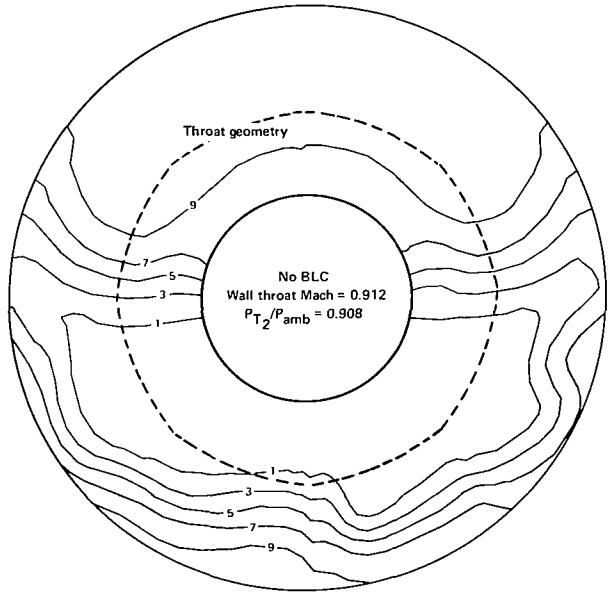

	Pressure recovery
1	0.99
3	0.96
5	0.92
7	0.88
9	0.84

(b) Diffuser exit total pressure distribution, no BLC

FIGURE A-7.–TOTAL PRESSURE DISTRIBUTIONS FOR ADJUSTABLE INLET MODEL (750-IN^2 THROAT AREA SIMULATION)

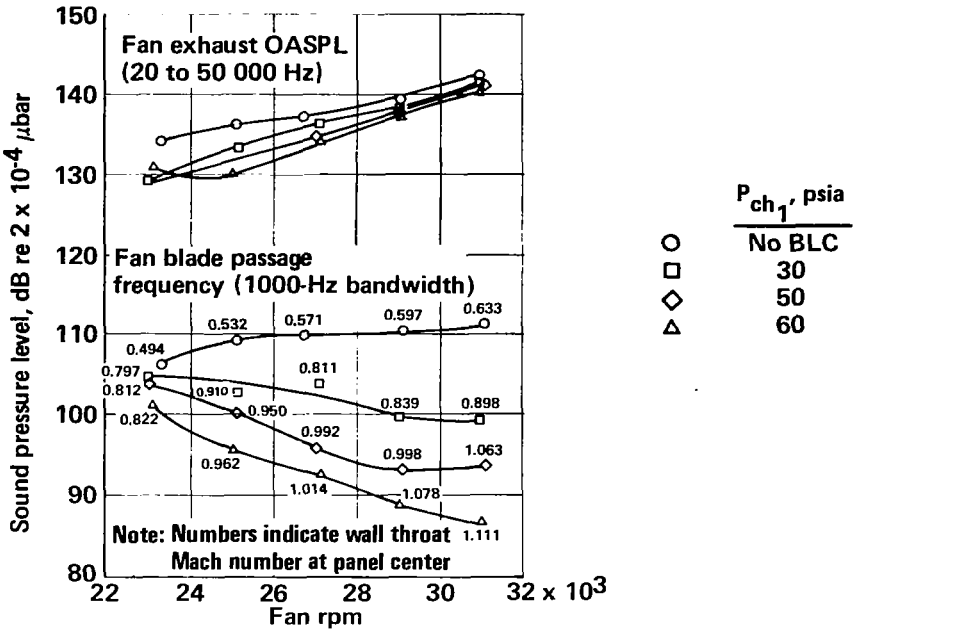

(a) Attenuation characteristics

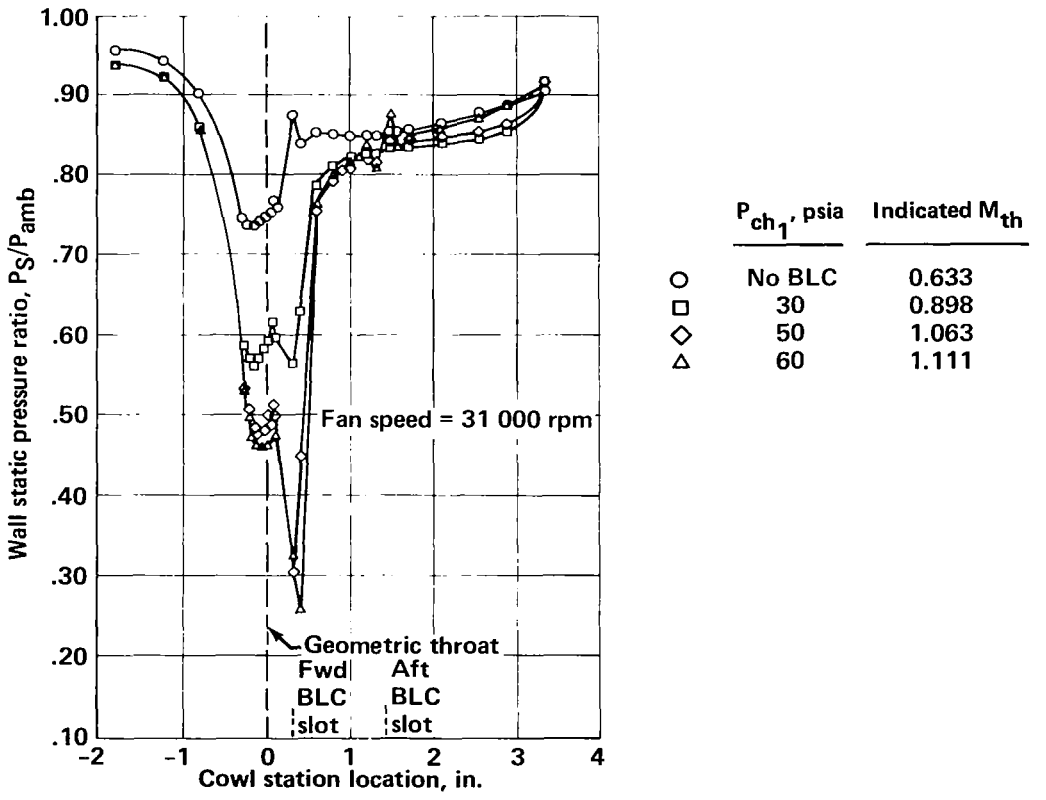

(b) Static pressure recovery

FIGURE A-8.—ATTENUATION AND STATIC PRESSURE RECOVERY OF ADJUSTABLE INLET MODEL (750-IN^2 THROAT AREA SIMULATION)

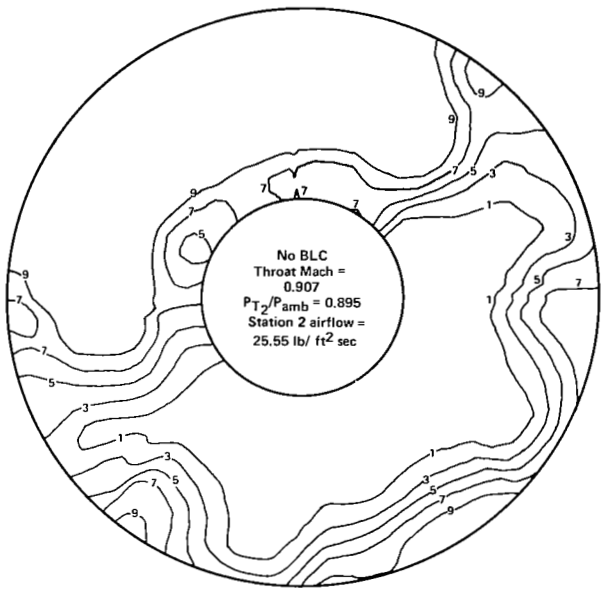

	Pressure recovery
1	0.99
3	0.96
5	0.92
7	0.88
9	0.84

(a) Diffuser exit pressure distribution, no BLC

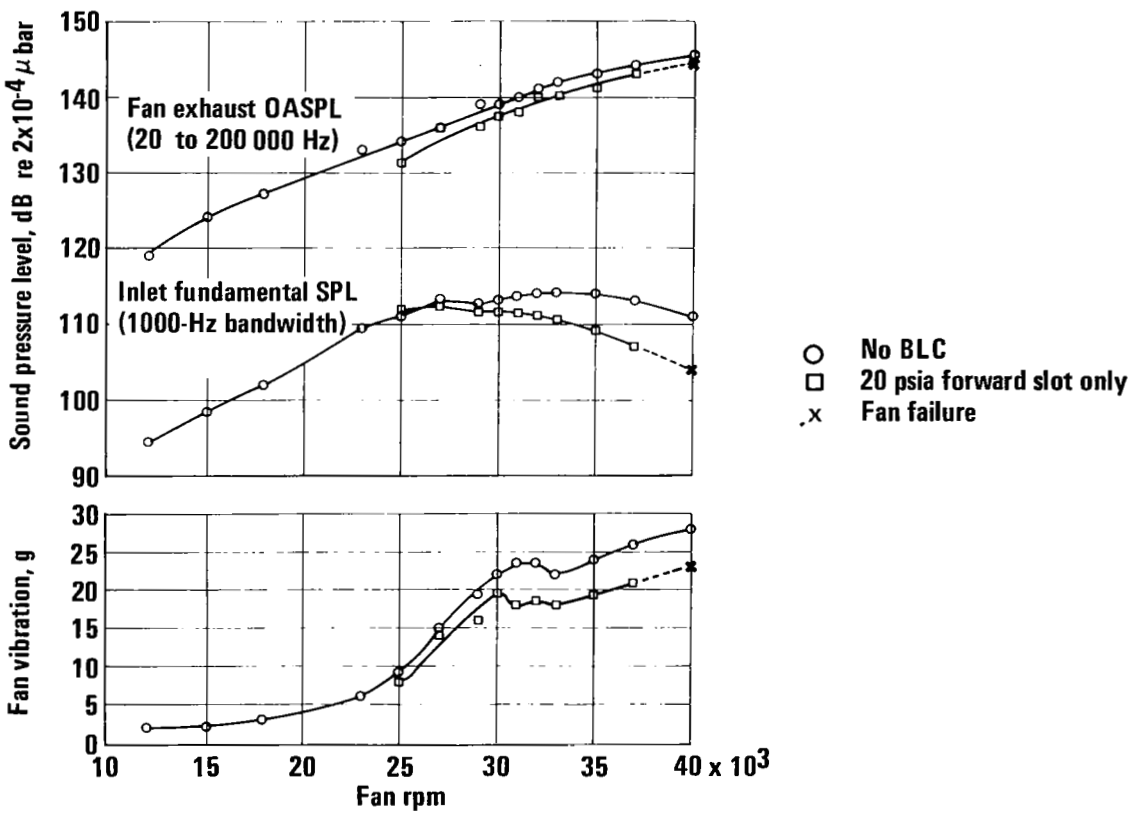

(b) Acoustic and vibration measurements

FIGURE A-9.–ACOUSTIC AND AERODYNAMIC CHARACTERISTICS OF ADJUSTABLE INLET MODEL (900-IN^2 THROAT AREA SIMULATION)

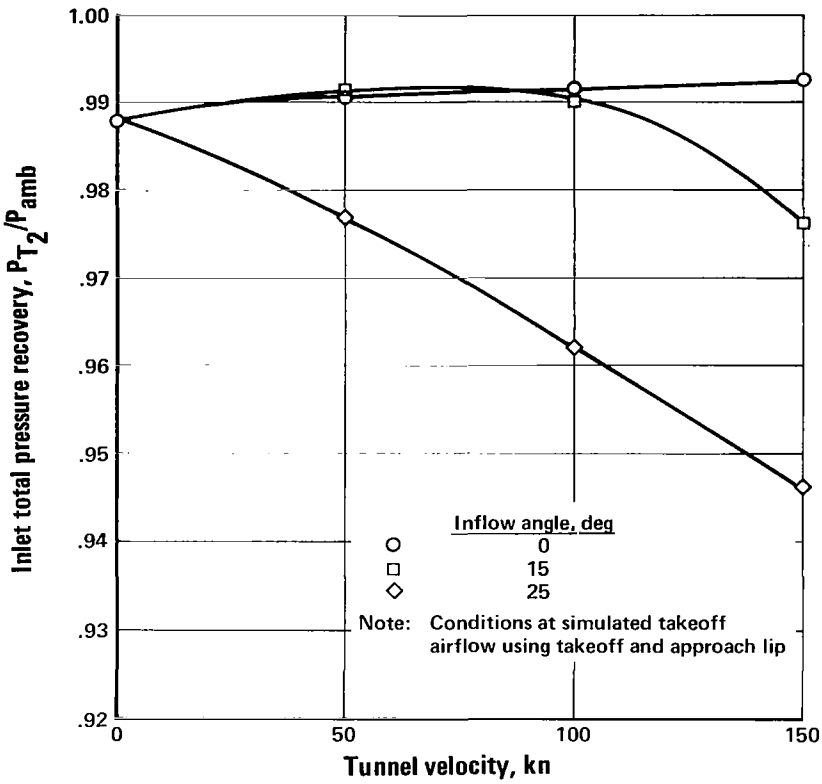

(a) Various inflow angles

	Pressure recovery
1	0.99
2	0.98
3	0.96
4	0.94

(b) Diffuser exit pressure distribution at 0°, 150 kn

FIGURE A-10.—TOTAL PRESSURE RECOVERY OF ADJUSTABLE INLET MODEL IN TAKEOFF CONFIGURATION WITH 1570-IN^2 THROAT AREA SIMULATION

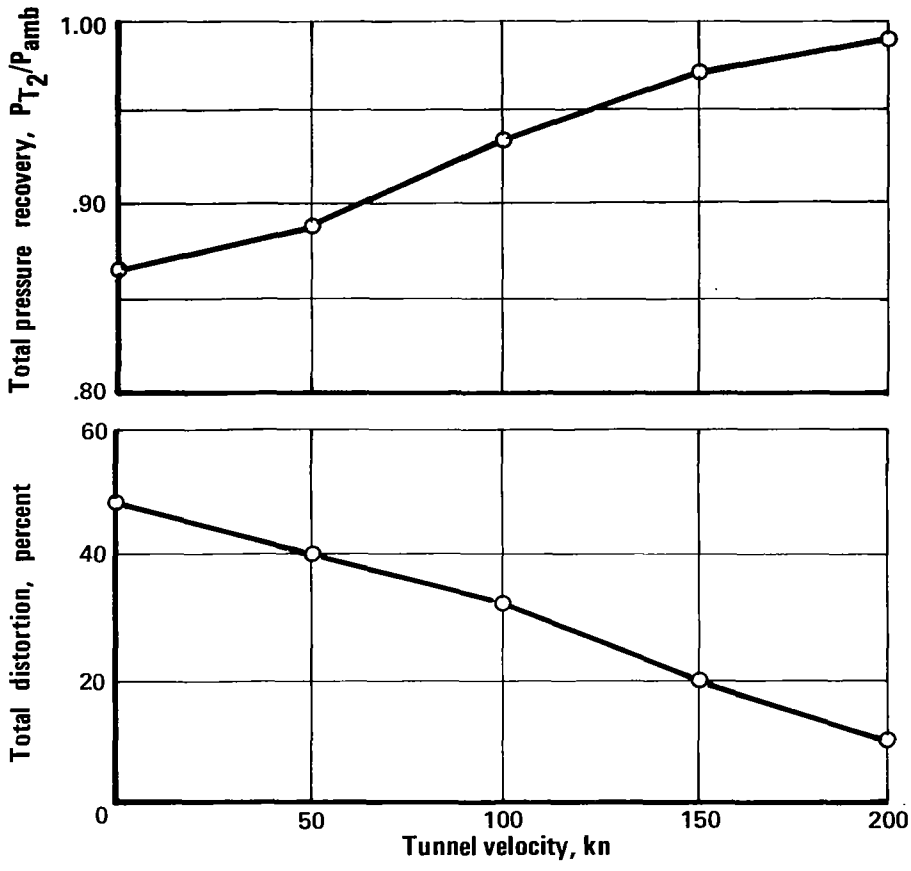

(a) Small-radius cruise lip

	Pressure recovery
1	0.99
2	0.98
3	0.96
4	0.94

(b) Cruise simulation bellmouth

FIGURE A-11.—TOTAL PRESSURE RECOVERY OF ADJUSTABLE INLET MODEL AT SIMULATED CRUISE CONDITIONS

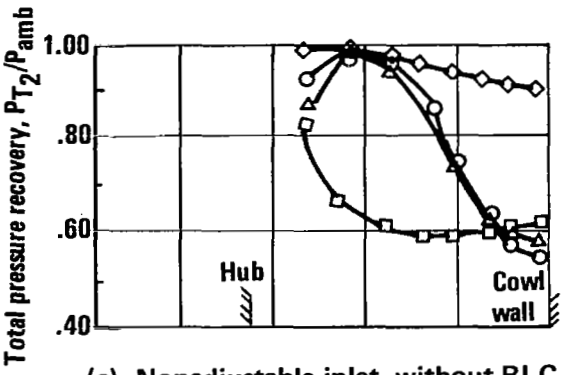

(a) Nonadjustable inlet, without BLC

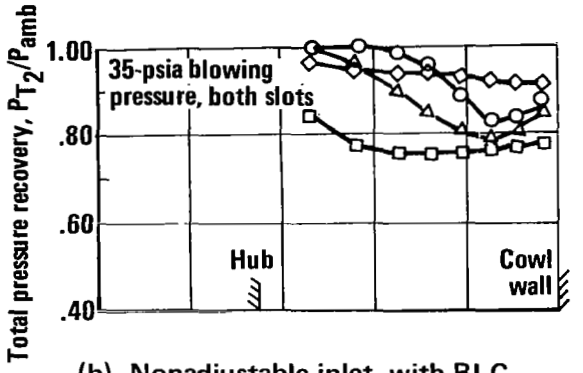

(b) Nonadjustable inlet, with BLC

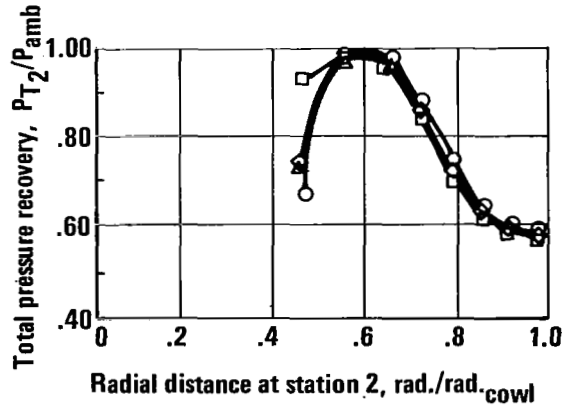

(c) Non-BLC inlet

Rake position, deg
○ 0
□ 90
◇ 180
△ 270

Choked condition

FIGURE A-12. –TOTAL PRESSURE RECOVERY OF NONADJUSTABLE AND NON-BLC INLET MODELS

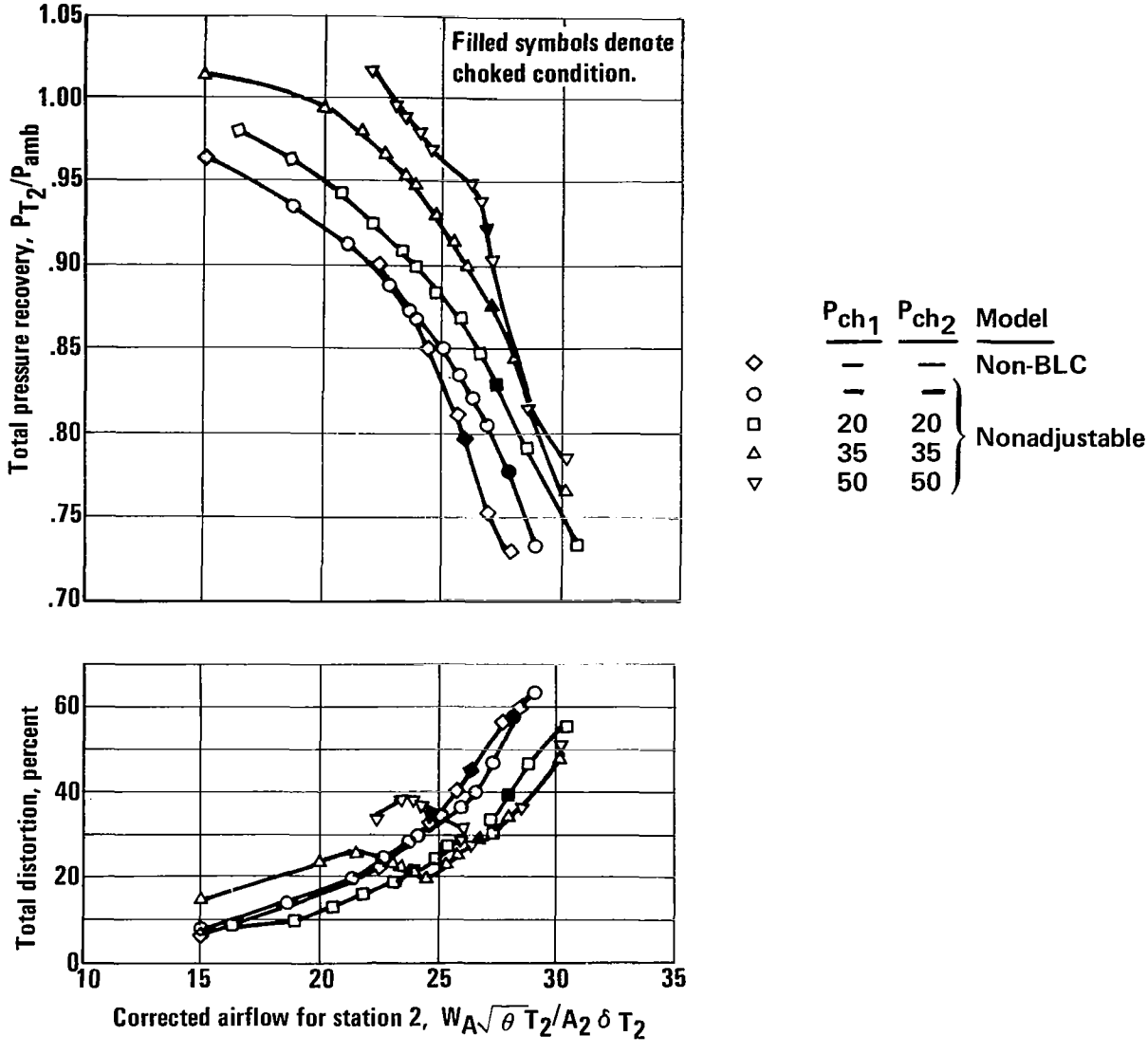

(d) Effect of varying BLC pressure

FIGURE A-12.—TOTAL PRESSURE RECOVERY OF NONADJUSTABLE AND NON-BLC INLET MODELS—Continued

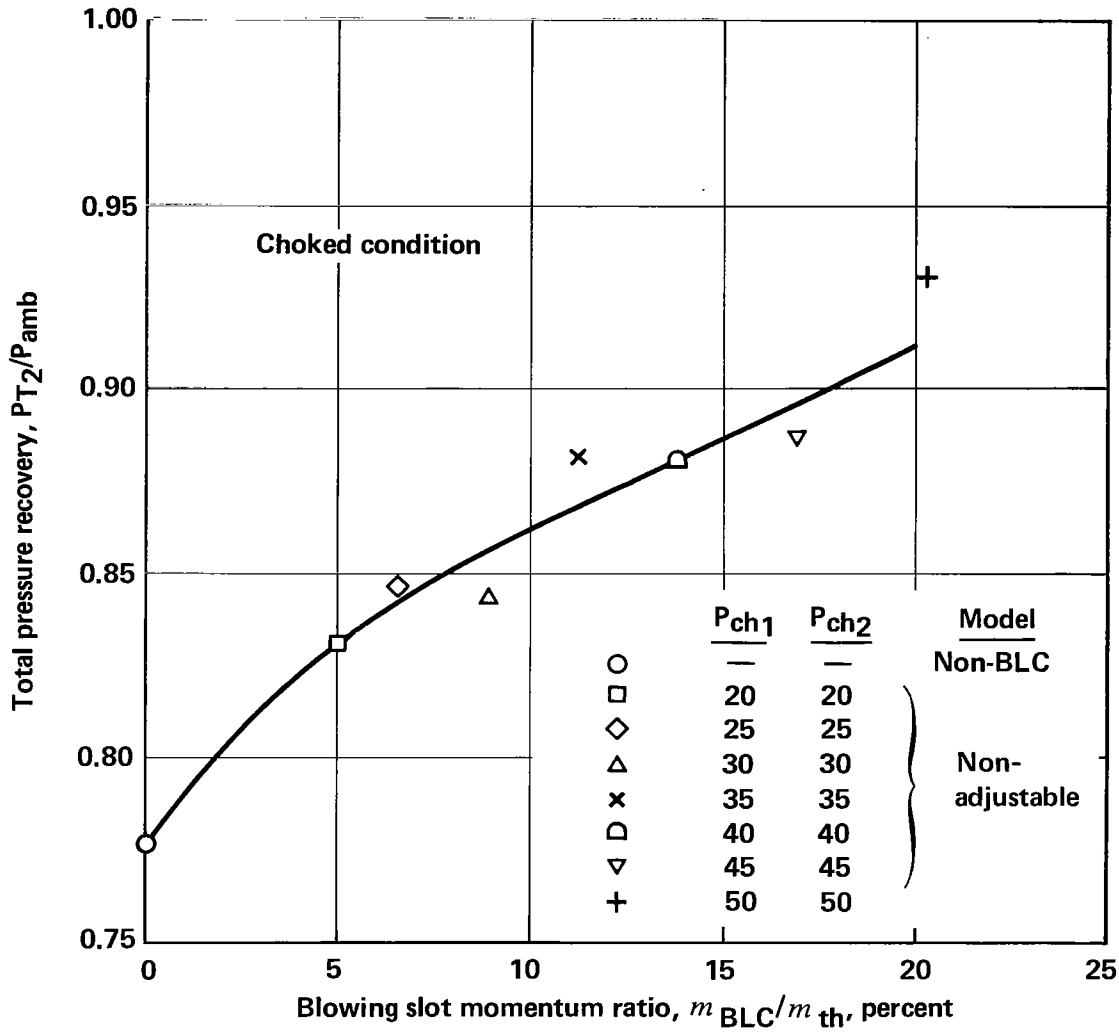

(e) Effect of blowing momentum on total pressure recovery

FIGURE A-12.—TOTAL PRESSURE RECOVERY OF NONADJUSTABLE AND NON-BLC INLET MODELS—Concluded

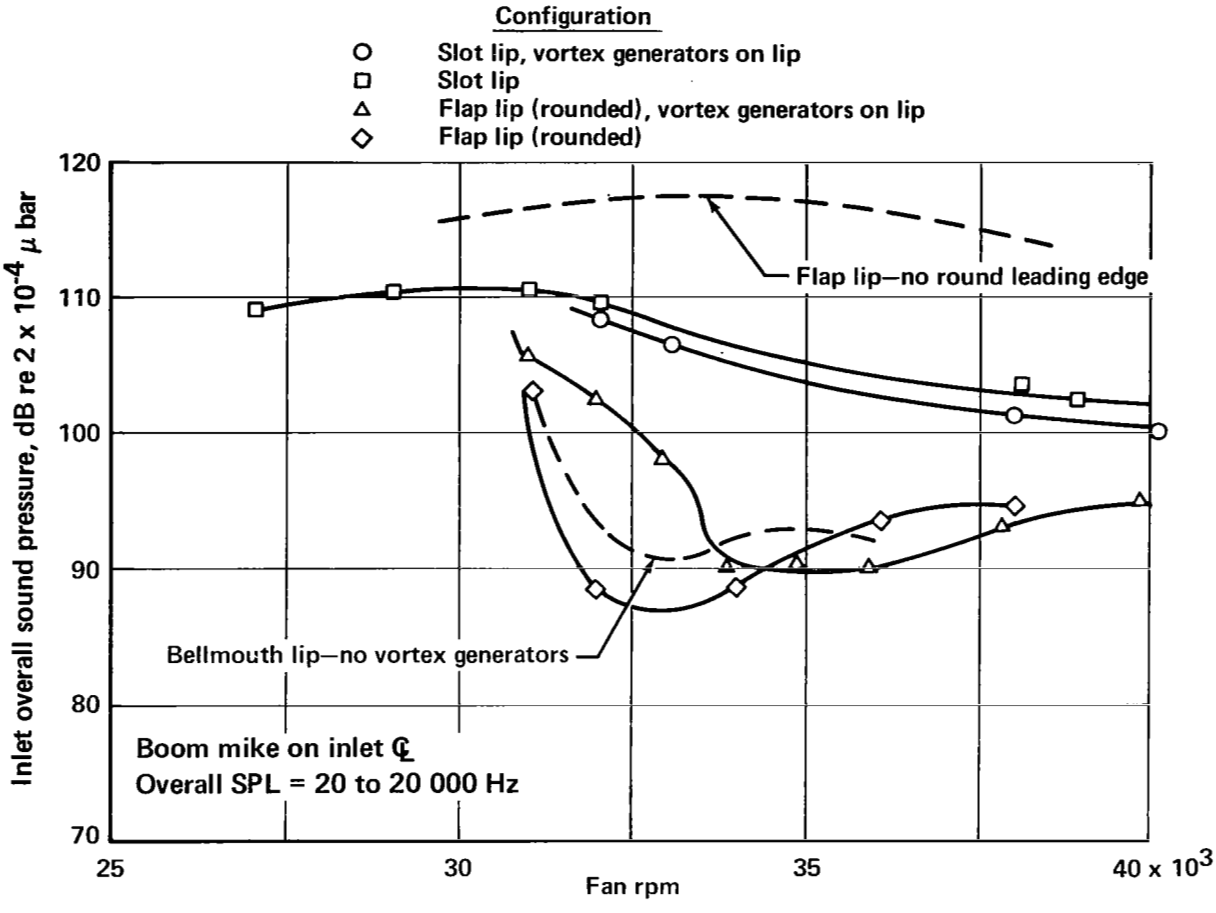

FIGURE A-13.–ATTENUATION CHARACTERISTICS OF FIVE-DOOR INLET MODEL IN LANDING APPROACH CONFIGURATION

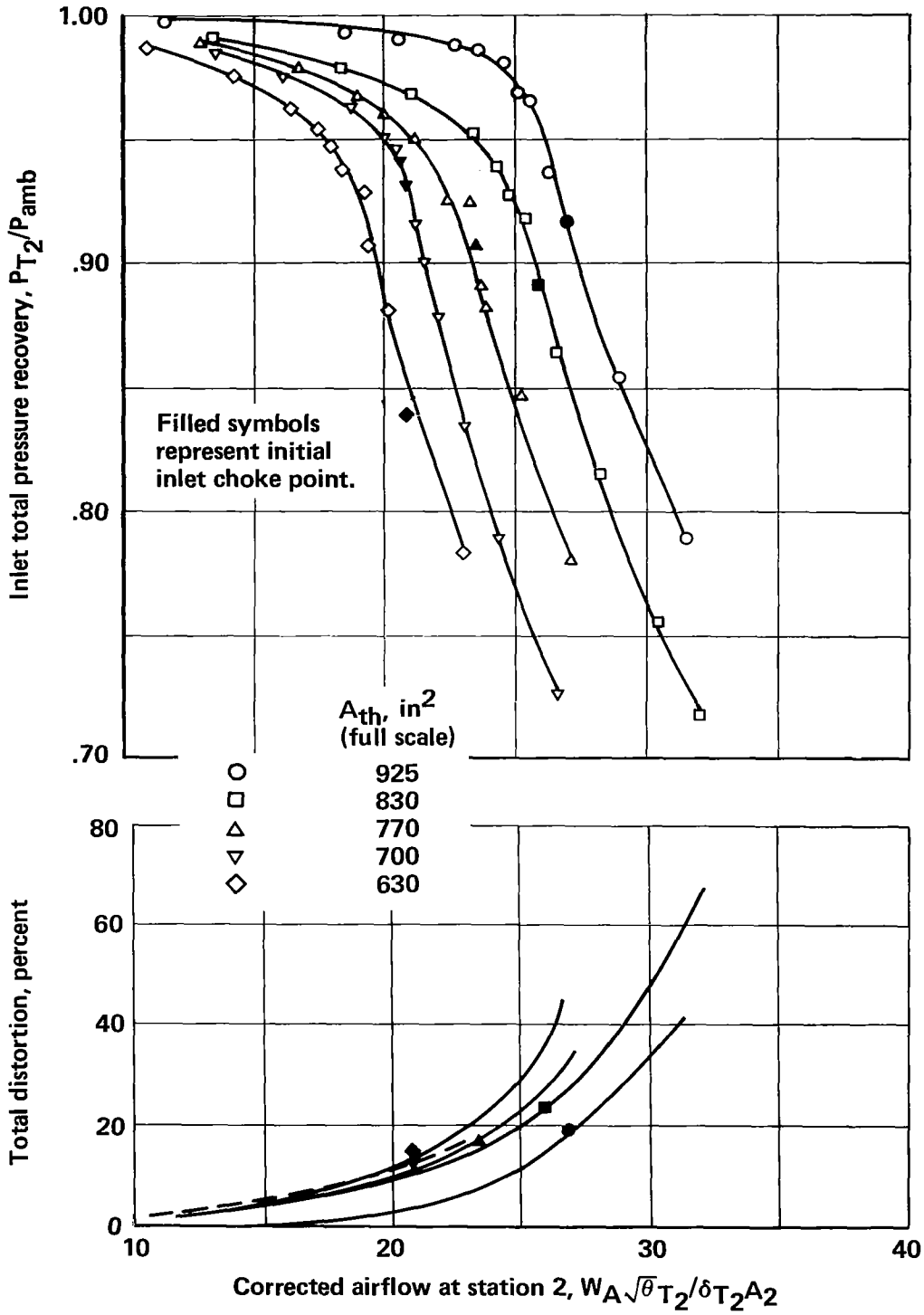

(a) Effect of varying throat area by means of extended centerbodies

FIGURE A-14.—TOTAL AND STATIC PRESSURE RECOVERY OF FIVE-DOOR INLET MODEL FOR VARIOUS CENTERBODIES AND THROAT AREAS

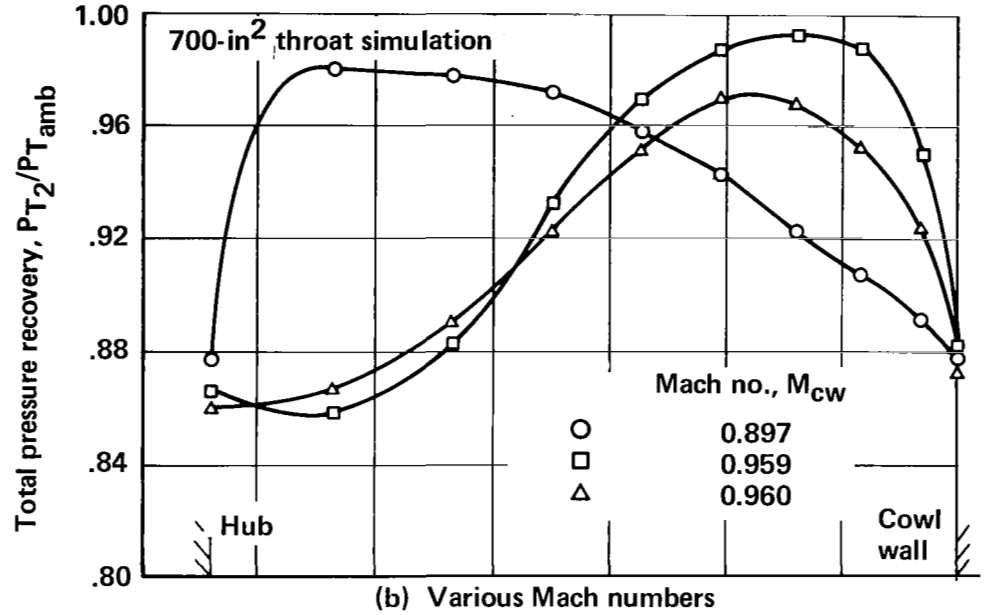

(b) Various Mach numbers

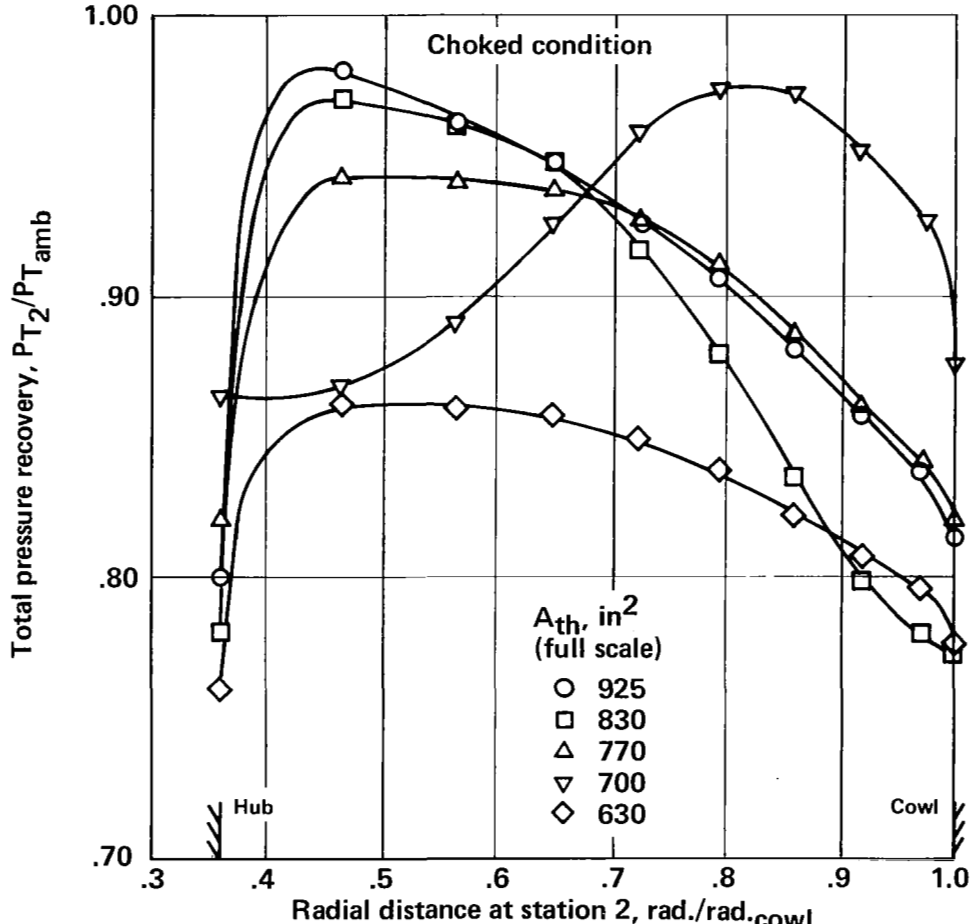

(c) Various throat areas

FIGURE A-14.–TOTAL AND STATIC PRESSURE RECOVERY OF FIVE-DOOR INLET MODEL FOR VARIOUS CENTERBODIES AND THROAT AREAS–Continued

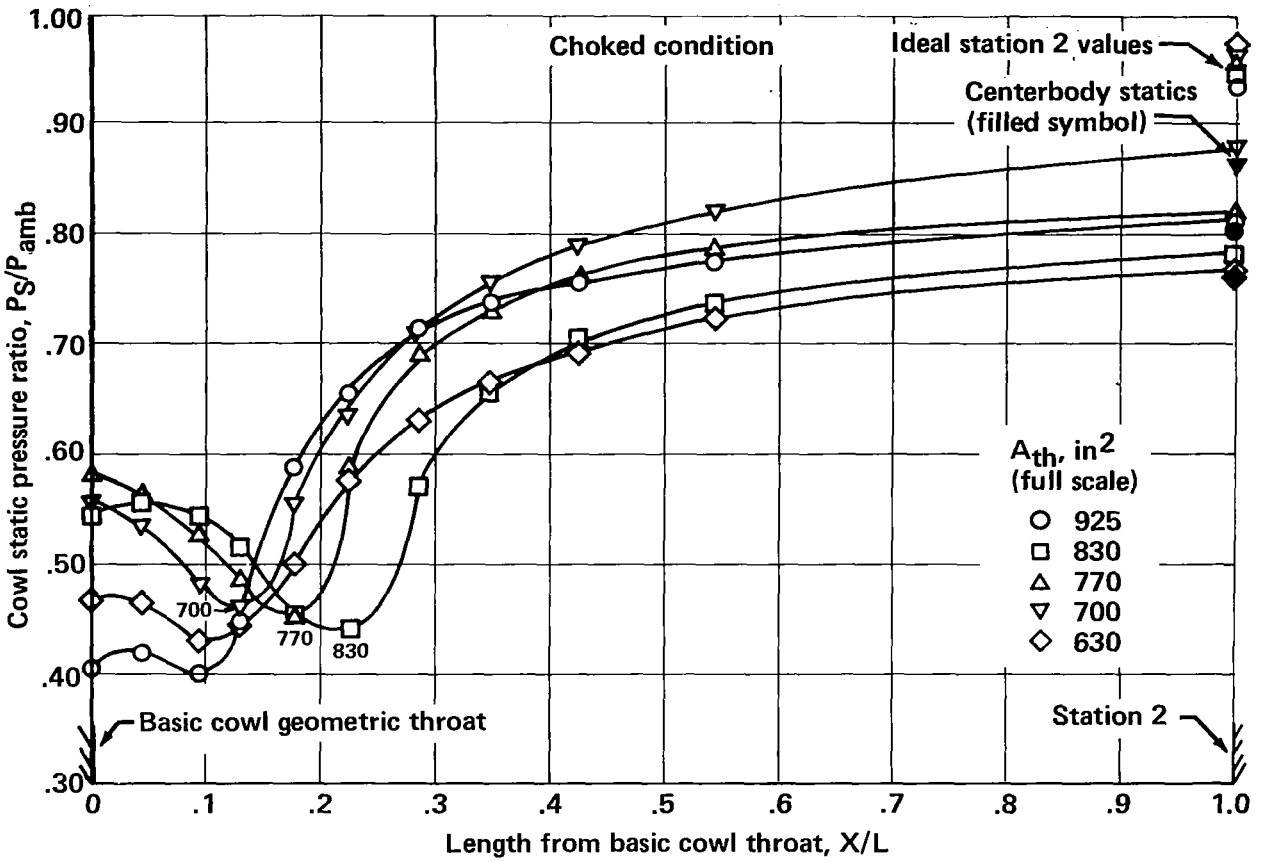

(d) Static pressure recovery

FIGURE A-14.–TOTAL AND STATIC PRESSURE RECOVERY OF FIVE-DOOR INLET MODEL FOR VARIOUS CENTERBODIES AND THROAT AREAS–Concluded

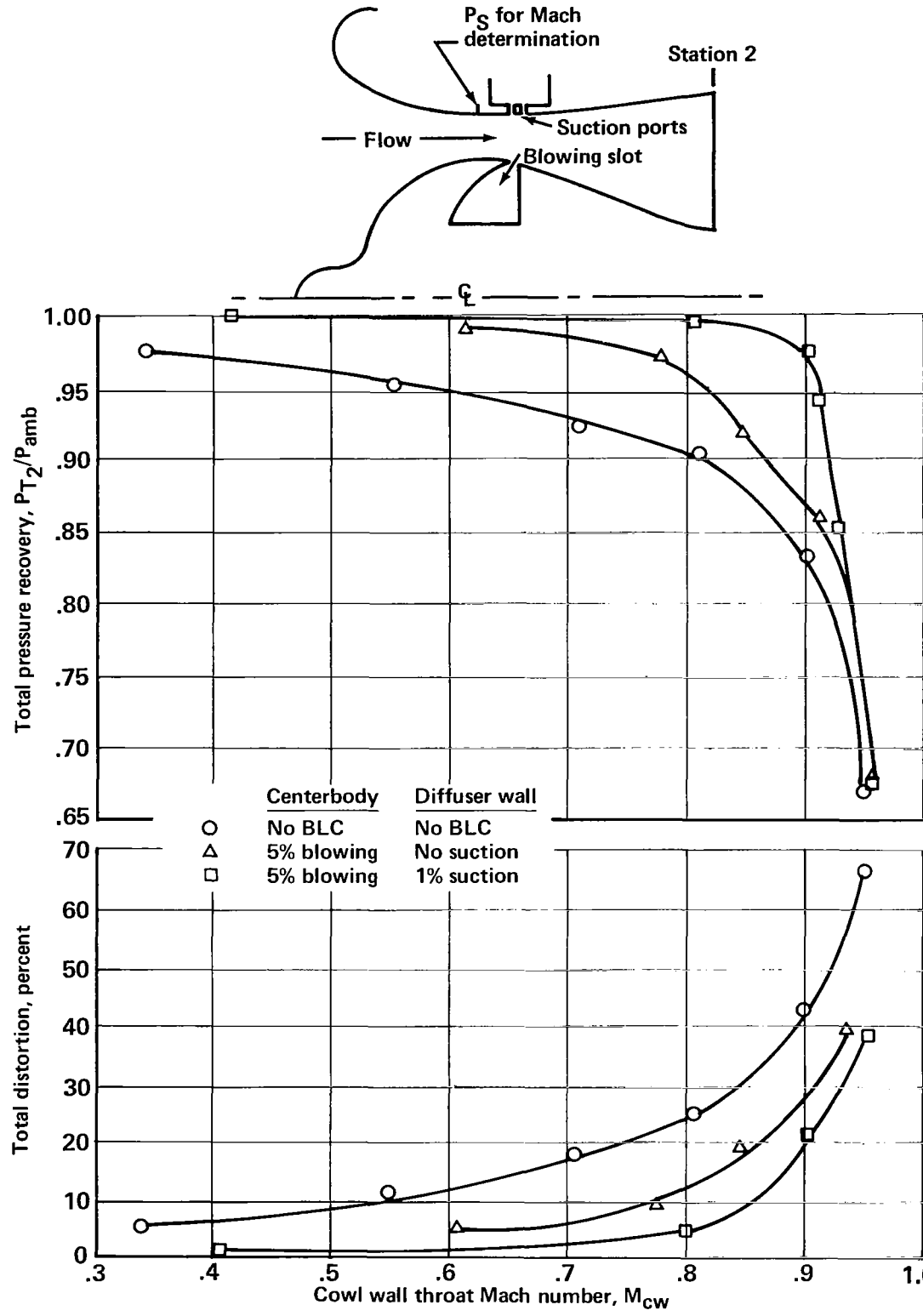

FIGURE A-15.–TOTAL PRESSURE RECOVERY OF EXPANDING CENTERBODY INLET MODEL FOR VARIOUS AMOUNTS OF BLC

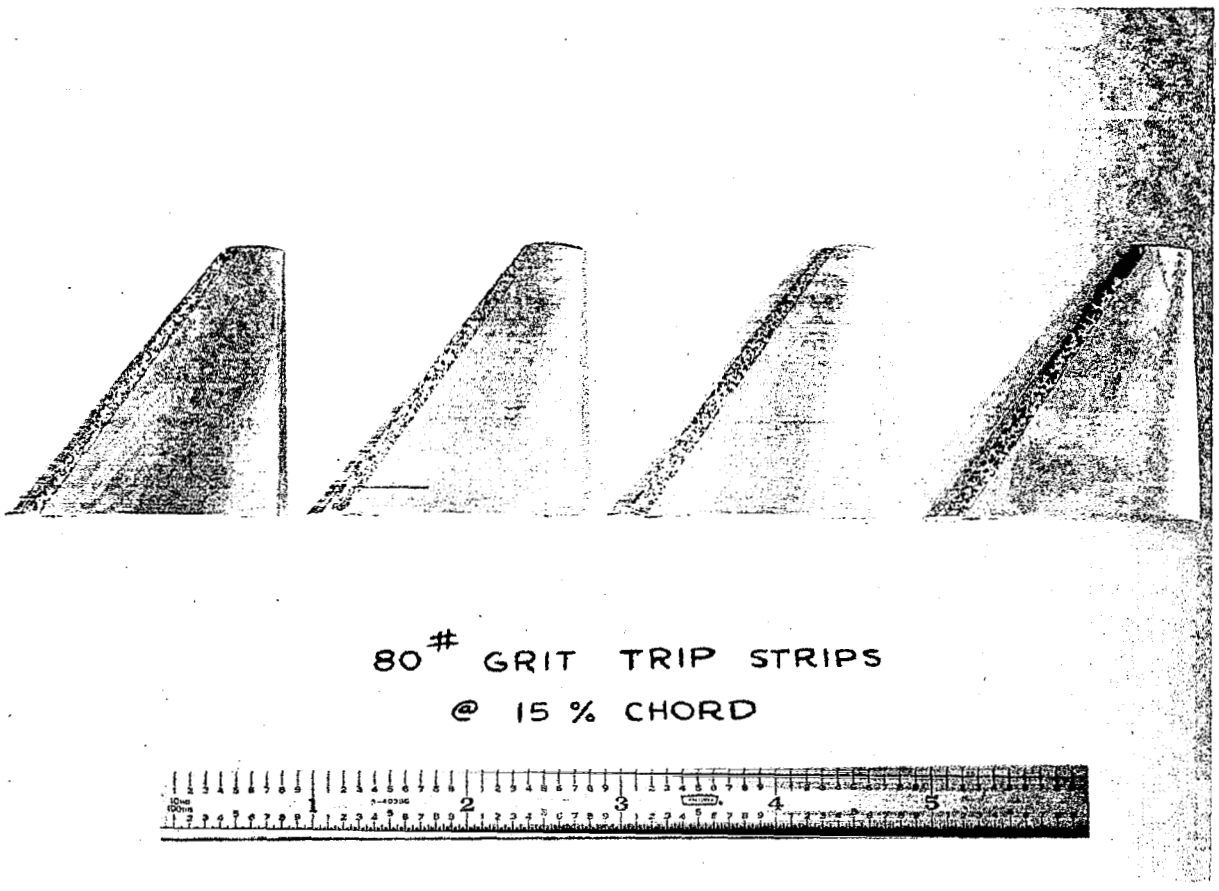

FIGURE A-16.—MODIFICATION OF RADIAL VANES

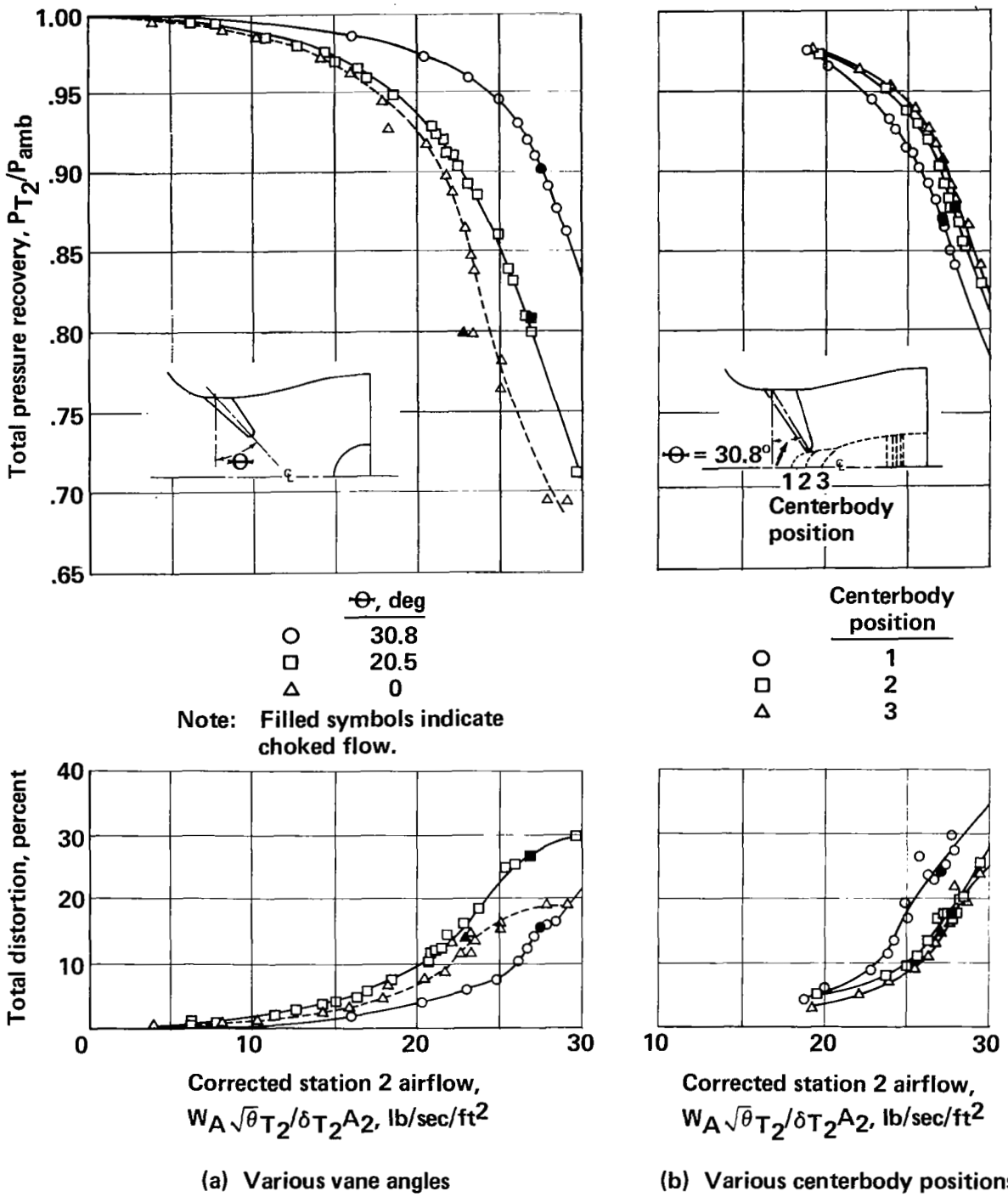

FIGURE A-17.—TOTAL PRESSURE RECOVERY OF RADIAL VANE INLET MODEL

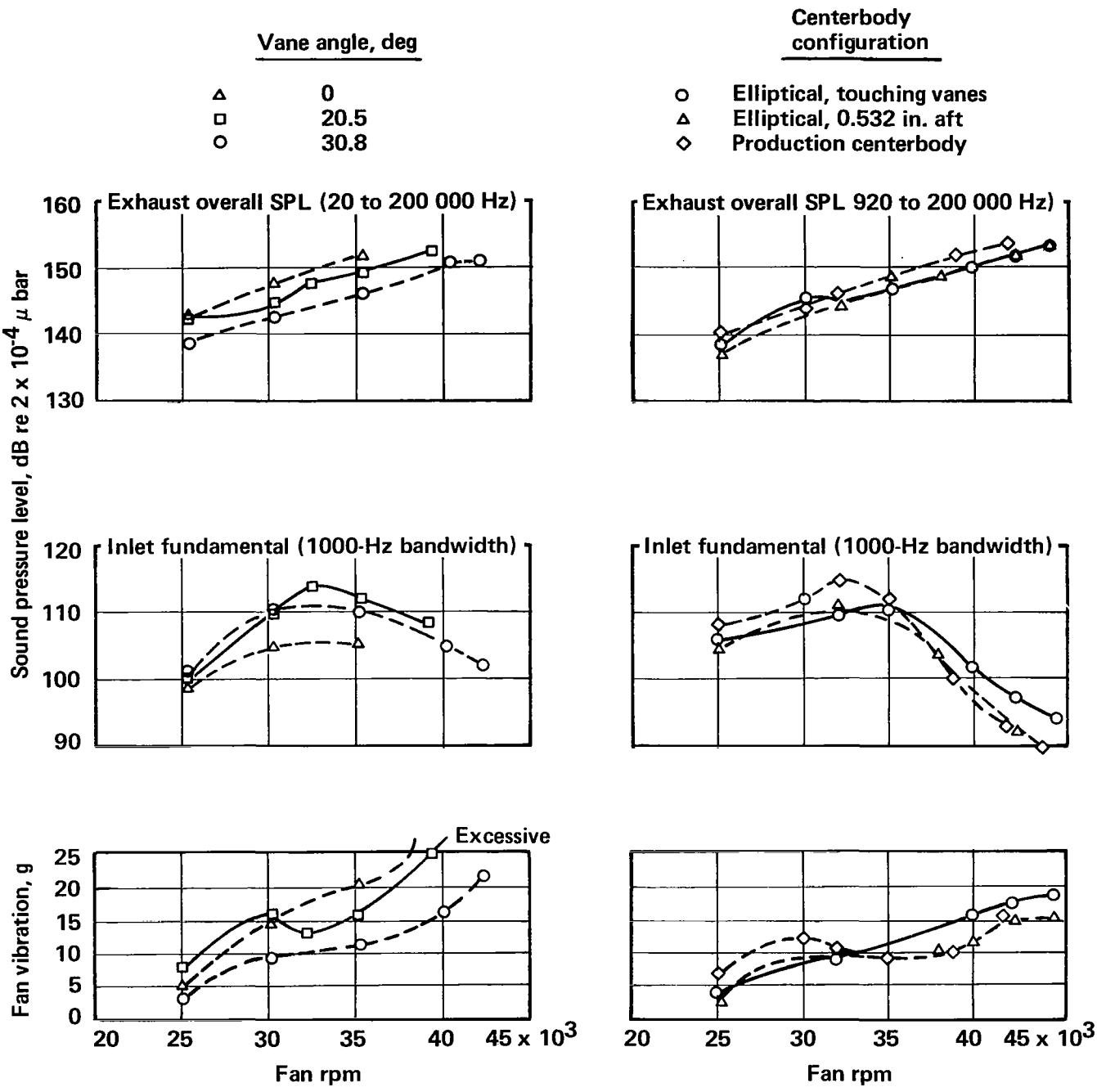

(a) Various vane angles

(b) Various centerbody positions, ⊖ = 30.8°, 3.36-in. cowl extension

FIGURE A-18.–ACOUSTIC AND VIBRATION CHARACTERISTICS OF RADIAL VANE INLET MODEL

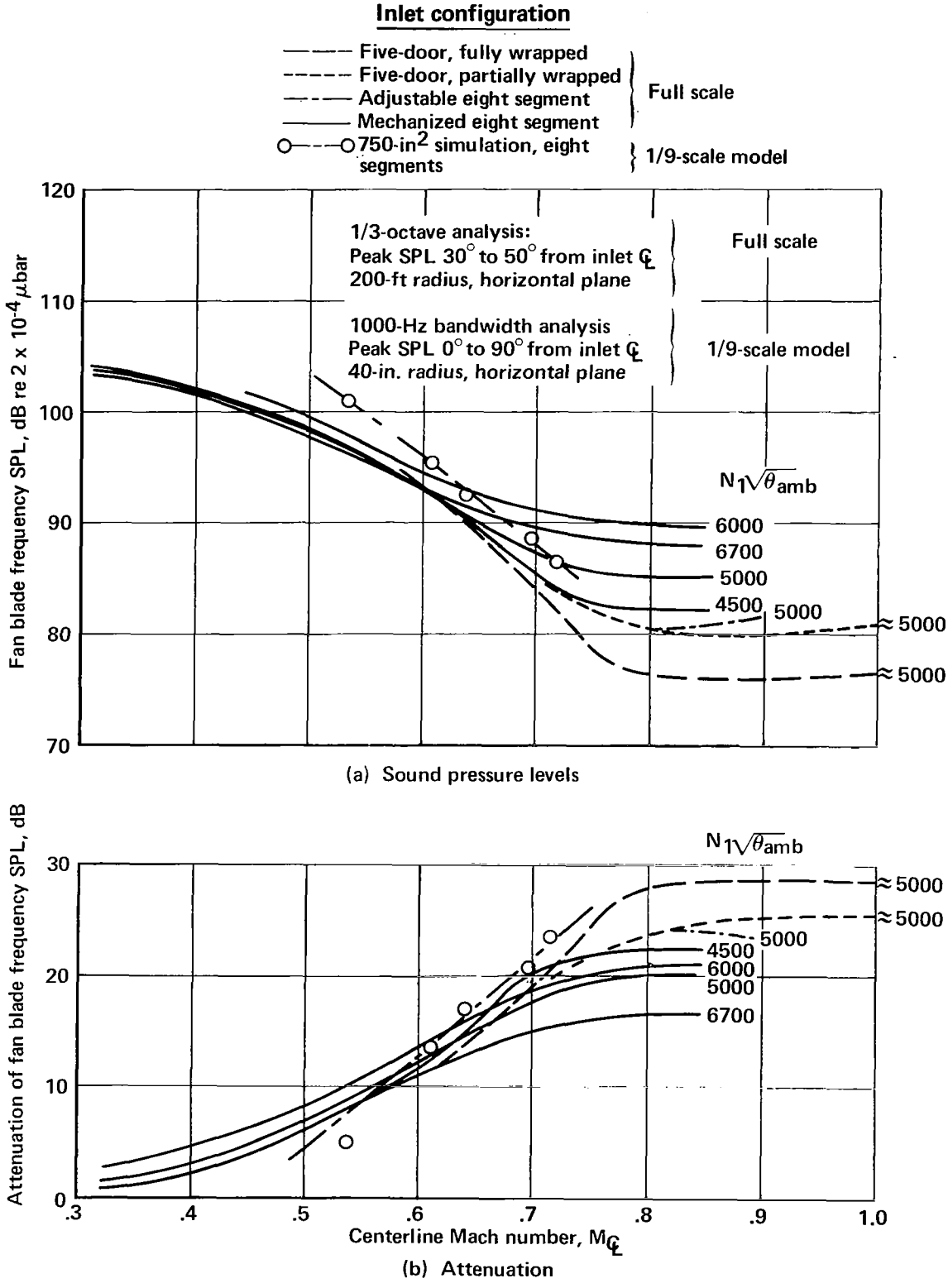

FIGURE A-19.–COMPARISON OF MODEL AND FULL-SCALE ACOUSTIC CHARACTERISTICS

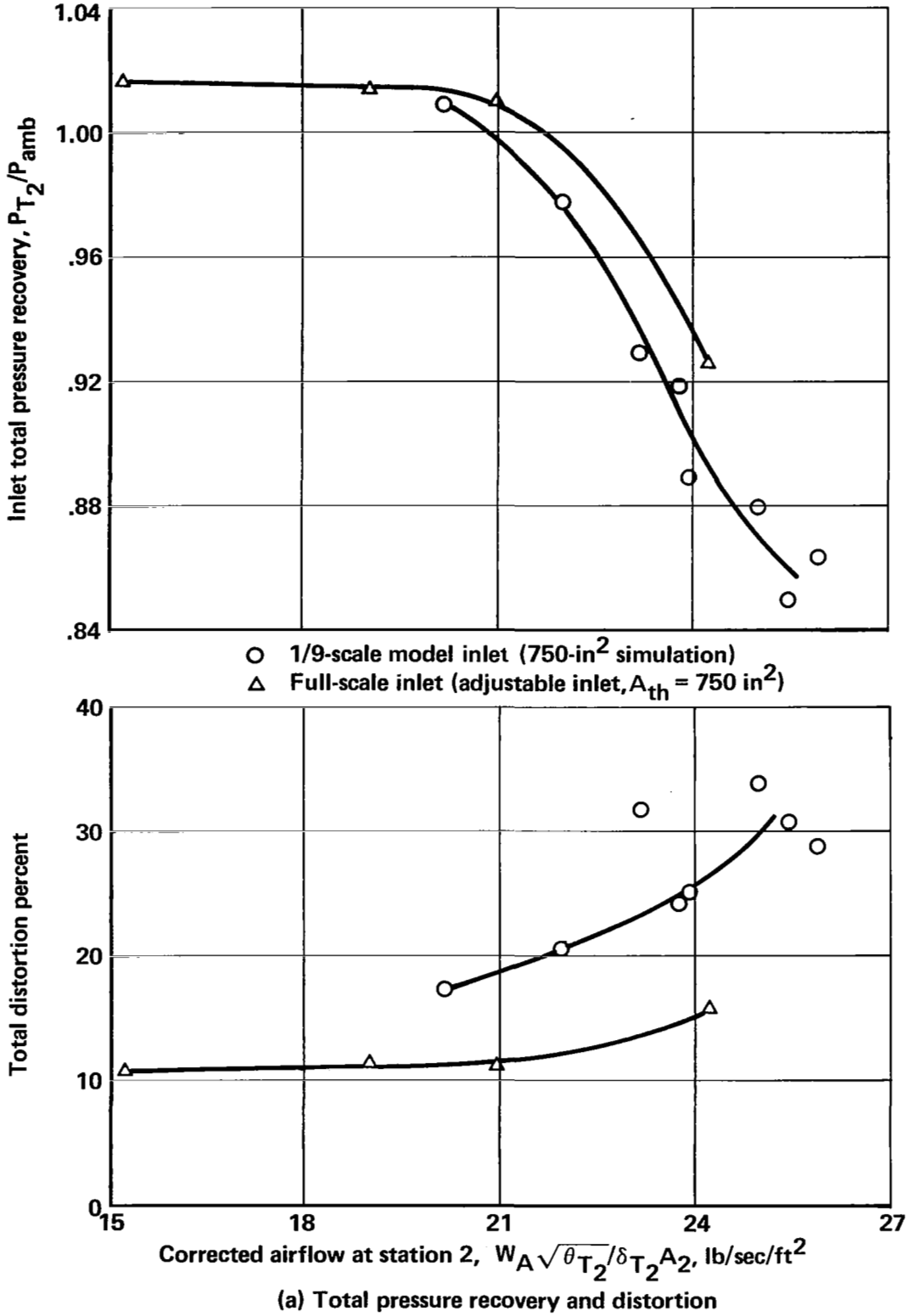

(a) Total pressure recovery and distortion

FIGURE A-20.—COMPARISON OF MODEL AND FULL-SCALE INLET PERFORMANCE

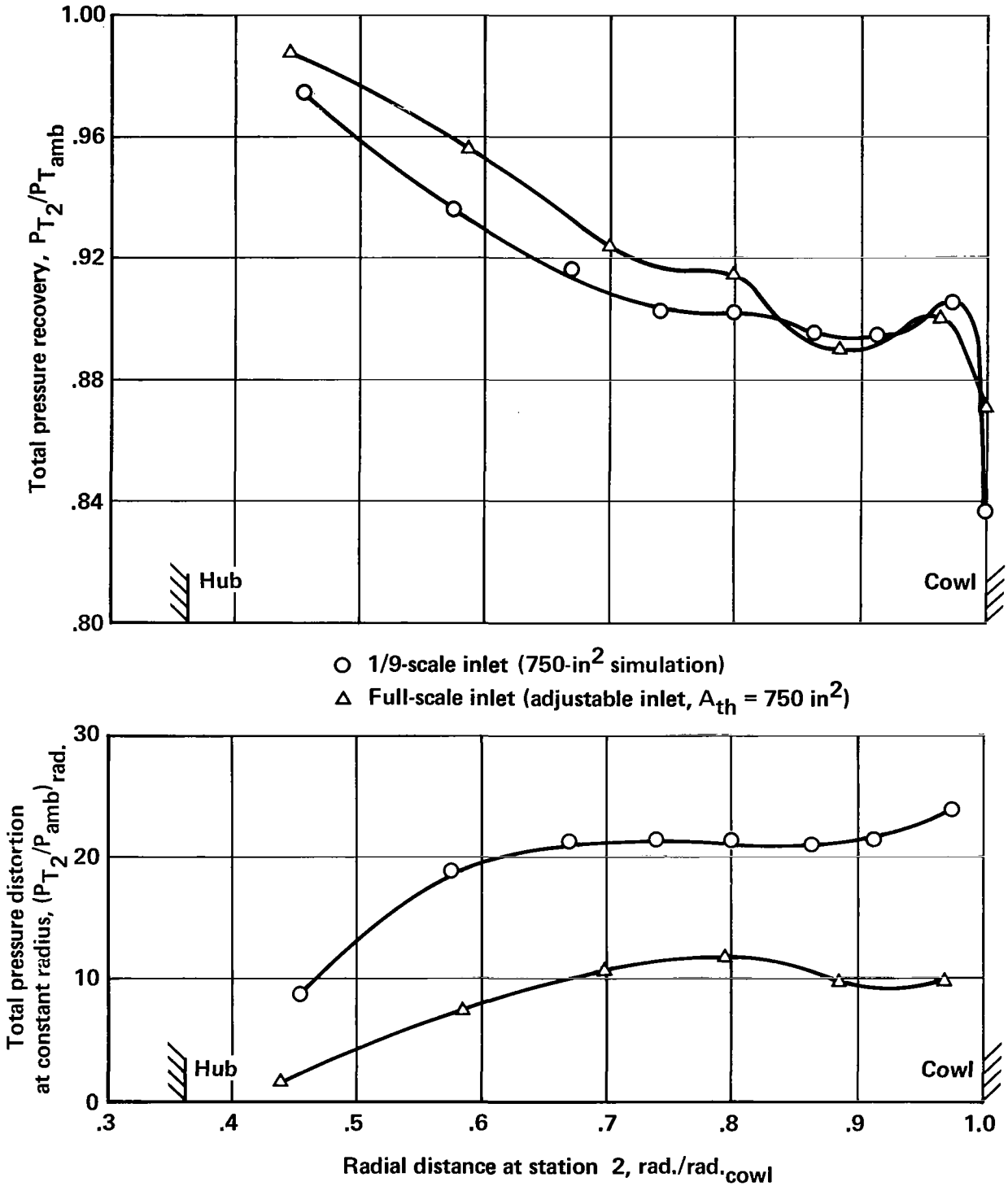

(b) Radial and circumferential recovery and distortion

FIGURE A-20.– COMPARISON OF MODEL AND FULL-SCALE INLET PERFORMANCE–Continued

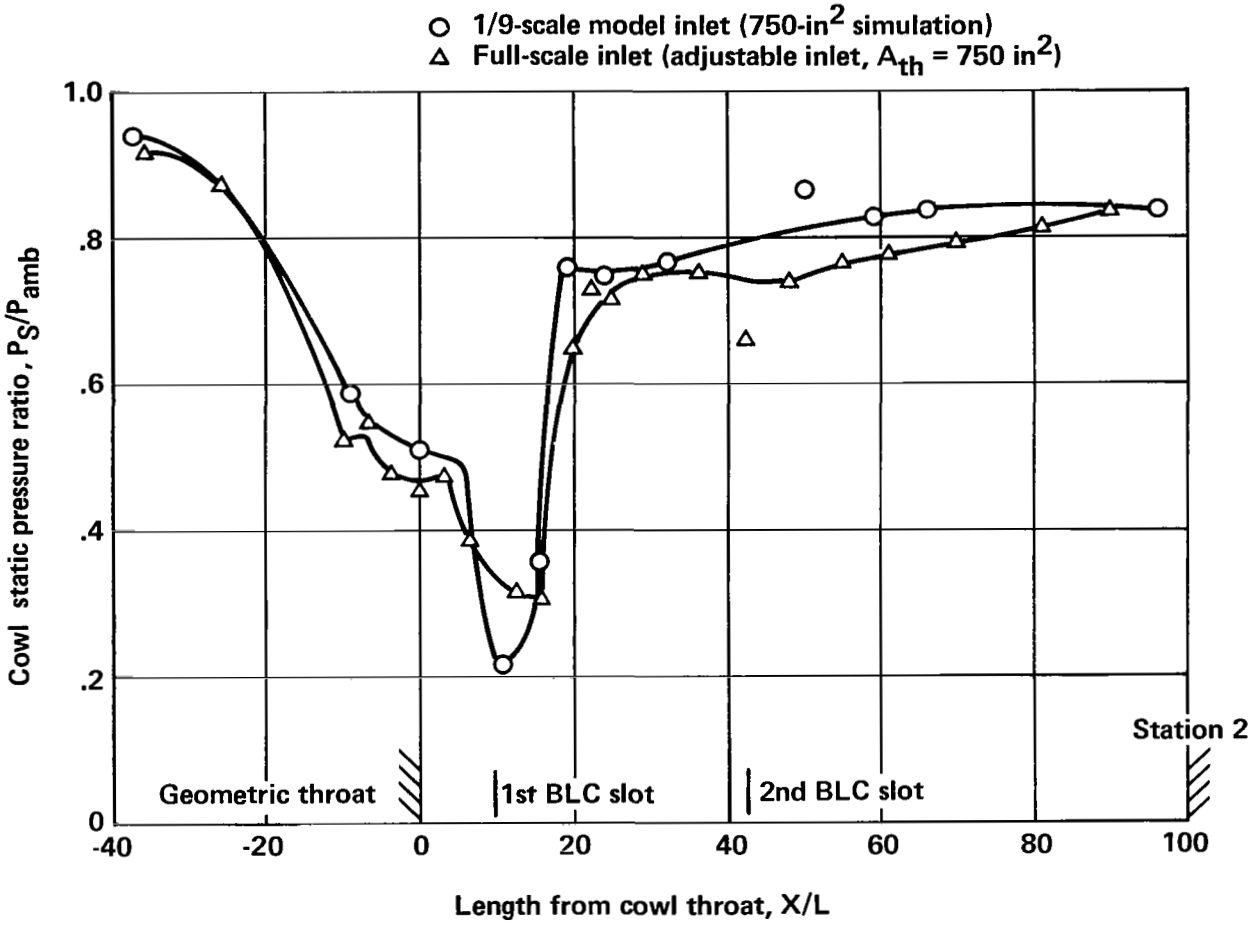

(c) Static pressure recovery

FIGURE A-20.– COMPARISON OF MODEL AND FULL-SCALE INLET PERFORMANCE–Concluded